

2019

Light Matter Interaction in Single Molecule Magnets

Rebecca Cebulka
University of Central Florida

 Part of the [Physics Commons](#)

Find similar works at: <https://stars.library.ucf.edu/etd>

University of Central Florida Libraries <http://library.ucf.edu>

This Doctoral Dissertation (Open Access) is brought to you for free and open access by STARS. It has been accepted for inclusion in Electronic Theses and Dissertations by an authorized administrator of STARS. For more information, please contact STARS@ucf.edu.

STARS Citation

Cebulka, Rebecca, "Light Matter Interaction in Single Molecule Magnets" (2019). *Electronic Theses and Dissertations*. 6343.

<https://stars.library.ucf.edu/etd/6343>

LIGHT-MATTER INTERACTION IN SINGLE
MOLECULE MAGNETS

by

REBECCA S. CEBULKA
B.S. Rutgers University, 2014
M.S. University of Central Florida, 2016

A dissertation submitted in partial fulfillment of the requirements
for the degree of Doctor of Philosophy in Physics
in the Department of Physics
in the College of Sciences
at the University of Central Florida
Orlando, Florida

Spring Term
2019

Major Professor: Enrique Del Barco

© 2019 Rebecca S. Cebulka

ABSTRACT

This dissertation includes a series of experimental realizations which focus on studying the coupling between photons and single-molecule magnets (SMMs) in both the weak and strong coupling regimes. In the weak coupling regime, the aim is to achieve coherent control over the time evolution of the spin of SMMs while applying rapid microwave pulses at sub-Kelvin temperatures, where polarization of the spin bath may be achieved without large magnetic fields, allowing the suppression of dipolar dephasing. The continuing results of this experiment will be to provide a window into fundamental sources of decoherence in single-crystal SMMs in an energy range not thoroughly investigated. We expect that these conditions would allow us to study the quantum dynamics of the spins as governed by the intrinsic molecular magnetic anisotropy, which should give rise to non-well-defined Rabi oscillations of the spin state, including metastable precessional spin states. In the strong coupling regime, high quality factor superconducting CPW resonators have been designed and fabricated to investigate the vacuum Rabi splitting between a photon and the SMM spin. The proposed setup will permit measurements of coherent collective coupling between molecular spins and a low number of photons, ideally down to a single photon. This experiment may ultimately provide the opportunity for reaching the strong coupling regime with a single spin. Finally, this thesis also documents a research study into the impact of service-learning methodology on students' depth of learning and critical thinking skills during a novel nanoscale science and technology course offered in the UCF Physics Dept. The overall learning of students was assessed and results clearly showed improvement in both multiple choice pre/post-tests and critical reflection papers. We associate this improvement at least partially to the service-learning experience.

This dissertation is dedicated to my family, my friends, and my loved ones, without whom none of this would have been possible.

ACKNOWLEDGMENTS

I would like to acknowledge the immense support, encouragement, and assistance given to me by my advisor, Dr. Enrique Del Barco, as well as my committee members Dr. Richard Klemm, Dr. Fernando Luis, and Dr. Eduardo Mucciolo. I would in addition like to thank each of my collaborators, particularly Dr. Jonathan Friedman and Dr. Charles Collett.

I would like to also thank both the National Science Foundation and the UCF Physics Department for their support throughout this process; especially my committee member and physics department chair Dr. Eduardo Mucciolo and the office staff including Esperanza Soto, Jessica Brooks, Shelley Glaspie, and Elizabeth Rivera. Also, many thanks to Amy Zeh, the Program Director of Service Learning at UCF, for her assistance with some of the work in this thesis.

I would like to express my appreciation and gratitude to all of the people in my research group, both former and current, for the invaluable assistance they have provided me: Dr. James H. Atkinson, Dr. Alvar Rodriguez, Dr. Marta Anguera, Priyanka Vaidya, Cameron Nickle, Gyanu Khatri, and Tyler Townsend. Additionally, I would like to mention special thanks to the new Dr. Tommy Boykin, who has helped me especially with regards to the formatting and editing of this thesis.

Finally, I would like to express how deeply grateful I am to my parents, without whom I never would have made it this far; my siblings, Jessica and Joshua, for their unwavering support; and friends, including George Chandler IV and Caitlin O'Malley, for helping to keep me sane throughout the process.

TABLE OF CONTENTS

LIST OF FIGURES.....	x
LIST OF TABLES.....	xii
LIST OF ABBREVIATIONS	xiii
CHAPTER 1: AN INTRODUCTION	1
1.1 Spin $\frac{1}{2}$	3
1.1.1 The Stern-Gerlach Experiment and the Electron's Magnetic Moment	5
1.1.2 Free Electron in an External Magnetic Field	6
1.1.3 Transitions Between Spin Levels.....	8
1.2 Single Molecule Magnets.....	10
1.2.1 Types of SMMs.....	11
1.2.2 The Spin Hamiltonian: A Double-Well Potential	13
1.2.3 QTM: Quantum Tunneling of the Magnetization	16
1.3 EPR: Electron Paramagnetic Resonance	20
1.3.1 The Basic Physics.....	21
1.3.2 Continuous Wave EPR	23
1.3.3 Pulsed EPR.....	24
1.4 The Spin-Photon Interaction	28
1.4.1 Decoherence in SMMs	28

1.4.2 Spins and Photons: the Jayne-Cummings Hamiltonian.....	30
1.4.3 Strong vs Weak: The Spin-Photon Coupling.....	32
References	37
CHAPTER 2: SUB-KELVIN TIME-RESOLVED EPR SPECTROSCOPY FOR STUDIES OF QUANTUM DYNAMICS OF LOW-DIMENSIONAL SPIN SYSTEMS AT LOW FREQUENCIES AND MAGNETIC FIELDS	
2.1 Background	45
2.1.1 Rabi Oscillations	49
2.1.2 Thermal Polarization for Spin $\frac{1}{2}$	50
2.2 Instrumentation and Methods.....	51
2.2.1 The Spin Echo Circuit.....	51
2.2.2 The Resonator	53
2.2.3 The Dilution Refrigerator	55
2.3 Experimental Results.....	57
2.3.1 Polarization of the Spins; Heating the Sample	58
2.3.2 Spin-Spin Relaxation Time	60
2.4 Discussion and Summary	61
References	64
CHAPTER 3: COLLECTIVE COUPLING OF MOLECULAR SPINS TO LOW NUMBERS OF PHOTONS IN THE STRONG COUPLING REGIME	
3.1 Vacuum Rabi Oscillations.....	70

3.1.1 The Jaynes-Cummings Hamiltonian, Revisited	71
3.2 The Strong Coupling Limit: The Story so Far	73
3.2.1 An Example: Fe_8	75
3.2.2 Magnetic Dilution.....	77
3.3 Superconducting, Nano-constricted, CPW Resonators	78
3.3.1 Design.....	80
3.3.2 Fabrication	83
3.4 Conclusions	84
References	87
CHAPTER 4: THE IMPACT OF SERVICE-LEARNING COURSEWORK ON UNDERGRADUATE STUDENTS’ LERANING PROCESS	91
4.1 Background	93
4.2 Methodology.....	96
4.2.1 Research Participants.....	96
4.2.2 Course Design.....	96
4.2.3 Assessments	99
4.3 Results	100
4.3.1 Pre/Post-Tests.....	102
4.3.2 Critical Reflections.....	103

4.3.3 Post-Survey.....	105
4.4 Discussion and Summary	106
References	109
CHAPTER 5: CONCLUSION.....	111
APPENDIX A: AUTHOR COPYRIGHT POLICY FOR PRISM: A JOURNAL OF REGIONAL ENGAGEMENT.....	115
APPENDIX B: IRB APPROVAL LETTER.....	117
APPENDIX C: DETAILED LIST OF SPIN ECHO CIRCUIT COMPONENTS.....	119
APPENDIX D: MICROSTRIP RESONATOR FABRICATION RECIPE	123
APPENDIX E: CRYOGENIC AMPLIFIER.....	125
APPENDIX F: NANOSCIENCE AND TECHNOLOGY CONCEPT INVENTORY.....	127
APPENDIX G: DEAL MODEL RUBRIC USED TO SCORE CRITICAL REFLECTIONS	132
APPENDIX H SERVICE-LEARNING POST-SURVEY	134

LIST OF FIGURES

Figure 1.1: Classical Angular Momentum	4
Figure 1.2: Spin $\frac{1}{2}$ Energy Diagrams.....	8
Figure 1.3: The Double-Well Potential.....	15
Figure 1.4: “Easy,” “Medium,” and “Hard” Axes	16
Figure 1.5: Mn_{12} and the Quantum Tunneling of the Magnetization.....	17
Figure 1.6: Energy Level Diagram for $S=10$ System	20
Figure 1.7: The Zeeman Effect	22
Figure 1.8: Free Induction Decay	25
Figure 1.9: Inversion Recovery.....	26
Figure 1.10: Spin Echo.....	27
Figure 1.11: Decoherence Rates for Fe_8	30
Figure 1.12: Coupled Spin-Photon Transition.....	32
Figure 1.13: Normal Mode Splitting.....	35
Figure 1.14: Weak vs Strong Coupling	36
Figure 2.1: The Spin Echo Circuit	52
Figure 2.2: The Microstrip Resonator	54
Figure 2.3: The Dilution Refrigerator	56
Figure 2.4: Spin Bath Polarization at Low Temperatures	59
Figure 2.5: Extracting the Spin-Spin Relaxation Time T_2	61
Figure 3.1: Coupling Regimes in Microstrip Resonators.....	74

Figure 3.2: Coherent Rabi Oscillations in Gd-doped CaWO_4	75
Figure 3.3: Strong Coupling in Fe_8	76
Figure 3.4: Resonant Geometries	78
Figure 3.5: Our Loop-Gap Resonator	79
Figure 3.6: Interlocked and Direct Coupling Gaps	81
Figure 3.7: The Parallel LRC Circuit	82
Figure 3.8: CPW Resonator Design	83
Figure 4.1: Participants Presenting in Middle Schools	98
Figure 4.2: Overall Concept Inventory Scores	102
Figure 4.3: Concept Inventory Scores by Topic	103
Figure 4.4: Critical Reflection Scores	104
Figure 4.5: Post-Survey Responses	106
Figure C.1: Spin Echo Circuit in Detail	120
Figure E.1: Cryogenic Amplifier.....	126

LIST OF TABLES

Table 4.1: Nanoscience Course Rubric.....	97
---	----

LIST OF ABBREVIATIONS

CPW	Coplanar Waveguide
CW	Continuous Wave
EDM	Electrical Discharge Machining
EPR	Electron Paramagnetic Resonance
GSA	Giant Spin Approximation
NHMFL	National High Magnetic Field Lab
NMR	Nuclear Magnetic Resonance
NSF	National Science Foundation
NV centers	Nitrogen-Vacancy centers
OFHC	Oxygen-Free High Thermal Conductivity
QED	Quantum Electrodynamics
QTM	Quantum Tunneling of the Magnetization
RWA	Rotating Wave Approximation
SMMs	Single Molecule Magnets
STEM	Science, Technology, Engineering, and Mathematics
UCF	University of Central Florida
YBCO	Yttrium Barium Copper Oxide
ZFS	Zero-Field Splitting

CHAPTER 1: AN INTRODUCTION

The theory of electromagnetism has been a driving force in innovation since it was explored by such early pioneers as Maxwell, Ampere, and Faraday [1,2]. Much of technology developed in the last century is based upon the creation and manipulation of electronic charges; in particular the use of transistors (which can act as an electronic switch, particularly in computers where they allow complex calculations to be performed); diodes (used to preferentially allow electric current to flow in one direction, for example in computers to perform certain logic operations utilizing large numbers of transistor components); and other hallmarks of modern electronic circuits. Today, technology is moving towards the manipulation of the magnetic properties of systems for a variety of purposes; here, that basic component is the intrinsic angular momentum of quantum particles, which is referred to as *spin*. In fact, the field of *spintronics* has emerged as a viable alternative to electronics where rather than movement of an electron's charge driving operations, the change of electronic spins can be used. Advantages of spintronics include the relative ease of switching spins when compared to maintaining an electric current, as well as the decreased power consumption required when compared to electronics. Some of the more widely researched applications include spin valves, giant magneto resistance, magnetic tunnel junctions, single spin logic, and spin-based transistors [3]; spin pumping and spin torque transfer, especially recent research done concerning antiferromagnets, where the electronic spins align antiparallel to their neighbors; and perhaps the most current "hot topic", quantum computing and the search for ideal qubits (quantum bits).

Molecular nanomagnets revealed their potential to act as magnetic bits at the quantum level with the discovery of magnetic hysteresis in molecular clusters of Mn₁₂ acetate. The 1996 discovery of the resonant quantum tunneling of the magnetization (QTM) [4-6] is considered to be a landmark in the

physics of spin [7]. In addition to QTM, the overall magnetic properties of single molecule magnets (SMMs) [8-23] make them extremely attractive for use in ultra-high-density integration and quantum information processing [24-26]. In fact, Grover's algorithm, a quantum algorithm designed to identify the correct input to a "black box" function which produces a given output, has recently been demonstrated in an individual SMM [27]. Of particular relevance is reducing and influencing sources of decoherence (such as interactions between electronic spins and nearby nuclear spins, magnons, or phonons, discussed further in section 1.4) in these systems, which will enable the substantial number of logic gate operations required by quantum algorithms and error correction protocols [28-31] (especially in samples which allow isotopic purification). In addition, the capability of a magnetic qubit, the quantum computing analog of the standard computing bit, such as a SMM [32] to coherently transform from a distinct excitation to a solitary photon is crucial for essential quantum information processes including the conveyance of information (read/write processes); this ability is characteristic of strong coupling between the qubit and its resonant modes [33]. Eventually, the ability to couple single spins to single photons in this regime would allow for unparalleled advances in quantum technologies – imagine individual spins being entangled across huge distances, allowing for virtually instantaneous communication; or perhaps calculations being performed by individual photons moving through a series of isolated spins, pushing Moore's law to the absolute limit. Another evolving area of interest in which molecular nanomagnets are becoming a significant contribution is the developing field of *molecular* spintronics [34-44]; that is, the integration of elements of quantum magnetism and molecular electronics to create electronic devices with exciting new functionalities [45-47]. There are specific instances in which SMMs will provide a significant advantage over other systems (for example, N-V centers in diamond) with respect to spin manipulation and control, such as coupling to quantum circuits using superconducting resonators [48-50].

This dissertation primarily concerns itself with the exploration of quantum dynamics of spin in SMMs, most notably in an energy regime that has not been well-studied and is dominated by the intrinsic properties of the molecules. Specific interest is paid to experiments devoted to ultra-low temperature pulsed electron paramagnetic resonance (EPR) studies in the weak coupling regime, the goal being to facilitate understanding of fundamental sources of decoherence in these spin systems to further their potential use in quantum information science. I then discuss methods of reaching the strong coupling regime with an ensemble of spins and a low number of photons and enhancing the coupling between the two systems, along with some preliminary results that relate to this path. Additionally, I will describe some physics education research work that has been done regarding service learning in a nanoscience course as a way to bring the experimental side of nanomagnetism to light in a broader context.

The remainder of this first chapter consists of a general introduction to the most basic spin system, a free electron, followed by a discussion of molecular nanomagnets in particular; an overview of one of the main experimental techniques used in this thesis; and a brief summary of light-matter interaction as it relates to spins. Chapter 2 discusses the main technical work I have performed pertaining to decoherence studies in SMMs. Chapter 3 puts forth our ideas for reaching the strong coupling regime with low numbers of photons. Chapter 4 describes my work in nanomagnetism education research. Finally, Chapter 5 will conclude this dissertation and present a general discussion of what has been accomplished.

1.1 Spin $\frac{1}{2}$

Portions of this section have been written using references [51,52].

When physicists talk about the spin of an electron, they are referring to an intrinsic property of the particle that is analogous to angular momentum due to the rotation of the electron around its own

axis, similar to how the Earth is spinning around its own axis while also orbiting the sun. This is somewhat of a simplification, as it is not strictly possible to physically observe an electron spinning in this manner, but spin in general obeys the same mathematical principles and laws as classical angular momentum (Figure 1.1). That is, spin gives an electron a magnetic moment, and is constrained by a conservation law similar to that of angular momentum. Referring to an electron as spin “up” or spin “down” simply denotes the direction of the axis of rotation; thought about in a different way, it specifies whether the electron can be viewed as being analogous to a ball of charge rotating clockwise or counterclockwise. Contrary to classical angular momentum, however, spin is a completely quantum mechanical property and can take only quantized, discrete values. It cannot be described by classical physics.

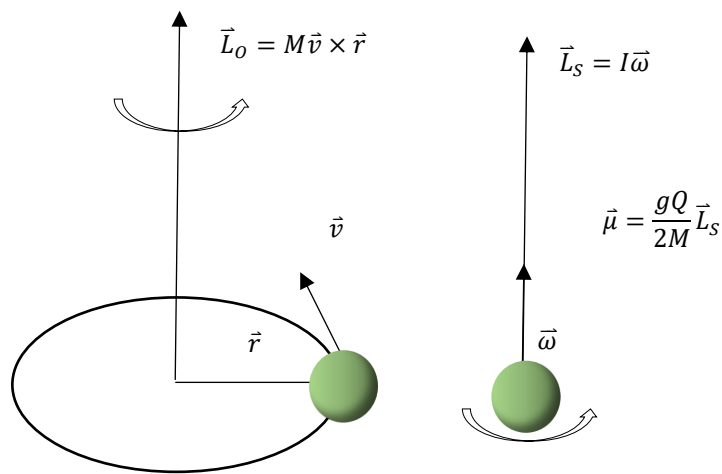


Figure 1.1: Classical Angular Momentum

A classical representation of the orbital angular momentum for an electron in a circular orbit (Left) and the spin angular momentum for a rotating electron (Right). The classical magnetic moment due to a rotating ball of charge is shown on the far right.

In determining the state of a quantum mechanical system, one can turn to linear algebra. The state is said to be an *eigenstate* of the system if it has a measurable value, the *eigenvalue*, that can be observed. For example, an eigenstate of the spin angular momentum operator for an electron would be spin up; the electron’s spin can be measured to be $+1/2$. Typically, such a system will have multiple

possible eigenstates; for a free electron there are two, spin up and spin down. The system in general, at any time, can be described by summing over all possible eigenstates, with appropriate coefficients to describe the probability of the system to be observed in each state at any given time. This summation is called the *wavefunction* of the system. Thus, to fully describe any quantum mechanical system one should identify the eigenstate coefficients from the equations of motion and construct the wavefunction. The observable properties are extracted from the eigenvalues and eigenstates of a specific operator (such as the spin angular momentum operator \vec{S}). As another example, the eigenvalues derived from applying the Hamiltonian operator to a system's wavefunction will return the measurable energies of that system. To better understand this in the context of spin, we will look at the most basic spin system: the free spin $\frac{1}{2}$ particle.

1.1.1 The Stern-Gerlach Experiment and the Electron's Magnetic Moment

The first real indication of the electron having some spin was found in 1922 in Germany, by Otto Stern and Walther Gerlach. They sent beams of silver atoms (with one unpaired electron in the valence shell) through an inhomogeneous magnetic field to observe any deflection. The results showed unequivocally that silver atoms had quantized magnetic moments that could take one of two possible values. However, it took several years (and Wolfgang Pauli) before this information became a framework for quantum mechanical spin.

If we start from a classical treatment and picture the electron as a tiny spinning ball of charge, then we know from classical mechanics that it should have both an angular momentum \vec{L} and a magnetic moment $\vec{\mu}$ which are related by the charge Q and mass M as

$$\vec{\mu} = \frac{Q}{2M} \vec{L} \quad (1.1)$$

[51]. Although an electron is most definitely *not* a physical spinning ball, it does have an intrinsic angular momentum usually denoted as \vec{S} , and the charge and mass are well known. Accounting for the dimensionless g-factor, which is an effective proportionality constant specific to a system and ≈ 2 for a free electron, this would give a semi-quantum expression for the spin magnetic moment $\vec{\mu}_S$ of

$$\vec{\mu}_S = \frac{-g\mu_B\vec{S}}{\hbar} \quad (1.2)$$

where μ_B is the Bohr magneton, \hbar is the reduced Planck's constant, and the negative sign comes from the fact that the electron has a negative charge and thus, the magnetic moment will point opposite the angular momentum.

1.1.2 Free Electron in an External Magnetic Field

In the presence of an external magnetic field \vec{B} , the classical potential energy of a magnetic moment $\vec{\mu}$ is

$$U_B = -\vec{\mu} \cdot \vec{B}. \quad (1.3)$$

However, we know that spin is quantized and thus requires a quantum mechanical treatment. We introduce the operator that represents the observable projection of the spin onto the quantization axis \hat{S}_Z as

$$\hat{S}_Z = \frac{\hbar}{2} \begin{bmatrix} 1 & 0 \\ 0 & -1 \end{bmatrix} \quad (1.4)$$

where the quantization axis is given by the applied magnetic field \vec{B} in this case ($|\vec{B}|$ is assumed to be large, on the order of 1T). The eigenvectors of this matrix are easily found to be $[1, 0]$ and $[0, 1]$ with respective eigenvalues of +1 and -1, telling us that measuring the spin of an electron along the defined

quantization axis will return a value of either $+\hbar/2$ or $-\hbar/2$ belonging to a spin that is either parallel or antiparallel to the axis (spin “up” or spin “down”). We can use this operator to construct the Zeeman Hamiltonian operator, the quantum mechanical analog to the classical potential U_B , defined as

$$H = -g\mu_B S_z B_z . \quad (1.5)$$

It is important now to distinguish the z-component of the magnetic field, B_z , from the total applied field \vec{B} as the component that lies along the whatever direction the spin vector points; this comes from the dot product between \vec{S} and \vec{B} . In this simple free electron system, of course, the spin vector will be aligned with the external field; however, in more complicated systems there may be additional internal fields that will affect the spin vector. One of the main goals of this thesis is to investigate these exact types of systems, where intrinsic magneto-anisotropy plays a large role in the spin dynamics (see Chapter 2). From this Hamiltonian operator it can immediately be seen that the energy will be a minimum when the spin vector and the magnetic field are aligned (S_z and B_z have the same sign), and the eigenvalues can be plotted as a function of B_z to give an energy level diagram for the system. Figure 1.2 on the next page displays a plot of the classical potential U_B as a function of magnetic field next to the energy level diagram for the simple spin $\frac{1}{2}$ system discussed.

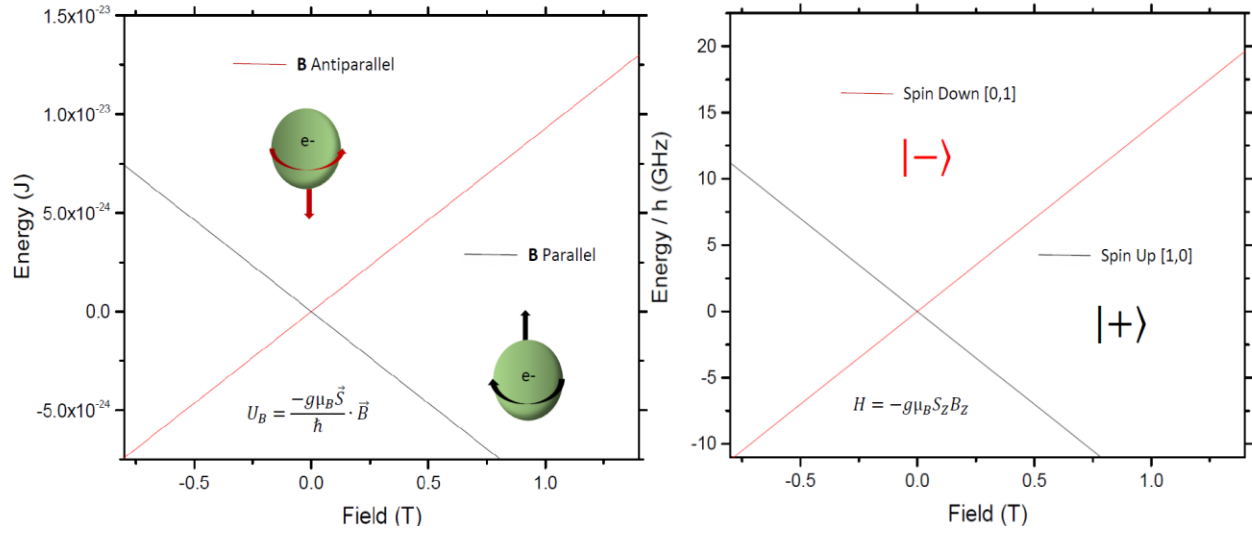


Figure 1.2: Spin ½ Energy Diagrams

Left: Graph of the semiclassical energies for the parallel (black) and antiparallel (red) orientations of a free electron's magnetic moment in an external magnetic field. Inset are classical representations of the electron's spin, illustrating an effective "right-hand rule" as explanation for the magnetic moment. Note that the directions have been reversed due to the negative charge of the electrons. Right: Energy level diagram of the two states (spin-up, black, and spin-down, red) for an isolated electron in a magnetic field. The arrow points to an energy difference of approximately 10GHz between the ground and excited states.

1.1.3 Transitions Between Spin Levels

It is in many cases easiest to analyze a quantum mechanics problem through the use of matrices.

We can define the basis states of our spin ½ system as $|+\rangle$ and $|-\rangle$ such that

$$\hat{S}_Z|+\rangle = +\frac{\hbar}{2}|+\rangle, \quad \hat{S}_Z|-\rangle = -\frac{\hbar}{2}|-\rangle \quad (1.6)$$

meaning $|+\rangle$ corresponds to the spin up state $[1, 0]$ and $|-\rangle$ corresponds to the spin down state $[0, 1]$.

What would happen if we wanted to look at the probability to change orientations from state $|+\rangle$ to state $|-\rangle$? Let us look at a two state Hamiltonian matrix in its most general form:

$$H = \begin{bmatrix} E_{11} & E_{12} \\ E_{21} & E_{22} \end{bmatrix}. \quad (1.7)$$

The diagonal matrix elements (E_{11} and E_{22}) of the Hamiltonian gives the eigenvalues, or observable energies, of each individual state $|+\rangle$ and $|-\rangle$. But the off-diagonal elements (E_{21} and E_{12}) are in fact the amplitudes for possible transitions *between* the states and describe the coupling between them. For example, if the off-diagonal terms in the Hamiltonian matrix are all zero, there will be no transitions allowed at all between the states. With our current definition of the Zeeman Hamiltonian, including only S_z as a spin operator, the Hamiltonian matrix is diagonal, and no transitions will occur. We must therefore include a dependence of the spin projection into the plane transverse to the z-axis of the form

$$\hat{S}_x = \frac{\hbar}{2} \begin{bmatrix} 0 & 1 \\ 1 & 0 \end{bmatrix}, \quad \hat{S}_y = \frac{\hbar}{2i} \begin{bmatrix} 0 & -1 \\ 1 & 0 \end{bmatrix}. \quad (1.8)$$

These, taken with \hat{S}_z , are none other than the well-known Pauli spin operators $\hat{\sigma}_x, \hat{\sigma}_y, \hat{\sigma}_z$ multiplied by $\hbar/2$.

Now the so-called matrix transition element for the two states, $M = \langle + | H | - \rangle$, will be nonzero, allowing for some transition probability. This is the driving force behind EPR measurements, where a cavity excitation (photon) is coupled to a spin through a nonzero transition matrix element; when the photon's energy matches the energy difference between the two levels $|+\rangle$ and $|-\rangle$ a transition can occur. The rate of this transition occurring can be found from Fermi's golden rule [53] to be

$$\Gamma_{+ \rightarrow -} = \frac{2\pi}{\hbar} |M = \langle + | H | - \rangle|^2 \delta(E_{ph} - \Delta) \quad (1.9)$$

where E_{ph} is the photon energy and Δ is the energy difference between the two states. The delta function effectively prevents a transition unless the photon energy exactly matches the energy gap; in practice, of course, there is not a discrete set of infinitely sharp lines marking the transitions. There are a host of other contributions, including dynamic effects (such as spontaneous relaxation) and static effects (such

as unresolved hyperfine splittings and small variations of magnetic properties across the sample) that lead to line-broadening [54-58]. Finally, it is not explicitly stated in (1.9), but due to spin conservation the photon spin must be equal to that of change in spin of the system ($\Delta S = \pm 1$). The next section will discuss the significantly more complicated situation with SMMs, a larger spin system, and introduce intrinsic anisotropy within a molecular nanomagnet.

1.2 Single Molecule Magnets

Portions of this section have been written using references [52,59-61].

SMMs are magnetic particles which function as a single domain and can be thought of as a bottom-up approach to magnetic materials at the nanoscale. They consist of a magnetic core, typically rare-earth ions or transition metals, that is surrounded by non-magnetic ligands (molecules that bind to a central metal atom to form a coordination complex) which help minimize intermolecular interactions. In contrast to a free electron, they exhibit many spin eigenstates with a potential energy barrier separating opposite spin projections, marking them as a spin system that is significantly more interesting to study. Their net spin is typically many times that of an electron alone, and they are characterized by a strong intrinsic magneto-anisotropy due to the couplings within the molecule itself. This anisotropy manifests as the energy barrier to reversing the spin orientation (“up” to “down”). A hallmark of the SMM is the quantum tunneling of the magnetization (QTM) [6], a way of allowing classically forbidden transitions to occur through this barrier, which will be discussed in more detail in section 1.2.3. They are of particular interest in the fields of spintronics and quantum information science, as they are definitively quantum objects with the capability of their spin to be used as a quantum bit, and their long magnetic relaxation times particularly at low temperatures [13,62-64] provide excellent candidates for improving magnetic storage techniques. Although there has been a wealth of concentrated study performed on such

molecular nanomagnets, they are still far not completely understood. The scientific community has only recently begun to increase our understanding of the effects of the light-matter interaction on SMMs and the intrinsic sources of decoherence in their solid-state form, limited primarily by dephasing due to dipolar fluctuations [29,63,65]. Major efforts have thus been aimed towards the investigation of the quantum dynamics of molecular magnets as it pertains to their potential use in quantum information technologies [17,26,31,32,66-70] as well as a way to expand our knowledge of decoherence at the nanoscale [28,62,63,71,72].

As an example, in recent years solid evidence has been obtained regarding the importance of internal molecular degrees of freedom to the behavior of basic QTM properties. In particular, molecular site symmetry is a central factor in the quantum Berry-phase interference (BPI) patterns observed in SMMs [73], and the relative orientations of the single-ion anisotropy tensors have a significant effect on the QTM spin selection rules [74]. BPI patterns are essentially oscillations in the spin tunneling probability as a function of the applied magnetic field (perpendicular to the easy axis/along the hard axis of anisotropy) which are due to quantum phase interference of different tunneling paths along the topological anisotropy energy landscape of the molecule [75]. The spin selection rules for QTM will be discussed further in section 1.2.3; they are what govern which forbidden transitions are permitted to occur. From a purely physical perspective, SMMs offer an intriguing playground in which to observe quantum behaviors in a relatively well-defined system.

1.2.1 Types of SMMs

In large part due to the recent increase in understanding of the intrinsic properties of molecular nanomagnets, the SMM community has shifted interest towards lanthanide-based mononuclear systems, where the magnetism arises from a single magnetic ion. The discovery that inorganic mononuclear

lanthanide polyoxometalates (POMs; a polyatomic ion consisting of at least three transition metal oxyanions, which are negatively charged molecules containing at least one oxygen atom, linked by shared oxygen atoms) also show quantum tunneling effects and can behave as SMMs [76-78] uncovered a new paradigm in molecular magnetism. The versatility and structural potential of this new class of purely inorganic SMMs has allowed for unprecedented control over key parameters such as the net spin, local symmetry, and hyperfine and dipolar interactions. As an interesting note, the SMM-like behavior in these compounds results from a significant orbital contribution to the ground state angular momentum J and the resultant anisotropy imposed by the surrounding ligands. These types of lanthanide-based nanomagnets present new possibilities to explore; several have recently been found to exhibit magnetic hysteresis at 60 K [79,80], and just this past fall a dysprosium-based SMM showed hysteresis even above liquid nitrogen temperature [81]. The family of mononuclear SMMs has also been recently expanded to include single-ion magnets (SIMs), where a solid-state lattice has embedded within it a single magnetic ion which supplied all the magnetic properties of the system.

In contrast, polynuclear SMMs, which may contain multiple magnetic constituents per molecule, are molecules made up of multiple transition metal or lanthanide ions which are bridged by organic ligands. The central magnetic ions are strongly coupled to each other by the exchange interaction (which determines the magnetic ordering of the spins, i.e. ferromagnetic or antiferromagnetic) [82], yielding large magnetic moments per molecule. This allows for a large spin, \vec{S} , which when combined with a splitting of spin degeneracies even at zero applied magnetic field (this is the so-called zero-field splitting, or ZFS) provides an anisotropy barrier to magnetization reversal and separates spin projections, S_z , with opposite sign by some nonzero energy barrier. These properties make the systems even more attractive

as a form of memory storage; the high temperature and low-field requirements lower costs and allow for simpler engineering.

In general, solid crystals of SMMs have several advantages over other magnetic structures. Chiefly, all molecules in a single crystal have identical spin amplitude and orientation, magnetic anisotropy, and atomic constituents, and are weakly interacting with respect to each other – that is to say, the molecular nanomagnet crystals are *monodisperse*. This facilitates the study of behavior intrinsic to the magnetic nanostructure but experimentally inaccessible in other classes of magnetic materials due to a lack of summation of individual spin responses. In point of fact, hundreds of different SMMs have been synthesized to date. Recent discoveries place SMMs as an already viable quantum magnetic system for technological applications and point to a trend that leads to magnetic hysteresis of a single-molecule at even higher temperatures.

1.2.2 The Spin Hamiltonian: A Double-Well Potential

The spin Hamiltonian for a SMM in general consists of two main parts: the Zeeman term (discussed in section 1.1) and the so-called *Zero-Field Splitting (ZFS)* terms, which describe the internal magnetic behavior of the system in the absence of an applied magnetic field. At low temperatures the SMM may be modeled as an isolated ground state with a well-defined spin value \vec{S} ; this is due to the fact that particularly with a large exchange coupling within the magnetic core of the molecule, excited spin multiplets are unpopulated. For example, Ni_4 may be assumed to be a “pure” spin 4 system at low temperatures; this is known as the Giant Spin Approximation (GSA). While the Zeeman term should be familiar to any senior physics student,

$$H_{\text{Zeeman}} = -g\mu_B \vec{S} \cdot \vec{B} \quad (1.10)$$

the zero-field splitting terms can be generally described, in the GSA, by the Stevens operators [83] as

$$H_{ZFS} = \sum_{k=2,4,6..} \sum_{q=-k}^k B_k^q O_k^q \quad (1.11)$$

where the coefficients B_k^q are real and the operators O_k^q are Hermitian. In systems with total spin ≤ 2 , terms up to second order are usually sufficient to describe the system; namely, the uniaxial anisotropy term DS_Z^2 and the transverse anisotropy term $E(S_X^2 - S_Y^2)$. The full spin Hamiltonian can thus be written as

$$H = H_{Zeeman} + H_{zfs} = -g\mu_B \vec{S} \cdot \vec{B} + DS_Z^2 + E(S_X^2 - S_Y^2) + \text{higher order anisotropy terms} \quad (1.12)$$

The first term on the right-hand side of (1.12) represents the Zeeman energy contribution from the interaction of the spin of the molecule with an externally applied magnetic field. The second term represents the uniaxial anisotropy resulting from the spin-orbit interaction, defines an “easy axis” for the magnetic moment of the molecule, and establishes an energy barrier DS_Z^2 separating opposite spin projections. The remaining terms correspond to transverse anisotropies (S_X^2, S_Y^2) and inter- or intra-molecular interactions such as dipolar, exchange, or hyperfine interactions.

To illustrate what this means for the molecule’s energy landscape, let us examine a molecule with only a uniaxial anisotropy term (DS_Z^2) and no external magnetic field. One can plot the shape of these energies as a function of the projection angle θ of the spin by using the classical approximation $S_Z = \cos(\theta)$, giving rise to the so-called double-well potential. A magnetic field applied along the easy axis of the molecule will tilt the potential energy wells, energetically favoring the spin projections along the direction of the applied field. Figure 1.3 shows a plot of this potential, along with the energy levels of the various spin alignments, for an $S=10$ system. Because SMMs have such a strong uniaxial anisotropy, even

in the presence of a moderate external magnetic field the shape of the potential remains. There are certain values of the applied field, referred to as “QTM resonances” where

$$H_k \approx \frac{kD}{g\mu_B}, k = 0, 1, 2 \dots \quad (1.13)$$

for which a pair of energy levels across the anisotropy barrier coincide in energy. The right side of Figure 1.3 shows the effect a magnetic field would have on the energy levels, shifting and equalizing different pairs of levels and allowing for various resonances to occur (denoted by the black horizontal arrows in the figure).

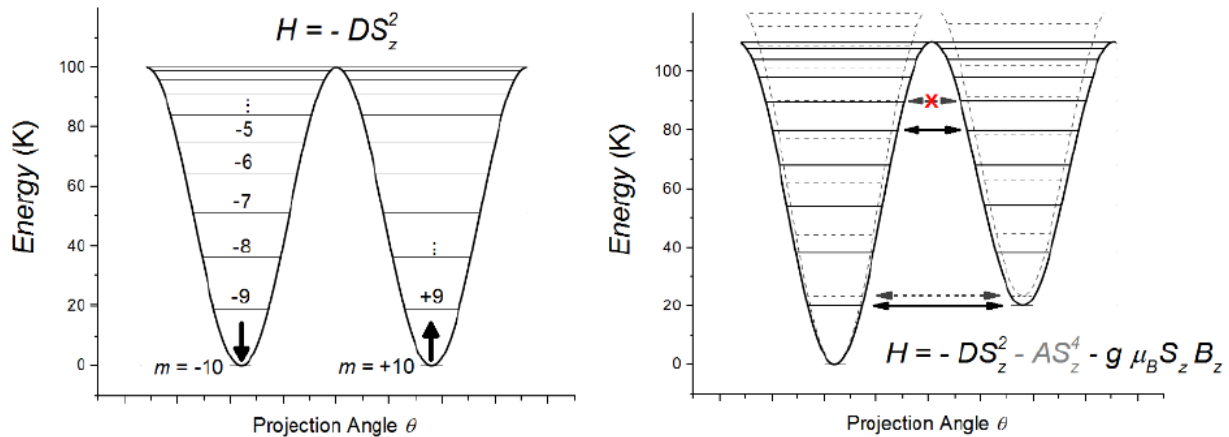


Figure 1.3: The Double-Well Potential

Left: Potential in the absence of an external magnetic field, with energy levels on resonance. Right: Potential in the presence of a longitudinal (applied along the easy axis) magnetic field. The energy levels have been shifted vertically, and the shape of the potential well has been altered to give preference to those states aligned with the field. The dashed line denotes the effect of higher order anisotropy terms in the Hamiltonian; in this case, a 4th order axial term [52].

Now, if we were to look at this in three dimensions we might observe something similar to what is shown in Figure 1.4. For a solely 2nd order uniaxially anisotropic system, a “hard plane” is formed as an energy barrier between opposite spin orientations that is isotropic in the transverse plane. If the system

were to exhibit 2nd order *transverse* anisotropy, we now see the development of both a “medium” and “hard” axis within the transverse plane. The anisotropy specific to each system determines what the energy landscape looks like, and what symmetries are observed; however, in each case the SMM will have some “easy” axis along which the spin will tend to align easily either parallel or antiparallel. The anisotropy barriers act to prevent transitions between spins with opposite orientations along this axis.

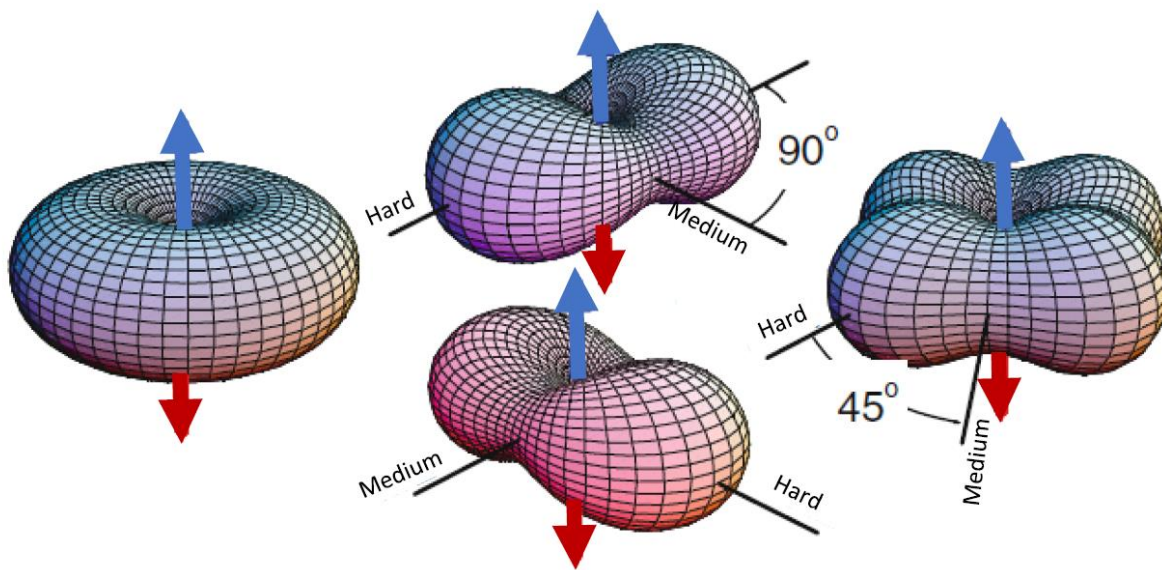


Figure 1.4: “Easy,” “Medium,” and “Hard” Axes

3D anisotropy barriers shown for a uniaxially anisotropic system (left) and a system with 2nd order transverse anisotropy (center two), and one with 4th order anisotropy (right). The spin tends to preferentially align along the easy-axis depicted as the red and blue arrows, with the hard axis representing the most difficult direction for the spin to travel. The shape of the energy landscape is determined by the symmetry of the system, i.e. two-fold, four-fold, etc. [84].

1.2.3 QTM: Quantum Tunneling of the Magnetization

Magnetic hysteresis is a consequence of the strong magnetism in some systems wherein application of a magnetic field along a certain direction will preferentially magnetize the system, so that subsequent observations will show a different behavior. At low temperatures, the magnetization hysteresis curves of SMMs will show discrete steps, signifying a dramatic acceleration of the magnetic

relaxation at the resonant fields H_k discussed in the previous section. These steps are a direct consequence of the appearance of quantum tunneling between opposite projections of the molecular spin, known as the quantum tunneling of the magnetization (QTM). This phenomenon was first observed in 1996 by Friedman et al [4] in a Mn_{12} -acetate SMM; an example is shown in Figure 1.5, right. In short, the ability of SMMs to exhibit QTM results from their significant intrinsic, *transverse*, anisotropy.

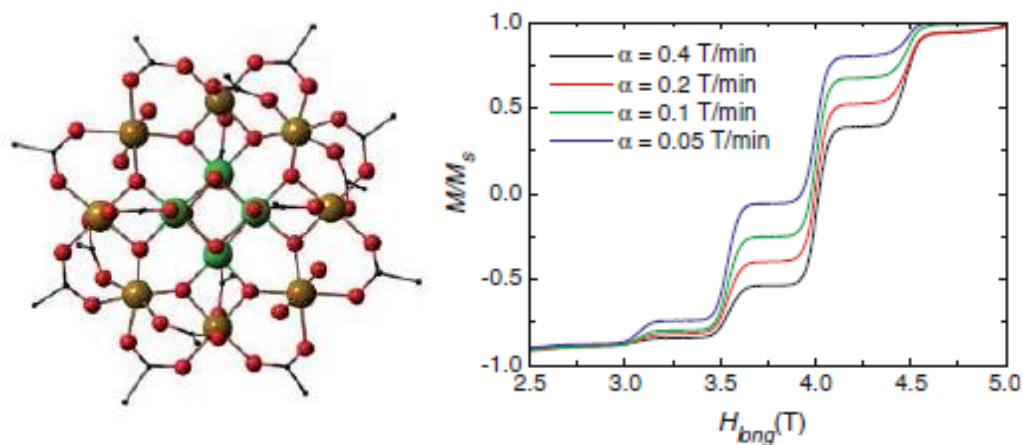


Figure 1.5: Mn_{12} and the Quantum Tunneling of the Magnetization

Left: A drawing of the Mn_{12} molecule. Right: Magnetization curve of Mn_{12} at $T = 0.6$ K. The jumps are due to quantum tunneling at the resonance fields. The different colors represent different sweep rates of the longitudinal applied magnetic field [84,85].

Apart from creating an interesting graphical energy landscape, having a significant transverse anisotropy plays a crucial role in one of the hallmark behaviors of SMMs – it links different eigenstates to allow transitions between spin up and spin down states. Transverse anisotropy terms do so by allowing off-diagonal terms in the spin Hamiltonian to be nonzero; graphically, they break the isotropic symmetry in the transverse plane (as in Figure 1.4). It is important to note that this can be accomplished in many different ways, including through molecular design (a transverse anisotropy intrinsic to the molecule) or most straightforwardly by applying a transverse magnetic field B_{XY} .

Let us revisit our treatment of the spin $\frac{1}{2}$ system and extend it to a SMM. We will write our spin Hamiltonian as

$$H = -g\mu_B \vec{S} \cdot \vec{B} + DS_Z^2 + E(S_X^2 - S_Y^2). \quad (1.14)$$

We may instead rewrite S_X and S_Y in terms of the spin raising and lowering operators, S_+ and S_- respectively, to put them in the S_Z basis, as such:

$$S_X = (S_+ + S_-)/2, S_Y = (S_+ - S_-)/2i. \quad (1.15)$$

The full Hamiltonian will then include terms which include multiple operations of the spin raising and lowering operators, including the rhombic term $E(S_+^2 + S_-^2)$. These sorts of operations will induce a transition in a similar manner to a photon-induced transition for a simple 2-level atom, but a different constraint on the total change in spin; for instance, this rhombic term will mix only levels with a total spin change of $\pm 2n$ (where n is an integer). This difference in spin constraints leads to the *spin selection rules* for SMM tunneling transitions, which states that the allowed transitions due to anisotropic mixing of eigenstates *must* have a spin difference equal to an integer multiple of the transverse symmetry of the system. That is, for a system with a rhombic anisotropy $E(S_+^2 + S_-^2)$ the allowed transitions will be for multiples of $\Delta S = \pm 2$; for a system with tetragonal anisotropy $C(S_+^4 + S_-^4)$ the allowed transition will be for multiples of $\Delta S = \pm 4$; and so on.

Now what happens in an external longitudinal (along the easy axis) magnetic field? We have already established that as the external field is swept, the energy levels of the spin states on opposite sides of the double-well potential will shift and occasionally become resonant with each other. When two levels whose difference in spin matches that allowed by the spin selection rules are perfectly on resonance, rather than the two states becoming degenerate the mixing between them will hybridize the

states into symmetric and antisymmetric superpositions. These hybridized levels differ by an energy equal to the tunnel splitting Δ_k , where k denotes the resonance (for example with 2nd order anisotropy terms, $k=2n$). The locations of these resonances are given in (1.13) by H_k . This manifests on an energy level diagram as the energy difference between two states in an anticrossing: where rather than continuing along its energy path, the spin as it passes through the resonance will suddenly flip and follow its counterpart's energy path instead. A comparison between resonance with and without transverse anisotropy playing a role is illustrated in Figure 1.6, which shows a resonance between the $S = \pm 10$ states (normal crossing) and a resonance between the $S = \pm 4$ states (anticrossing) for a system with tetragonal symmetry. The probability of a spin completing such a tunneling transition can be found from the Landau-Zener formula

$$P_k = 1 - \exp \left[- \frac{\pi \Delta_k^2}{2g\mu_B(m - m')\alpha} \right] \quad (1.16)$$

where α is the rate at which the external magnetic field is swept, m and m' denote the two levels involved in the transition, and g is the gyromagnetic ratio. These transitions are part of what traditional EPR aims to study in molecular nanomagnetism.

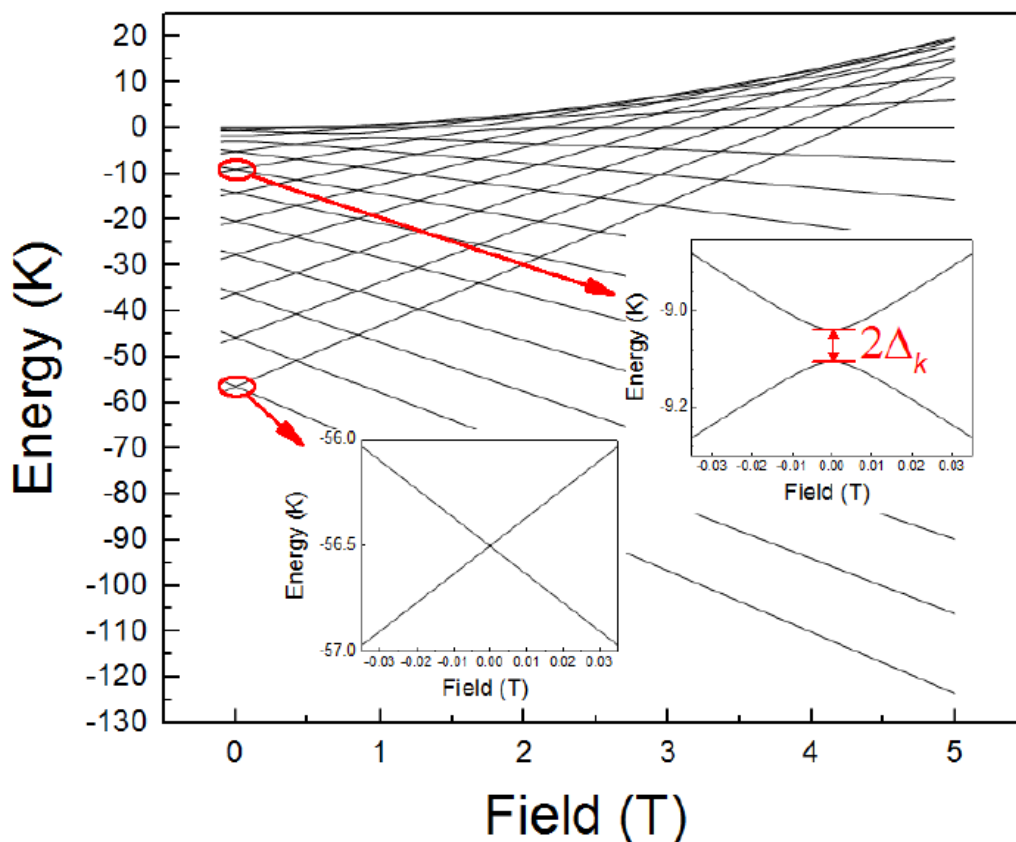


Figure 1.6: Energy Level Diagram for $S=10$ System

Energy level diagram for the energy levels of an $S=10$ system with a significant transverse anisotropy. This system has a tetragonal symmetry. The first inset shows a normal crossing ($S = \pm 10$), while the second shows an anticrossing due to level-mixing of states separated by the transverse symmetry of the system ($S = \pm 4$). The fourfold symmetry allows otherwise forbidden transitions where $\Delta m = \pm 4$. [52]

1.3 EPR: Electron Paramagnetic Resonance

Electron paramagnetic resonance (EPR) is similar in principle to the arguably more widely known nuclear magnetic resonance (NMR), the main difference being (as the name suggests) EPR's use of the electronic spin rather than the nuclear spin. EPR is a technique based on the *resonant* absorption of electromagnetic radiation, typically microwaves, to facilitate transitions between energy levels of the electron(s) spin. It has applications ranging from understanding the fundamentals of physics, to characterizing and designing new compounds in material and earth sciences, to uses in biology and

medicine, and can be performed on a host of samples including crystalline solids and liquid solutions [86]. There are two main classifications of EPR spectroscopy: continuous wave (CW) EPR and pulsed EPR, both of which will be discussed in this section.

1.3.1 The Basic Physics

A traditional EPR spectrum consists of the first derivative of microwave radiation absorption plotted as a function of the magnetic field intensity. This is achieved by sweeping the magnetic field around a resonance location B_0 , corresponding to the fixed microwave frequency that is irradiating the sample. The fundamental equation of EPR highlights the relation between this field and frequency: $h\nu = g\mu_B B_0$, where h is Planck's constant and ν is the photon frequency. This relation is simply due to energy conservation, as the energy of the absorbed photon must be equal to the energy difference of the two spin states. The electron spin is the quantity of interest and supplies all of the interesting physics here; as such, a good EPR sample must have at least one unpaired electron. In particular, the driving mechanism behind EPR is the behavior of an unpaired electron spin when placed in a magnetic field – the Zeeman effect [87]. We discussed the mathematical impact this has on the spin Hamiltonian in section 1, but we follow a more intuitive approach here to illustrate the underlying physics of EPR.

The electron is a spin $\frac{1}{2}$ particle; therefore, the only states it can exist in are spin up ($S_z = +\frac{1}{2}$) or spin down ($S_z = -\frac{1}{2}$). The energies of these two states are the same and the two states are degenerate for a free, single unpaired electron. However, in the presence of an external magnetic field with intensity B_0 the two energies split into

$$E_{\pm} = \pm\left(\frac{1}{2}\right)g\mu_B B_0 . \quad (1.17)$$

This splitting is what's known as the Zeeman effect, and is illustrated in Figure 1.7. There must be a difference in energies between the two states if they are no longer degenerate, and it can be clearly seen from (1.17) to be $\Delta E = g\mu_B B_o$. If we now irradiate the electron with a photon, then provided the photon's energy matches that of the energy gap between the states, the electron may absorb the photon energy to flip from the lower energy state to the higher energy state. This is nothing more than a straightforward derivation of the previously mentioned fundamental EPR equation:

$$h\nu = E_+ - E_- = g\mu_B B_o . \quad (1.18)$$

It is important to note that in order for the radiation to be absorbed it should be polarized perpendicular to the applied field, with the oscillating magnetic field perpendicular to \vec{B}_o .

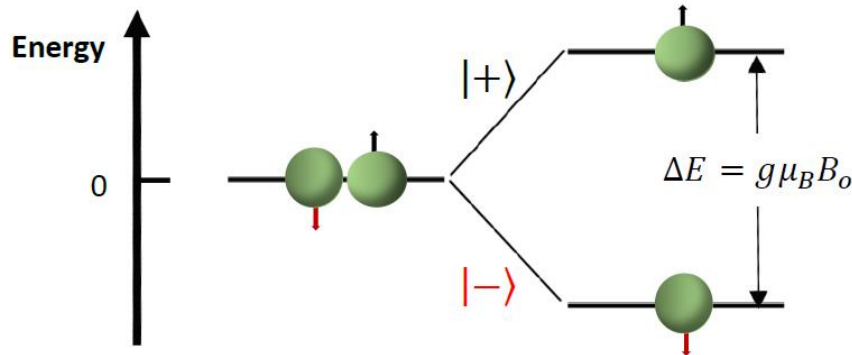


Figure 1.7: The Zeeman Effect

Splitting of the spin-up and spin-down states due to an external applied magnetic field. The two states are degenerate in the absence of the field but split by an energy difference ΔE which is proportional to the magnetic field strength.

This works well for an electron in the spin down state, as it has a lower energy and can absorb the photon energy to reach the spin up state. But what about an electron already in the spin up state? It's not possible for it to absorb an additional photon. Instead it may undergo the process of stimulated emission, wherein an oscillating magnetic field with frequency corresponding to that of (1.18) is present and allows the transition from spin up to spin down by emission of a photon with energy $h\nu$. Thus, an

isolated electron may undergo transitions between the two states provided there is an external magnetic field \vec{B}_0 and the radiation applied has both the frequency specified in (1.18) and is polarized perpendicular to \vec{B}_0 . In point of fact, you will never perform EPR on an isolated, free unpaired electron; at minimum, you will have interactions with both the nucleus and the neighboring molecules. Likely, you will have dipolar interactions with neighboring unpaired electrons.

1.3.2 Continuous Wave EPR

In CW EPR, either the irradiating frequency is held constant while the magnetic field is swept around a resonance point, or the reverse (the frequency is swept at a constant field). It is typically easier experimentally to hold the frequency constant and scan through magnetic fields, so that is generally what is done. The magnetic field is swept until the resonance condition (1.18) is met, and the photon absorption is observed as a change in microwave signal through the sample [88]. This is the most basic form of EPR and is usually performed before any other related experiments to identify the resonant conditions. Information about the splitting between energy levels may be gleaned from the CW EPR spectrum of a sample, but it is difficult to extract information that directly pertains to the spin dynamics of the system. Indeed, although a CW EPR spectrum can contain a huge amount of information about a spin system (including g factor, spin relaxation times, hyperfine interactions with nearby nuclei, dipolar interactions with nearby electron spins) the sheer number of contributing parameters makes it difficult to accurately isolate any single one of them. This leads us to the following subsection on pulsed EPR, which is particularly good for controlling the generation of signal that contain only desired information by using various pulse sequences.

1.3.3 Pulsed EPR

An important modern technique within the EPR framework is pulsed EPR. Pulsed EPR is performed after the resonant conditions have been found, usually by CW EPR. The electronic spins are excited by a series of high-power microwave pulses and the resulting signal is observed in the absence of any radiation, in contrast to CW where there is a constant low power microwave background. Pulsed EPR allows the direct measurement of signals emitted by the spins after the radiation is turned off, and as such allows a direct link to the spin dynamics of the system [89]. There are many different pulse sequences which can be used, each designed to measure a specific type of signal, and many have already been identified and well-documented. This is one of the factors that makes pulsed EPR such a useful modern experimental tool.

In both pulsed and CW EPR, what we are observing is an ensemble of spins rather than a single, isolated unpaired electron. Luckily, we can approximate an ensemble of a large number of noninteracting, identical spins by a sum over all of them, commonly referred to as the magnetization, which behaves more or less as a vector in classical mechanics and makes life much easier as a consequence. In general, even for systems with a larger spin than $S = 1/2$, pulsed EPR can be described in this way so long as the transitions under study involve only two energy levels. Thus, we can look at a “spin packet” of identical spins and its net magnetization as what is being affected by each pulse [90].

The magnetization can be described as a vector \vec{M} , with components along x , y , and z like any other vector. Without the application of any external radiation, the behavior of this magnetization vector is simple: M_z will relax towards its thermal equilibrium value according to the spin lattice relaxation time constant T_1 , while M_x and M_y will decay towards zero according to the spin-spin relaxation time constant T_2 . T_1 characterizes a transfer of energy between the spin system and the lattice, while T_2 characterizes

energy exchanges within the spin system itself which have nothing to do with the lattice. M_z is directly proportional to the energy level population difference, and M_x and M_y precess around the applied magnetic field B_0 at the Larmour frequency, $\omega = -\gamma B_0 = \frac{eg}{2m} B_0$. This precession of the magnetization is a result of the torque exerted by the applied magnetic field on the electrons' magnetic moments. A pulse of resonant microwaves can be used to effectively convert M_z into M_x and M_y (and vice versa) by controlling the rotation of the magnetization vector around the applied magnetic field B_0 .

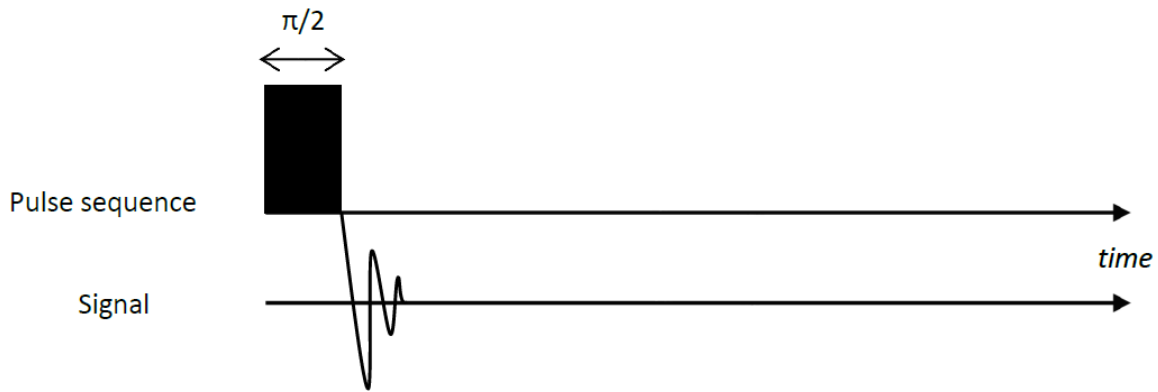


Figure 1.8: Free Induction Decay

An FID pulse sequence. A single pulse timed to rotate the spins by $\pi/2$ is applied, with the free induction decay signal immediately following the cessation of the pulse. It can be used to measure the spin-spin relaxation time T_2 as well as the resonant frequency.

The simplest possible pulse sequence is a single pulse as in Figure 1.8, which produces what is known as the free induction decay (FID) signal [91]. During the pulse, the magnetization is rotated towards the transverse plane. After the pulse, the magnetization of any spin packet with a resonant frequency matched by that of the applied microwaves will have been rotated to lie along the either the x or y-axis. The transverse components of \vec{M} will then precess about the z-axis while shrinking according to T_2 . FID is thus a reliable way to measure both the frequency and T_2 of a spin packet; however, it follows immediately after the pulse and can thus be extremely difficult to detect in some experimental setups due to the time required for the resonator and detector to recover from the intense pulse just applied.

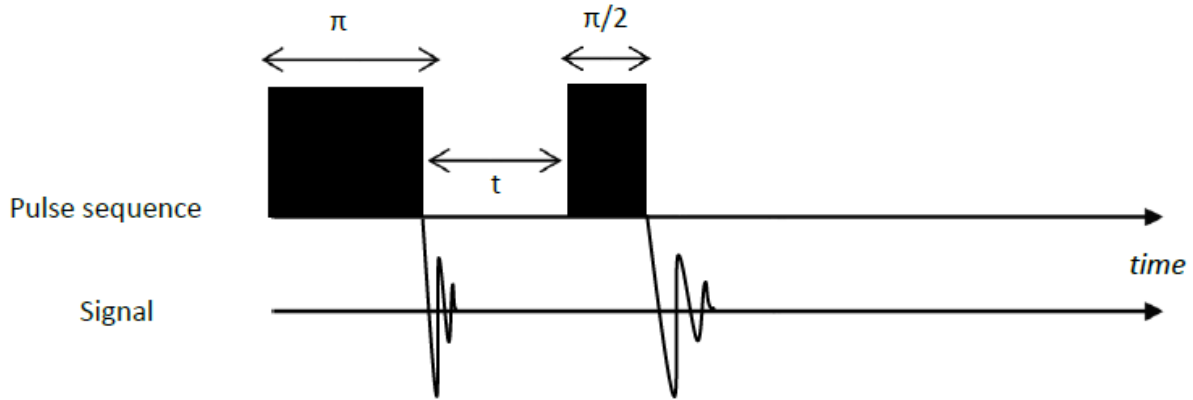


Figure 1.9: Inversion Recovery

An inversion recovery pulse sequence. A pulse timed to rotate the spins by π is applied, then after a delay time t a pulse timed to rotate the spins by an additional $\pi/2$ is applied. There will be FID signals following each pulse, and a small echo signal which should follow the second pulse by the same delay time t . Recording of the second FID signal as a function of delay time can be used to measure the spin-lattice relaxation time T_1 .

The next simplest would be a two-pulse sequence. These can be more or less divided into inversion recovery sequence and the spin echo sequence [91]. The inversion recovery sequence consists of a first pulse to rotate the magnetization, a delay time to allow M_z to relax according to T_1 , and a second pulse to measure the FID signal for the remaining part of M_z that has not yet decayed. If this FID amplitude is measured for a variety of delay times, it gives direct information about the T_1 relaxation time. The inversion recovery sequence is thus a reliable way of measuring T_1 . Typically, in this sequence the pulses are denoted as a π pulse followed by a $\pi/2$ pulse where the π (or 180°) rotates the magnetization from \vec{M} to $-\vec{M}$ and the $\pi/2$ (or 90°) rotates the remainder into the transverse plane. Figure 1.9 shows an example of an inversion recovery sequence.

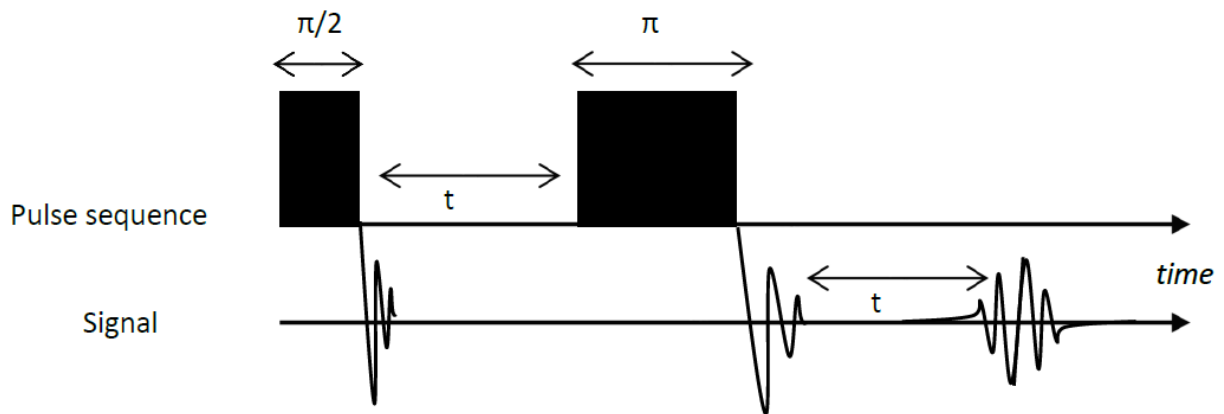


Figure 1.10: Spin Echo

A spin echo pulse sequence. A pulse timed to rotate the spins by $\pi/2$ is applied, then after a delay time t a pulse timed to rotate the spins by an additional π is applied. The transverse components of the spins then recombine a time t after the second pulse, resulting in a spin echo signal. This gives direct information about the spin-spin relaxation time T_2 .

The spin echo sequence consists of a first pulse to rotate the magnetization into the transverse plane (a $\pi/2$ pulse), a delay time where the transverse magnetization precesses around the z-axis while decaying according to T_2 , and a second pulse to rotate the transverse magnetization from M_x to $-M_x$ and M_y to $-M_y$ (a π pulse). There will still be an FID signal which may be able to be observed, but what is most striking is what occurs if there is a relatively wide distribution of resonant frequencies/fields among the spin packets. The sum of the FIDs after the first pulse from each spin packet will go to zero faster than it would according solely to T_2 relaxation, due to interference between the spin packets. But the magnetization reversal of the second pulse will reverse this destructive interference, so that at a time equal to the delay between pulses the spin packets will add their magnetizations to produce a spin echo signal (as in Figure 1.10). At this time, the magnetization should be equal to that after the first pulse aside from T_2 decay. In fact, the spin echo amplitude should decay as a function of the delay time between pulses according to the time constant T_2 ! Spin echo is therefore an excellent method to extract the spin-spin relaxation time.

1.4 The Spin-Photon Interaction

The spin-photon interaction is of particular interest to fields such as quantum computation. The photon is an ideal mobile qubit, to be used as a “messenger” in quantum circuits, and spin qubits in a solid may provide an optimal method of long-term quantum memory storage. Single crystal SMMs provide an excellent framework for the spin part of the equation, with their strong intrinsic anisotropy and comparatively isolated spin sites in a rigid lattice. However, there exist issues with their viability for use as magnetic storage bits, most obviously the intrinsic sources of decoherence [92,93]. Thus, there exist two primary regimes of spin-photon interactions: strong coupling, wherein the coupling between the spin and the photon is much larger than the decoherence rates of the system; and weak coupling, in which the photon lifetimes and spin decoherence dominate. In this section we will discuss decoherence as relevant to SMMs, as well as a model which can be used to describe the interaction of a spin and a photon.

1.4.1 Decoherence in SMMs

Overcoming decoherence in SMMs is crucial to many of their potential uses. The time needed to accomplish any measurement must be less than the time it takes for external systems to significantly affect your system; imagine trying to read out something from computer memory, only to find it disappeared before you could access it. Luckily, the main sources of decoherence in SMMs have already been identified to include hyperfine fluctuation (coupling to nearby nuclei), phonons (coupling to lattice vibrations), and magnons (coupling to locally oscillating magnetic fields; dipolar fluctuations) [92]. When photons are introduced, however, you must also ensure that the interacting cavity or resonator can ensure a high enough quality factor to support excitation lifetimes of a photon long enough to perform a measurement. These factors translate directly into experimental setups – your equipment *must* be

capable of overcoming the limitations of photon/spin state lifetimes, or you will be unable to observe anything at all.

There are ways to mitigate decoherence, however. Magnon and phonon coupling both tend to decrease significantly as temperature is lowered, with the bonus that at lower temperatures the spin bath may be polarized with respect to lower energy separations between transition states. Hyperfine interactions will also decrease, but at a smaller rate (\approx that of the fine structure constant, $1/137$); temperatures needed to see an appreciable decrease in decoherence will be much lower than for phonon or dipolar coupling. As an example, for an energy splitting of 250 GHz between the ground state and first excited state (which would require a magnetic field of approximately 9 T to observe the transition using EPR according to (1.18)) the spin bath may be nearly completely polarized at 2 K; for an energy splitting of 15-20 GHz (with a required field of <1 T) near-unitary polarization may be achieved below 100 mK. This decrease in energy required to observe the transitions not only makes the researcher's life easier, it also has the benefit of decreasing the phonon effect on decoherence rates.

A plot of various decoherence rates and their dependence on field, temperature, and splitting energy is shown in Figure 1.11. In addition to what is shown in there, magnetic dilution within a solid crystalline lattice is a promising technique to reduce the dipolar decoherence. This method replaces some magnetic ions in a crystal lattice with chemically similar, but non-magnetic, counterparts, maintaining the crystalline structure but reducing the impact of dipolar fluctuations. There also exist so-called atomic clock transitions where the transition is somewhat insulated from nearby dipolar interactions, due to the first and second order derivatives of the states' energies being near zero with respect to the magnetic field. That is, a small fluctuation in the local magnetic field does not significantly affect the system. One key point, as it relates to SMMs, is that studies of decoherence done at higher magnetic fields do not

reflect the intrinsic properties of the molecules. Rather, they are performed in an energy range dominated by the Zeeman effect of the applied magnetic field. In order to study the intrinsic effects pertaining to decoherence in these molecules, lower temperatures (and thus lower fields) are required.

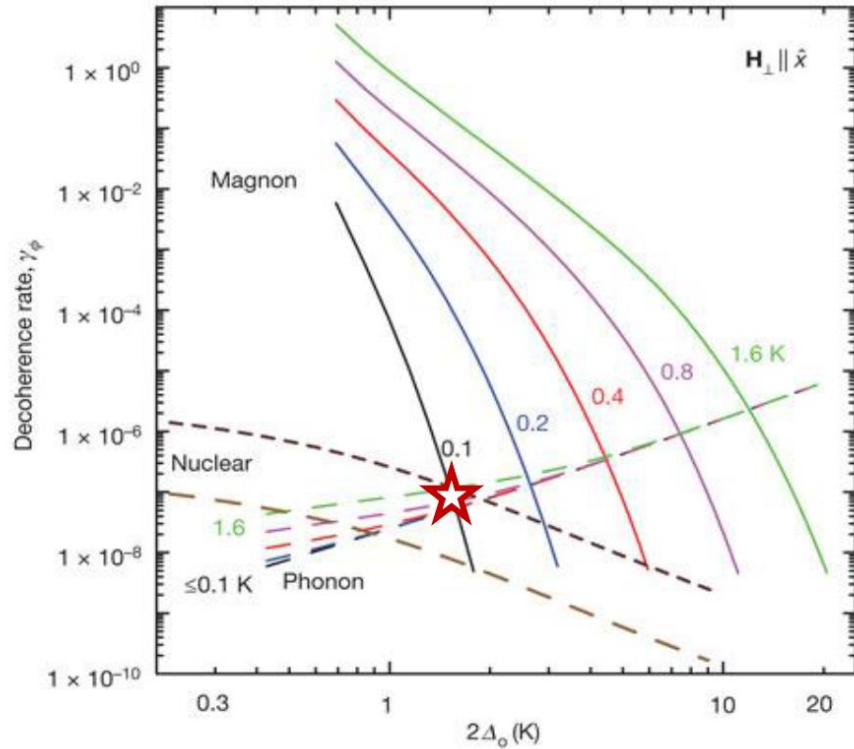


Figure 1.11: Decoherence Rates for Fe_8

Calculated contributions to decoherence in Fe_8 as a consequence of coupling between electron spins and nuclear spins, phonons, and magnons. Lower temperatures allow a smaller EPR frequency and field while maintaining spin polarization, and significantly decreases both magnon and phonon contributions. The ideal location on this graph is denoted by the star, where phonon and nuclear sources meet, and dipolar contributions may be ignored. [92]

1.4.2 Spins and Photons: the Jayne-Cummings Hamiltonian

To describe the interaction between a single spin and a single photon, at least three components are required: the spin energy, the photon energy, and the interaction energy. The Jaynes-Cummings model [94] illustrates this exceedingly well with its Hamiltonian:

$$H_{JC} = \frac{\hbar}{2} \omega_0 \sigma_z + \hbar \omega a^\dagger a + \hbar g (a^\dagger \sigma^- + a \sigma^+). \quad (1.19)$$

The first term describes the energy of the spin transitions $\hbar \omega_0$ and the spin orientation along the z-axis, the second term describes the energy of the field (having an individual photon energy of $\hbar \omega$) with the operator $a^\dagger a$ which counts the number of photon excitations, and the last term describes the spin photon interactions with the coupling parameter g as emission of a photon by the spin ($a^\dagger \sigma^-$) or absorption of the photon by the spin ($a \sigma^+$). Here, a^\dagger and a represent the photon creation and annihilation operators while σ^+ and σ^- represent the spin raising and lowering operators. The third term utilizes the rotating wave approximation (RWA), wherein terms that oscillate quickly in time have been neglected [95].

If we look at the Hamiltonian matrix for a single excitation between the spin and cavity, we can determine it to have the form

$$H = \hbar \begin{bmatrix} \omega & \gamma \\ \gamma & \omega_0 \end{bmatrix} \quad (1.20)$$

[96]. It is clear that in the absence of the coupling parameter γ , that is, for no off-diagonal mixing terms in the Hamiltonian, this gives the energies of two separate states. We can denote them as $|1, 0\rangle$, for a cavity excitation with energy $\hbar \omega$, and $|0, 1\rangle$, for a spin excitation with energy $\hbar \omega_0$. The eigenvalues can easily be solved to be

$$\frac{E_{1,2}}{\hbar} = \frac{\omega}{2} + \frac{\omega_0}{2} \pm \sqrt{\gamma^2 + \frac{1}{4}(\omega - \omega_0)^2}. \quad (1.21)$$

In a magnetic field, the energy of the spin transition is the same as the Zeeman splitting energy $g\mu_B B_0$. Thus, one can calculate the energy level diagram for a spin in a magnetic field interacting with a photon near resonance as shown in Figure 1.12. As the spin and photon energies approach resonance, they hybridize into symmetric and antisymmetric superpositions and form an anticrossing which allows them

to interact and “flip” between an excited spin state and an excited photon state. This is the basis for phenomena such as vacuum Rabi oscillations , where vacuum fluctuations drive oscillations between spin-photon emission and absorption [97].

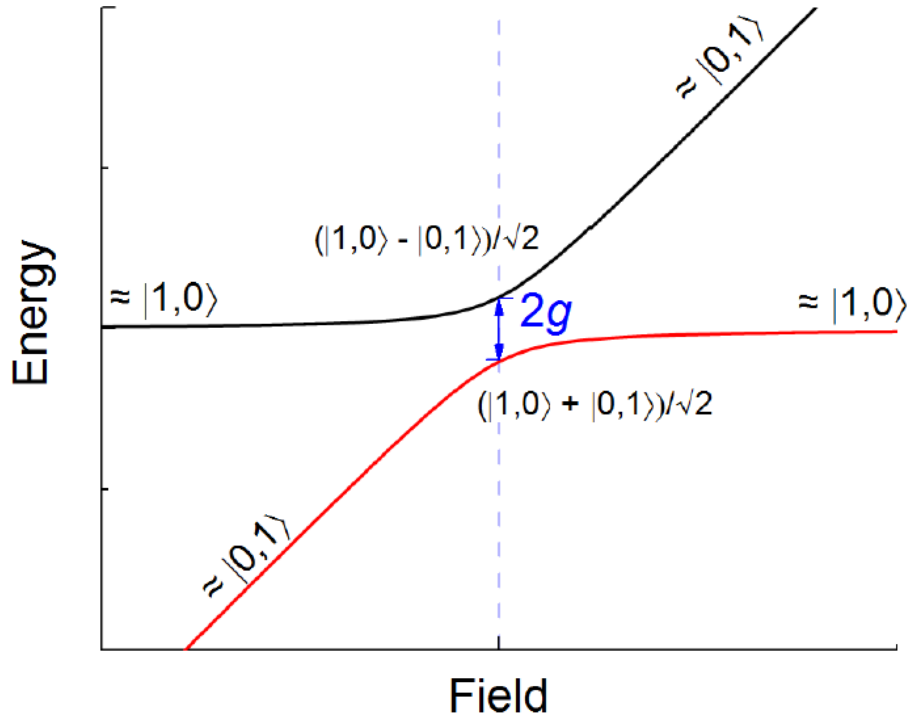


Figure 1.12: Coupled Spin-Photon Transition

An energy level diagram for a photon-spin interaction near resonance in the Jaynes’ Cummings model. An anticrossing is shown between the mixed spin and cavity eigenstates. The two branches are the symmetric (red) and antisymmetric (black) superpositions of the bare spin and photon states. [52]

1.4.3 Strong vs Weak: The Spin-Photon Coupling

Perhaps the final piece to the introductory chapter of this dissertation is the concept of the *strong* vs *weak* coupling regimes [94]. Section 1.4.1 discussed the behavior and most common sources of decoherence in spins, which strongly contribute to a system with weak coupling. The Jaynes-Cummings Hamiltonian from the previous section, along with observable vacuum Rabi oscillations, are hallmarks of strong coupling [98]. In point of fact, the only way to observe coherent vacuum Rabi oscillations is to have

a strong enough coupling between the spin and photon that many interactions can occur before the lifetime of either decays. To put this in a more mathematical sense, the coupling parameter γ between the photon and spin excitations must relate to the spin decay rate k_s and the photon decay rate k_p as such:

$$\frac{2\gamma}{k_s+k_p} \gg 1, \text{strong coupling}, \frac{2\gamma}{k_s+k_p} \ll 1, \text{weak coupling} . \quad (1.22)$$

Here, the spin decay rate comes from a combination of all significant sources of decoherence in the system, while the photon decay rate comes from the photon energy and the cavity quality factor Q as $k_p = \omega/Q$.

To illustrate the difference between these two regimes, Figure 1.13 shows the normal mode splitting of a coupled atom-cavity system as a function of coupling strength, while Figure 1.14 shows the oscillatory/exponential behavior of the excited state of an emitter (such as atomic spin) as a function of time for weak, strong, and nonexistent coupling. Both regimes are interesting to study – in the weak coupling regime, we may perform spin echo experiments at ultra-low temperatures in order to study the sources of decoherence inherent in a SMM. This is the subject of chapter 2, where we will attempt to coherently control the time evolution of the spin of SMMs upon application of fast pulsed microwave irradiation in the weak coupling regime at sub-Kelvin temperatures (> 50 mK), for which dipolar dephasing will be suppressed due to polarization of the spin bath without the need of large magnetic fields. This will open a window into the fundamental sources of decoherence in single crystals of SMMs in an energy range (frequencies < 10 GHz, and magnetic fields < 1 T) never before explored. Meanwhile, in the strong coupling regime, we may be able to couple very low numbers of photons to low numbers of spins, even potentially experimentally realizing the strong coupling regime for a single-spin (something not yet

achieved). This is the subject of chapter 3, where to investigate these interactions in the strong coupling regime between a vacuum photon mode and SMM spins (such as the vacuum Rabi splitting), we plan to utilize nano-constricted superconducting coplanar waveguide (CPW) resonators of extremely high quality factors, along with an experimental setup designed to allow measurements of the coherent collective coupling of a number of molecular spins and a low number of photons, including eventual single photon measurements. In the next chapter, I will discuss our work aimed towards the weak coupling regime; in the following chapter, I will do so for the strong coupling regime.

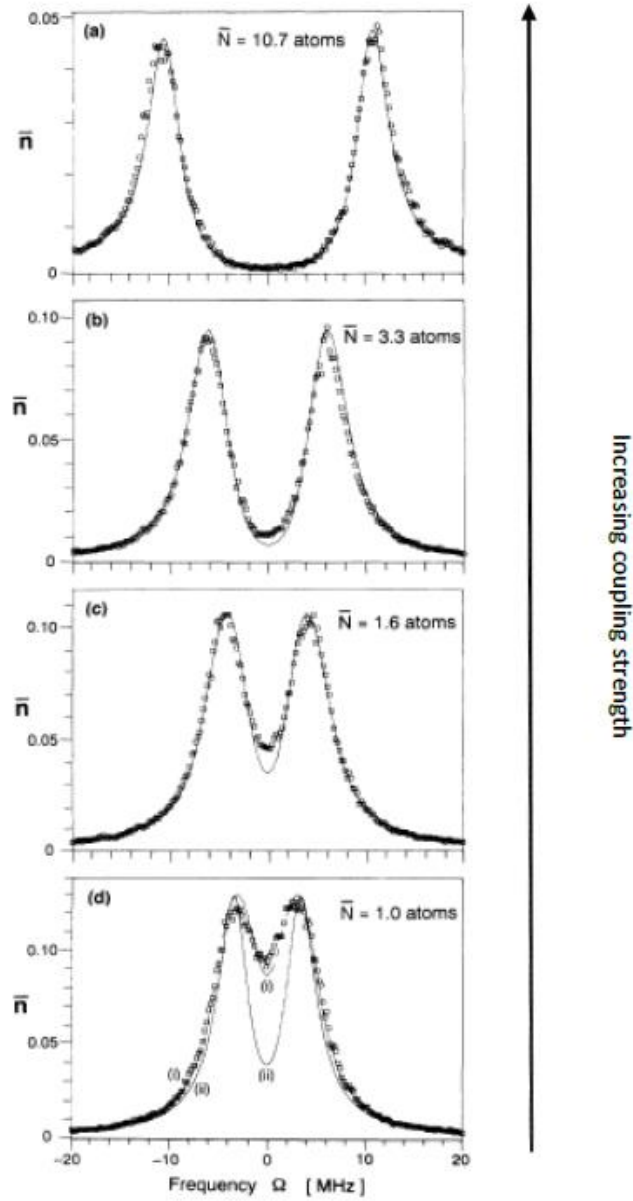


Figure 1.13: Normal Mode Splitting

Number of photons existing in the cavity as a function of frequency for various coupling strengths. Weak coupling shows a primarily single Lorentzian shape (bottom) while strong coupling exhibits two distinct peaks. This normal mode splitting is a hallmark of the strong coupling regime. [99]

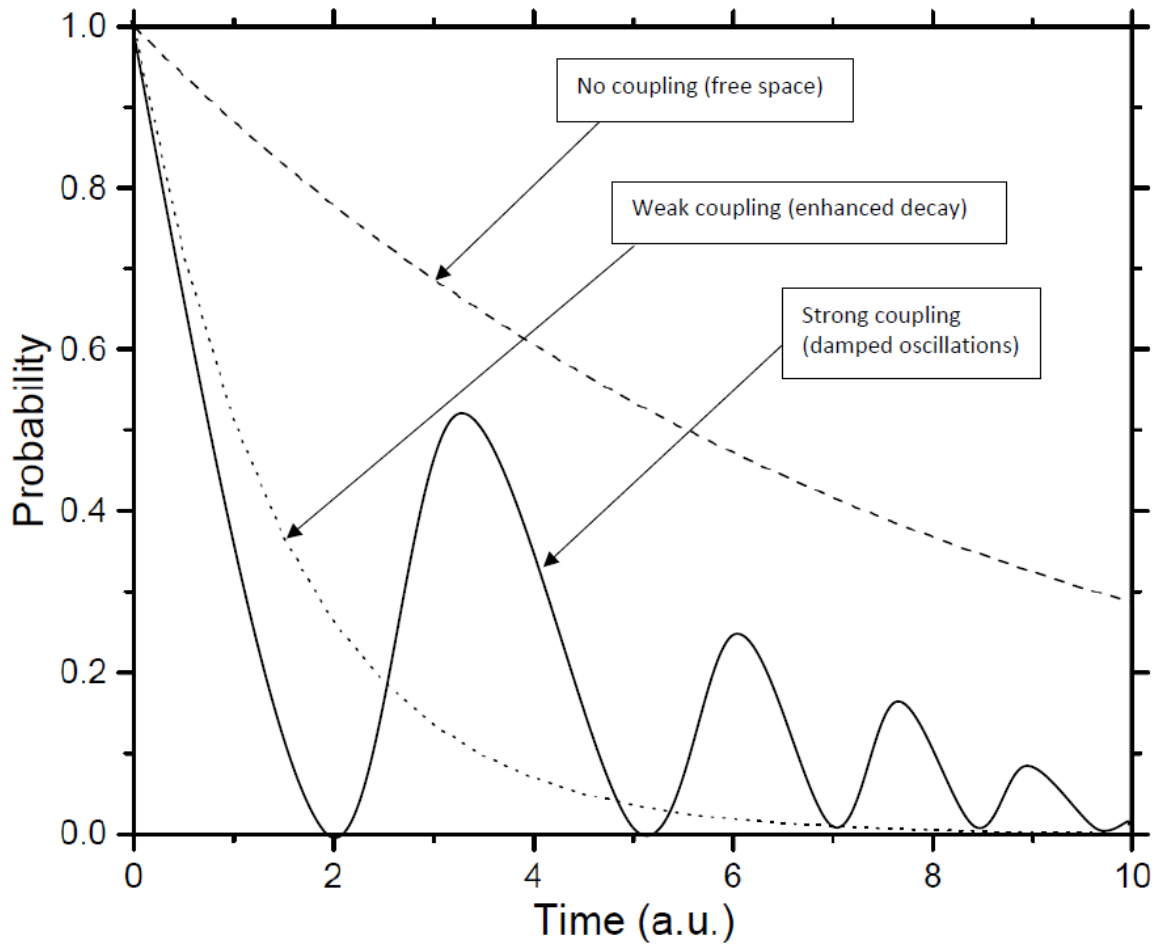


Figure 1.14: Weak vs Strong Coupling

Probability to find an emitter (electron spin) in its excited state as a function of time. The emitter begins in the excited state, with probability to reach the same excited state decaying rapidly in the weak coupling regime but oscillating somewhat coherently in the strong coupling regime.

References

- 1 Jackson, J. D. *Classical Electrodynamics: Third Edition*. John Wiley & Sons, Inc., (1999).
- 2 Landau, L. D. & Lifshitz, E. M. *Electrodynamics of Continuous Media (Second Edition)*. Pergamon, (1984).
- 3 Joshi, V. *Spintronics: A Contemporary Review of Emerging Electronics Devices*. Engineering Science and Technology, an International Journal **19**, 1503-1513, (2016).
- 4 Friedman, J. R., Sarachik, M. P., Tejada, J. & Ziolo, R. *Macroscopic Measurement of Resonant Magnetization Tunneling in High-Spin Molecules*. Physical Review Letters **76**, 3830-3833, (1996).
- 5 Hernández, J. M. *et al.* *Field Tuning of Thermally Activated Magnetic Quantum Tunnelling in Mn12–Ac Molecules*. Europhysics Letters (EPL) **35**, 301-306, (1996).
- 6 Thomas, L. *et al.* *Macroscopic Quantum Tunnelling of Magnetization in a Single Crystal of Nanomagnets*. Nature **383**, 145-147, (1996).
- 7 Ziemelis, K. *The Difficult Middle Ground*. Nature Physics, S19, (2008).
- 8 Caneschi, A. *et al.* *Alternating Current Susceptibility, High Field Magnetization, and Millimeter Band EPR Evidence for a Ground $S = 10$ State in $[\text{Mn}_{12}\text{O}_{12}(\text{CH}_3\text{COO})_{16}(\text{H}_2\text{O})_4] \cdot 2\text{CH}_3\text{COOH} \cdot 4\text{H}_2\text{O}$* . Journal of the American Chemical Society **113**, 5873-5874, (1991).
- 9 Hill, S. *et al.* *High-Sensitivity Electron Paramagnetic Resonance of Mn12-Acetate*. Physical Review Letters **80**, 2453-2456, (1998).
- 10 Caciuffo, R. *et al.* *Neutron Spectroscopy for the Magnetic Anisotropy of Molecular Clusters*. Physical Review Letters **81**, 4744-4747, (1998).
- 11 Fernández, J. F., Luis, F. & Bartolomé, J. *Time Dependent Specific Heat of a Magnetic Quantum Tunneling System*. Physical Review Letters **80**, 5659-5662, (1998).
- 12 del Barco, E. *et al.* *High-Frequency Resonant Experiments in Fe8 Molecular Clusters*. Physical Review B **62**, 3018-3021, (2000).
- 13 Prokof'ev, N. V. & Stamp, P. C. E. *Low-Temperature Quantum Relaxation in a System of Magnetic Nanomolecules*. Physical Review Letters **80**, 5794-5797, (1998).
- 14 Garg, A. *Lattice Distortion Mediated Paramagnetic Relaxation in High-Spin High-Symmetry Molecular Magnets*. Physical Review Letters **81**, 1513-1516, (1998).
- 15 Thomas, L., Caneschi, A. & Barbara, B. *Nonexponential Dynamic Scaling of the Magnetization Relaxation in Mn12 Acetate*. Physical Review Letters **83**, 2398-2401, (1999).

- 16 Saito, K., Miyashita, S. & De Raedt, H. *Effects of the Environment on Nonadiabatic Magnetization Process in Uniaxial Molecular Magnets at Very Low Temperatures*. Physical Review B **60**, 14553-14556, (1999).
- 17 Hill, S., Edwards, R. S., Aliaga-Alcalde, N. & Christou, G. *Quantum Coherence in an Exchange-Coupled Dimer of Single-Molecule Magnets*. Science **302**, 1015, (2003).
- 18 Evangelisti, M. *et al.* *Magnetic Long-Range Order Induced by Quantum Relaxation in Single-Molecule Magnets*. Physical Review Letters **93**, 117202, (2004).
- 19 Evangelisti, M., Luis, F., de Jongh, L. J. & Affronte, M. *Magnetothermal Properties of Molecule-Based Materials*. Journal of Materials Chemistry **16**, 2534-2549, (2006).
- 20 Luis, F., González, V., Millán, A. & García-Palacios, J. L. *Large Quantum Nonlinear Dynamic Susceptibility of Single-Molecule Magnets*. Physical Review Letters **92**, 107201, (2004).
- 21 Chudnovsky, E. M. & Garanin, D. A. *Superradiance from Crystals of Molecular Nanomagnets*. Physical Review Letters **89**, 157201, (2002).
- 22 Suzuki, Y. *et al.* *Propagation of Avalanches in Mn12-Acetate: Magnetic Deflagration*. Physical Review Letters **95**, 147201, (2005).
- 23 de Loubens, G., Garanin, D. A., Beedle, C. C., Hendrickson, D. N. & Kent, A. D. *Magnetization Relaxation in the Single-Molecule Magnet Ni4 Under Continuous Microwave Irradiation*. EPL (Europhysics Letters) **83**, 37006, (2008).
- 24 *Molecular Magnetism: From Molecular Assemblies to the Devices*. Vol. 321 Springer Netherlands, (1996).
- 25 Luis, F., L. Mettes, F., Tejada, J., Gatteschi, D. & Jongh, L. J. *Observation of Quantum Coherence in Mesoscopic Molecular Magnets*. Vol. 85, (2000).
- 26 Leuenberger, M. N. & Loss, D. *Quantum Computing in Molecular Magnets*. Nature **410**, 789, (2001).
- 27 Godfrin, C. *et al.* *Operating Quantum States in Single Magnetic Molecules: Implementation of Grover's Quantum Algorithm*. Physical Review Letters **119**, 187702, (2017).
- 28 Chudnovsky, E. M. *Universal Decoherence in Solids*. Physical Review Letters **92**, 120405, (2004).
- 29 Bertaina, S. *et al.* *Quantum Oscillations in a Molecular Magnet*. Nature **466**, 1006, (2010).
- 30 Stamp, P. C. E. & Gaita-Ariño, A. *Spin-based Quantum Computers Made by Chemistry: Hows and Whys*. Journal of Materials Chemistry **19**, 1718-1730, (2009).
- 31 Lehmann, J., Gaita-Ariño, A., Coronado, E. & Loss, D. *Quantum Computing with Molecular Spin Systems*. Journal of Materials Chemistry **19**, 1672-1677, (2009).

- 32 Tejada, J., Chudnovsky, E. M., Barco, E. del, Hernandez, J. M. & Spiller, T. P. *Magnetic Qubits as Hardware for Quantum Computers*. Nanotechnology **12**, 181-186, (2001).
- 33 Eddins, A. W., Beedle, C., Hendrickson, D. & Friedman, J. R. *Collective Coupling of a Macroscopic Number of Single-Molecule Magnets with a Microwave Cavity Mode*. **112**, 120501, (2014).
- 34 Park, K. & Pederson, M. R. *Effect of Extra Electrons on the Exchange and Magnetic Anisotropy in the Anionic Single-Molecule Magnet Mn₁₂*. Physical Review B **70**, 054414, (2004).
- 35 Romeike, C., Wegewijs, M. R., Hofstetter, W. & Schoeller, H. *Quantum-Tunneling-Induced Kondo Effect in Single Molecular Magnets*. Physical Review Letters **96**, 196601, (2006).
- 36 Romeike, C., Wegewijs, M. R. & Schoeller, H. *Spin Quantum Tunneling in Single Molecular Magnets: Fingerprints in Transport Spectroscopy of Current and Noise*. Physical Review Letters **96**, 196805, (2006).
- 37 Elste, F. & Timm, C. *Transport Through Anisotropic Magnetic Molecules with Partially Ferromagnetic Leads: Spin-Charge Conversion and Negative Differential Conductance*. Physical Review B **73**, 235305, (2006).
- 38 Misiorny, M. & Barnaś, J. *Spin Polarized Transport through a Single-Molecule Magnet: Current-Induced Magnetic Switching*. Physical Review B **76**, 054448, (2007).
- 39 Barraza-Lopez, S., Park, K., García-Suárez, V. & Ferrer, J. *First-Principles Study of Electron Transport through the Single-Molecule Magnet Mn₁₂*. Vol. 102, (2009).
- 40 Voss, S. et al. *Electronic Transport Properties and Orientation of Individual Mn₁₂ Single-Molecule Magnets*. Physical Review B **78**, 155403, (2008).
- 41 Ruiz-Molina, D. et al. *Isolated Single-Molecule Magnets on the Surface of a Polymeric Thin Film*. Vol. 15, (2003).
- 42 Cavallini, M., Biscarini, F., Gomez-Segura, J., Ruiz, D. & Veciana, J. *Multiple Length Scale Patterning of Single-Molecule Magnets*. Nano Letters **3**, 1527-1530, (2003).
- 43 Steckel, J. S. et al. *Monolayer and Multilayer Films of [Mn₁₂O₁₂(O₂CMe)₁₆]*. Nano Letters **4**, 399-402, (2004).
- 44 Burgert, M. et al. *Single-Molecule Magnets: A New Approach To Investigate the Electronic Structure of Mn₁₂ Molecules by Scanning Tunneling Spectroscopy*. Journal of the American Chemical Society **129**, 14362-14366, (2007).
- 45 *A Molecular Jigsaw Puzzle*. Nature Materials **16**, 499, (2017).
- 46 Cinchetti, M., Dediu, V. A. & Hueso, L. E. *Activating the Molecular Spininterface*. Nature Materials **16**, 507, (2017).

- 47 Guo, L., Gu, X., Zhu, X. & Sun, X. *Recent Advances in Molecular Spintronics: Multifunctional Spintronic Devices*. Advanced Materials **0**, 1805355, (2019).
- 48 Jenkins, M. *et al.* *Coupling Single-Molecule Magnets to Quantum Circuits*. New Journal of Physics **15**, 095007, (2013).
- 49 Bonizzoni, C., Ghirri, A. & Affronte, M. *Coherent Coupling of Molecular Spins with Microwave Photons in Planar Superconducting Resonators*. Vol. 3, (2018).
- 50 Bonizzoni, C., Troiani, F., Ghirri, A. & Affronte, M. *Microwave Dual-Mode Resonators for Coherent Spin-Photon Coupling*. Journal of Applied Physics **124**, 194501, (2018).
- 51 Zweibach, B. in *Spin One-Half, Bras, Kets, and Operators* (MIT OpenCourseWare, <https://ocw.mit.edu/>. License: Creative Commons BY-NC-SA, Massachusetts Institute of Technology, Fall 2013).
- 52 Atkinson, J. H. *Internal Degrees of Freedom and Spin Transitions in Single Molecule Magnets* Doctor of Philosophy thesis, University of Central Florida, (2016).
- 53 Zhang, J. M. & Liu, Y. *Fermi's Golden Rule: Its Derivation and Breakdown by an Ideal Model*. European Journal of Physics **37**, 065406, (2016).
- 54 Park, K., Dalal, N. S. & Rikvold, P. A. *Effect of Defects on the Line Shape of Electron Paramagnetic Resonance Signals from the Single-Molecule Magnet Mn₁₂: A Theoretical Study*. The Journal of Chemical Physics **117**, 11292-11300, (2002).
- 55 Bales, B. L., Meyer, M., Smith, S. & Peric, M. *EPR Line Shifts and Line Shape Changes due to Spin Exchange of Nitroxide Free Radicals in Liquids: 6. Separating Line Broadening due to Spin Exchange and Dipolar Interactions*. The journal of physical chemistry. A **113**, 4930-4940, (2009).
- 56 Gendell, J., Freed, J. H. & Fraenkel, G. K. *Line Shapes in Electron Spin Resonance Spectra*. Vol. 41, (1964).
- 57 Ryadun, A. A., Nadolinny, V. A., Pavlyuk, A. A., Solodovnikov, S. F. & Boguslavskii, E. G. *Reasons for the Line Broadening in the EPR Spectra of Copper Ions in Li₂-2xZn₂+x(MoO₄)₃ Lithium-Zinc Molybdate Crystals*. Journal of Structural Chemistry **54**, 59-64, (2013).
- 58 *Spectral Broadenings*, in <http://easyspin.org/documentation/broadenings.html> (2019).
- 59 Quddusi, H. *Role of Internal Degrees of Freedom in the Quantum Tunneling of the Magnetization in Single-Molecule Magnets* Doctor of Philosophy thesis, University of Central Florida, (2012).
- 60 Barbara, B. in *Molecular Magnets* (eds J. Bartolome, J. Fernandez, & F. Luis) Ch. 2, 17-60 (Springer, 2014).
- 61 Liu, J., Del Barco, E. & Hill, S. in *Molecular Magnets* (eds J. Bartolome, J. Fernandez, & F. Luis) Ch. 4, 77-112 (Springer, 2014).

- 62 Chiolero, A. & Loss, D. *Macroscopic Quantum Coherence in Molecular Magnets*. Physical Review Letters **80**, 169-172, (1998).
- 63 Stamp, P. C. E. & Tupitsyn, I. S. *Coherence Window in the Dynamics of Quantum Nanomagnets*. Physical Review B **69**, 014401, (2004).
- 64 Ardavan, A. *et al.* *Will Spin-Relaxation Times in Molecular Magnets Permit Quantum Information Processing?* Physical Review Letters **98**, 057201, (2007).
- 65 Schlegel, C., van Slageren, J., Manoli, M., Brechin, E. K. & Dressel, M. *Direct Observation of Quantum Coherence in Single-Molecule Magnets*. Physical Review Letters **101**, 147203, (2008).
- 66 Wernsdorfer, W., Aliaga-Alcalde, N., Hendrickson, D. N. & Christou, G. *Exchange-Biased Quantum Tunnelling in a Supramolecular Dimer of Single-Molecule Magnets*. Nature **416**, 406, (2002).
- 67 Affronte, M. *Molecular Nanomagnets for Information Technologies*. Journal of Materials Chemistry **19**, 1731-1737, (2009).
- 68 Affronte, M. *et al.* *Single Molecule Magnets for Quantum Computation*. Journal of Physics D: Applied Physics **40**, 2999-3004, (2007).
- 69 Amigó, R., Hernandez, J. M., García-Santiago, A. & Tejada, J. *High-Resolution Detection of Resonant Frequencies of Microwave Resonators via Magnetic Measurements*. Applied Physics Letters **82**, 4528-4530, (2003).
- 70 Bal, M. *et al.* *Non-Equilibrium Magnetization Dynamics in the Fe₈ Single-Molecule Magnet Induced by High-Intensity Microwave Radiation*. Europhysics Letters (EPL) **71**, 110-116, (2005).
- 71 Meier, F. & Loss, D. *Electron and Nuclear Spin Dynamics in Antiferromagnetic Molecular Rings*. Physical Review Letters **86**, 5373-5376, (2001).
- 72 Meier, F., Levy, J. & Loss, D. *Quantum Computing with Spin Cluster Qubits*. Physical Review Letters **90**, 047901, (2003).
- 73 Quddusi, H. M. *et al.* *Asymmetric Berry-Phase Interference Patterns in a Single-Molecule Magnet*. Physical Review Letters **106**, 227201, (2011).
- 74 Henderson, J. J. *et al.* *Manifestation of Spin Selection Rules on the Quantum Tunneling of Magnetization in a Single-Molecule Magnet*. Physical Review Letters **103**, 017202, (2009).
- 75 Wernsdorfer, W., Soler, M., Christou, G. & Hendrickson, D. N. *Quantum Phase Interference (Berry Phase) in Single-Molecule Magnets of [Mn₁₂]2-*. Journal of Applied Physics **91**, 7164-7166, (2002).
- 76 AlDamen, M. A., Clemente-Juan, J. M., Coronado, E., Martí-Gastaldo, C. & Gaita-Ariño, A. *Mononuclear Lanthanide Single-Molecule Magnets Based on Polyoxometalates*. Journal of the American Chemical Society **130**, 8874-8875, (2008).

- 77 AlDamen, M. A. *et al.* Mononuclear Lanthanide Single Molecule Magnets Based on the Polyoxometalates $[Ln(W_5O_{18})_2]^{9-}$ and $[Ln(\beta_2-SiW_{11}O_{39})_2]^{13-}$ ($Ln^{III} = Tb, Dy, Ho, Er, Tm, \text{ and } Yb$). *Inorganic Chemistry* **48**, 3467-3479, (2009).
- 78 Clemente-Juan, J. M. & Coronado, E. *Magnetic Clusters from Polyoxometalate Complexes*. *Coordination Chemistry Reviews* **193-195**, 361-394, (1999).
- 79 Guo, F.-S. *et al.* A Dysprosium Metallocene Single-Molecule Magnet Functioning at the Axial Limit. *Angewandte Chemie International Edition* **56**, 11445-11449, (2017).
- 80 Goodwin, C., Ortu, F., Reta, D., Chilton, N. & Mills, D. *Molecular Magnetic Hysteresis at 60 Kelvin in Dysprosocenium*. Vol. 548, (2017).
- 81 Guo, F.-S. *et al.* Magnetic Hysteresis up to 80 Kelvin in a Dysprosium Metallocene Single-Molecule Magnet. *Science* **362**, 1400, (2018).
- 82 Amjad, A. *Exchange Coupling In Molecular Magnets: Zero, One And Three Dimensions* Doctor of Philosophy thesis, University of Central Florida, (2013).
- 83 *Stevens Operators*, in <http://easyspin.org/documentation/stevensoperators.html> (2019).
- 84 del Barco, E. *et al.* Magnetic Quantum Tunneling in the Single-Molecule Magnet Mn_{12} -Acetate. *Journal of Low Temperature Physics* **140**, 119-174, (2005).
- 85 Escalera-Moreno, L., Baldoví, J. J., Gaita-Ariño, A. & Coronado, E. *Spin States, Vibrations and Spin Relaxation in Molecular Nanomagnets and Spin Qubits: A Critical Perspective*. Vol. 9, (2018).
- 86 Brustolon, M. & Giamello, E. in *Electron Paramagnetic Resonance : A Practitioner's Toolkit* Ch. 1, 3-35 (John Wiley & Sons, Incorporated, 2009).
- 87 in *Quantum Mechanics* (ed F. Schwabl) 259-269 (Springer Berlin Heidelberg, 2007).
- 88 Brustolon, M. & Giamello, E. in *Electron Paramagnetic Resonance : A Practitioner's Toolkit* Ch. 2 37-82 (John Wiley & Sons, Incorporated, 2009).
- 89 Brustolon, M. & Giamello, E. in *Electron Paramagnetic Resonance : A Practitioner's Toolkit* Ch. 5.1, 159-161 (John Wiley & Sons, Incorporated, 2009).
- 90 Brustolon, M. & Giamello, E. in *Electron Paramagnetic Resonance : A Practitioner's Toolkit* Ch. 5.2 162-171 (John Wiley & Sons, Incorporated, 2009).
- 91 Brustolon, M. & Giamello, E. in *Electron Paramagnetic Resonance : A Practitioner's Toolkit* Ch. 5.3 172-184 (John Wiley & Sons, Incorporated, 2009).
- 92 Takahashi, S. *et al.* Decoherence in Crystals of Quantum Molecular Magnets. *Nature* **476**, 76, (2011).

- 93 Takahashi, S. *et al.* *Coherent Manipulation and Decoherence of $S=10$ Single-Molecule Magnets*. Physical Review Letters **102**, 087603, (2009).
- 94 Fox, M. in *Quantum Optics: An Introduction* Ch. 10, 194-215 (Oxford University Press, 2006).
- 95 Cohen-Tannoudji, C., Dupont-Roc, J. & Grynberg, G. in *Atom-Photon Interactions: Basic Processes and Applications* Ch. 5A, 355-363 (John Wiley & Sons, 1992).
- 96 Zweibach, B. in *Two State Systems* (MIT OpenCourseWare, <https://ocw.mit.edu/>. License: Creative Commons BY-NC-SA, Massachusetts Institute of Technology, Fall 2013).
- 97 Fox, M. in *Quantum Optics: An Introduction* Ch. 9, 167-193 (Oxford University Press, 2006).
- 98 Stockklauser, A. *et al.* *Strong Coupling Cavity QED with Gate-Defined Double Quantum Dots Enabled by a High Impedance Resonator*. Physical Review X **7**, (2017).
- 99 Thompson, R. J., Rempe, G. & Kimble, H. J. *Observation of Normal-Mode Splitting for an Atom in an Optical Cavity*. Physical Review Letters **68**, 1132-1135, (1992).

CHAPTER 2: SUB-KELVIN TIME-RESOLVED EPR SPECTROSCOPY FOR STUDIES OF QUANTUM DYNAMICS OF LOW-DIMENSIONAL SPIN SYSTEMS AT LOW FREQUENCIES AND MAGNETIC FIELDS

The main objective of this dissertation is to study the nature of the light-matter interaction in SMMs and advance towards coherent quantum control over their molecular spins. The current chapter focuses on enabling coherent control of the quantum mechanical time evolution of molecular nanomagnet spins, by utilization of a time resolved electron paramagnetic resonance spectrometry setup designed to work at frequencies below 20 GHz and temperatures down to 50 mK. Capability to perform time-resolved EPR spectroscopy in this temperature range is crucial to our investigations of molecular nanomagnet quantum dynamics at X-band (≈ 10 GHz) frequencies, as the ensemble of spins will be completely thermally polarized into a single ground state without the need for large magnetic fields. The results show an increase in echo signal intensity as temperature is decreased until saturation as expected from the 99% spin polarization at 100 mK. Our technique allows tuning of the spin system in the pure state regime and minimization of dipolar fluctuations, the main contribution to decoherence in condensed single crystals of single-molecule magnets (SMMs), which are currently being tested for applications in quantum computation. The achievement of full spin polarization at 100 mK will allow for coherent control over the time evolution of spin systems without the need for large magnetic fields (which are commonly used to polarize the dipolar bath at higher temperatures) and high frequencies. In addition, the utilization of on-chip microstrip resonators will allow the extension of such studies into 2D films and individual molecules placed on the surface of the resonator line, something that is not possible with standard resonant cavities.

The following sections describe the experimental setup that I have designed in order to study the spin-photon interaction in the weak coupling regime, with the ultimate goals being to:

- i. Increase our knowledge of quantum coherent dynamics in SMM spins;
- ii. Explore and identify the role played by the intrinsic anisotropy and symmetry degrees of freedom inherent in SMMs as it relates to the quantum evolution of spin states; and,
- iii. Examine the potential of low-nuclearity SMMs as hardware for quantum computing and information technologies.

2.1 Background

SMMs first revealed their potential to act as magnetic bits at the quantum level with the discovery of magnetic hysteresis in molecular clusters of Mn_{12} acetate. The 1996 discovery of the resonant quantum tunneling of the magnetization (QTM) [1-3] is widely considered to be a landmark in spin physics [4], and these molecular nanomagnets provide a range of rich quantum behaviors [5-15] which make them promising candidates for qubits [16-20], the quantum computing analog of the classical computing bit. SMMs also happen to be ideally suited for studies concerning the confluence of classical and quantum magnetism and are of great interest in the field of molecular spintronics [21-29], merging elements of quantum magnetism and molecular electronics to create electronic devices with exciting new functionalities [30-32]. One exciting field where these molecules will provide an advantage over other spin systems, such as NV centers in diamond, with respect to the manipulation of the spins is the coupling of SMMs with quantum circuits (for example, superconducting resonators) [33]. Pulsed EPR spectroscopy is a powerful tool for the study of quantum dynamics and the determination of decoherence rates in magnetic systems [34-39]. In particular, it has been recently used to characterize the quantum dynamical properties of spins in SMM systems [16,40-46], which offer great potential for applications in quantum computation and information technologies [17-20,47-54].

The molecular magnetism community has in recent years begun to increase understanding of the effects of light-matter interaction on SMMs and the intrinsic sources of decoherence in their solid-state form, limited primarily by dephasing due to dipolar fluctuations in crystalline samples where magnetic molecules interact by means of dipolar interactions [55-57]. Aside from dipolar dephasing, intrinsic sources of decoherence in SMMs are associated to hyperfine interactions (with fluctuating nuclear spins of the constituent molecular atoms) and to spin-phonon interactions. Previous works [58] have found that it is necessary to first eliminate this dephasing due to fluctuating dipolar interactions before one may begin to study the intrinsic decoherence mechanisms of electron spins in SMMs which are associated to nuclear spins and coupling to the lattice vibrational modes. There are several valid and well-established approaches to study this decoherence while avoiding dipolar dephasing, including sample dilution in solution [59,60], solid state magnetic dilution [61-63], and polarization of the spin bath by application of large magnetic fields [45,64]. However, these approaches have some significant drawbacks. Dilution of molecular magnets in solution to separate them far enough apart that the molecular spins do not react to each other results in a dispersion of the spin orientations and anisotropy axes, causing individual molecules within the sample to react differently to an external perturbation (such as a magnetic field) and losing the monodispersity inherent to crystalline SMM samples. Magnetic dilution in crystals is only achievable with mononuclear SMMs, where the molecular magnetism arises from a single magnetic ion. Finally, polarization of the spin bath by the application of strong magnetic fields to generate a large energy splitting between the ground and excited spin states by Zeeman interactions restricts the experiments to large magnetic fields, where substantially high frequency (>100 GHz) microwave pulses are required. Aside from the technical restrictions, in the latter approach the Zeeman interaction governs the spin dynamics, dominating over the intrinsic magnetic anisotropy that is characteristic of SMMs and makes

these systems unique ($g\mu_B\vec{S} \cdot \vec{B} \gg DS_z^2$); among other things this enables the possibility to work with states resulting from quantum superposition of spin states generated by transverse anisotropy tensors.

Time-resolved EPR spectroscopy consists of irradiating the test device with specific patterns of short microwave pulses while the reflection or transmission of the signal is recorded as a function of time. In this work, we examine only the spin-spin or transverse relaxation time (T_2) as a measure of how quickly the transverse magnetization M_{XY} decays to equilibrium after being excited with an initial high-power microwave pulse. Similar experiments that have been performed at the National High Magnetic Field Lab (NHMFL) in Tallahassee are limited to temperatures above 1.6 K, requiring magnetic fields in excess of 8 T to separate the spin levels enough to avoid population of the excited state. This requires the use of EPR frequencies in the sub-Terahertz range (greater than 0.2 THz). More specifically, in studies performed at NHMFL on Fe8 (see Figure 1.11) microwave frequencies in excess of 125 GHz were used which allowed for this form of spin polarization (via a negligible population of the first excited state) to occur for temperatures in excess of 1 K. While this may seem attractive, in order to separate the spin states of the system so that their energy difference matched the applied microwave energy, a magnetic field greater than 10 T was needed. In this regime, the Zeeman coupling would dominate, and the applied field would become the quantization axis in contrast to the intrinsic anisotropy axis of the molecule. The net effect of this is to lower the mixing between spin states, which when combined with the EPR spin transition selection rules would make observing spin-echo for most SMMs virtually impossible (irrespective of the fact that the spin bath is polarized).

New and innovative techniques are therefore required in order to more fully comprehend the nature of the light-matter interaction and contributions to decoherence in molecular nanomagnets while both maintaining the degree of monodispersity inherent in single crystals and remaining within the energy

landscape produced by the intrinsic magneto-anisotropy of the molecules. A recent report in Review of Scientific Instruments [65] shows the accomplishment of pulsed EPR experiments in a resonant cavity at temperatures down to 12.3mK. In reaching such low temperatures, researchers were able to achieve near complete thermal polarization of the spin bath in a $\frac{1}{2}$ spin system. However, the use of a resonant cavity as in [65] does not allow for coupling to low-dimensional spin systems (including SMMs, 2D films or individual molecules) to the extent possible with other resonating devices, such as on-chip microstrip resonators. Strong spin-photon coupling is particularly important for studies of the quantum dynamics of the spin of SMMs (strong candidates for reliable qubits) in view of applications in quantum computation. The intrinsically small coupling of spins with the magnetic component of electromagnetic radiation, a factor c (the speed of light) smaller than the electric field component, prevents reaching the strong spin-photon coupling regime in standard resonating cavities, even in high quality factor superconducting cavities. Recently, it has been shown that a substantial enhancement of the microwave magnetic field in nano-constricted, on-chip, coplanar waveguide superconducting resonators can increase the spin-resonator coupling by several orders of magnitude [66], which together with the strong coupling of photons to superposition states (only possible for low or no magnetic fields), high spin values, and long coherent times in SMMs open the door to unequivocally proving the potential of SMMs for quantum computation for the first time. Therefore, it is important to develop time resolved EPR spectroscopic techniques at ultra-low temperatures with the use of on-chip microstrip resonators.

Our solution to this open research question has been to develop an in-house experimental setup capable of applying high-power EPR pulses to a sample mounted on a planar microstrip resonator at temperatures below 100 mK, polarizing the spin bath with the ground and excited states being separated by much lower energies while suppressing dipolar dephasing, and allowing EPR to be performed at

frequencies down to 10 GHz. Of course, the temperature required to polarize the spin bath in this manner depends directly on the energy spacing between the ground and first excited states; however, this polarization may be reached with magnetic fields of less than 1 T so as to preserve the inherently anisotropic nature of SMMs. This will enable research studies into the much richer quantum dynamics associated with the intrinsic magneto-anisotropy of molecular nanomagnets. Along these lines, planar microstrip resonators deliberately designed for enhanced sensitivity and homogeneity of the magnetic field at the sample location have been fabricated and are employed in this work. They are complemented by a careful engineering of stainless steel, copper, and niobium superconducting coaxial lines which carry the microwave stimuli down to the sample position (in our Oxford Instruments KelvinoxMX100 dilution cryostat) while preserving the base temperature of below 50 mK. The ultra-low temperature of the system will force the molecular spins to remain in their ground state, avoiding population of excited states and thus minimizing spin fluctuations.

2.1.1 Rabi Oscillations

As previously stated, the energy region we desire to work in will enable studies of a variety of molecular nanomagnets without destroying the role of the intrinsic molecular anisotropy by the use of large magnetic fields. These large magnetic fields become an even more significant factor when, for example, inducing Rabi oscillations via pulses of electromagnetic radiation. In a Zeeman dominated regime, transitions between spin states which are eigenstates of the Hamiltonian (namely, the S_i states with $g\mu_B S_i B_i \gg DS_Z^2$, where $i=x, y, \text{ or } z$ denotes the direction of the applied magnetic field) may be easily induced. They will correspond to simple, well-defined Rabi oscillations between the two states involved, which can be calculated analytically. However, if the Zeeman energy is comparable to the anisotropy barrier ($g\mu_B S_i B_i \sim DS_Z^2$), the induced transitions may instead involve states with

symmetric/antisymmetric superpositions of the Hamiltonian eigenstates ($|\Psi_S\rangle$ or $|\Psi_A\rangle$ states which are determined by $DS_Z^2 + g\mu_B S_i B_i$, for i orthogonal to z). In this situation, the Rabi oscillations are no longer either simple or well-defined, and the magnetic state of the molecule may develop excited precessional states. The experimental setup described in this chapter will allow the study of spin quantum dynamics in single-crystal SMMs which are governed by the intrinsic molecular anisotropy, permitting these anisotropy-driven quantum dynamics to be observed.

2.1.2 Thermal Polarization for Spin $1/2$

The experimental setup realized in the following sections provides a window into the fundamental sources of decoherence in non-dilute single-crystal SMMs in an energy range (frequencies below 18 GHz and magnetic fields below 1 T) not yet achieved, while allowing for the possibility to couple to 2D films and eventually individual molecules that may be placed on the surface of the resonator line. These low temperature, low frequency experiments will allow measurements of decoherence rates orders of magnitude smaller than those found at the NHMFL; this energy range also provides the opportunity to potentially examine all three of these main sources of decoherence (dipolar, nuclear, and phonon dephasing) in the same experimental setup. The three decoherence rate curves cross at (for Fe_8) approximately 0.1 K and 20 GHz, shown by the red star in Figure 1.11, exactly within the parameters of our setup.

We will examine only the T_2 (spin-spin) relaxation time as a measure of how quickly the transverse magnetization M_{XY} decays to equilibrium after being excited; for this, we use the classic Hahn Echo sequence of $\frac{T}{2} \rightarrow t_{\text{delay}} \rightarrow T \rightarrow t_{\text{delay}} \rightarrow \text{echo}$ where $\frac{T}{2}$ denotes the “ $\frac{\pi}{2}$ ” pulse which rotates the electronic spins by 90° into the transverse plane, t_{delay} denotes the time during which no radiation is applied where the spins dephase in the transverse plane, T denotes the “ π ” pulse which rotates the spins

by 180° within the transverse plane, and *echo* denotes the signal produced from the sample as the electronic spins recombine in the transverse plane. By plotting the magnitude of this echo signal as a function of the dephasing time t_{delay} one will observe an exponential decay, the time constant of which gives a good estimate of T_2 . The results shown in this chapter were achieved according to this process. In the remaining sections I showcase the in-house setup I have built which is capable of applying high-power EPR pulses to a sample mounted on a microstrip resonator down to 50 mK, with the ability to apply magnetic fields below 1 T in any direction. We also demonstrate the achievement of the pure-state regime in a well-known spin $\frac{1}{2}$ coal marker sample, whose thermal equilibrium polarization P can be described at a temperature T by

$$P = \tanh\left(\frac{\hbar\gamma_e B_0}{2k_B T}\right) \quad (2.1)$$

where \hbar is the reduced Plank's constant, γ_e is the electron gyromagnetic ratio, B_0 is the externally applied magnetic field strength, and k_B is the Boltzmann constant. This technique allows tuning of the spin system in the pure state regime and minimization of dipolar fluctuations, as well as coherent control over the time evolution of spin systems without the need for large magnetic fields and high frequencies. In addition, the utilization of on-chip microstrip resonators will allow the extension of such studies into 2D films and individual molecules placed on the surface of the resonator line, something that is not possible with standard resonant cavities.

2.2 Instrumentation and Methods

2.2.1 The Spin Echo Circuit

Our home-built experimental setup is shown in Figure 2.1. First, a PNA microwave source (A) provides a 10dBm signal in the range of 6-18 GHz to the circuit, which is then divided by a directional

coupler (B) between a line to the sample (~90% of signal) and a line to the mixer used as a detector (~10% of signal). Next, the signal is passed through a circulator to a switch which pulses the signal to the described Hahn echo sequence (C, D). The resultant pulses are filtered using a 2-18 GHz bandpass filter and then amplified by a high-gain (40dB) high output power (30dBm) Agilent amplifier (E), before being sent through a DC block to the coaxial lines in the dilution refrigerator (F). The setup is configured for transmission experiments, and the spin echo pulses are directed through a series of copper, stainless steel, and niobium superconducting semirigid coaxial lines to the resonator (G).

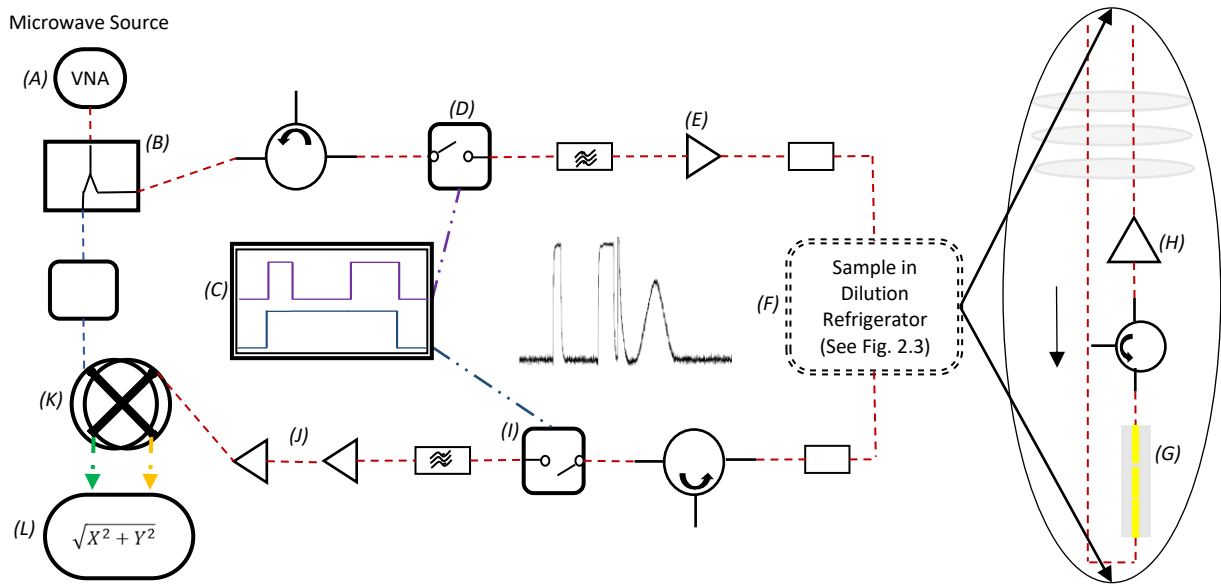


Figure 2.1: The Spin Echo Circuit

Schematic of the pulsed EPR setup. Key components labeled by italicized letters in parentheses are: (A) microwave source (Agilent E8364B), (B) directional coupler (Agilent 87301D Opt 240), (C) pulse generator (Agilent 81110A), (D) pulsing switch (HP SPST 33144A with HP 33190B driver), (E) pulse amplifier (Agilent 83020A), (F) dilution refrigerator (KelvinoxMX100) inside vector magnet (3-axis American Magnetics Inc), (G) microstrip resonator (fabricated in-house), (H) cryogenic signal amplifier (CIT618 Cryogenic HEMT from CalTech), (I) screening switch (AMC SWM-DJV-1DT-2ATT Opt 20F), (J) signal amplifiers (Mini-Circuits ZVE-3W-183+ and CTT APM/180-2741-22), (K) quadrature mixer (Stellex M38UC), (L) oscilloscope (Agilent Infiniium DS08194A).

Once the pulses reach the sample, the spin echo signal is directed through the resonator to another series of copper, superconducting, and stainless steel coaxials. We have allowed for the option to include a cryogenic amplifier (H) between the copper and stainless steel coaxials, intentionally designed for future investigations in experiments with a low number of photons (Appendix E). Should this amplifier be used, a cryogenic circulator will also be placed between it and the sample to prevent high power reflections. Once out of the fridge the resulting signal is passed through another DC block and a circulator, which is used to prevent any spurious noise from traveling back to the resonator and sample. Finally, a screening switch (I) is added and programmed to remain closed to screen out the initial echo pulse sequence, opening only to allow the resultant spin echo signal to pass through at full power. It is further filtered via a 2-18GHz bandpass filter and fed through two amplifiers (J) for a total gain of 80dB (maximum output power of 40 dBm). The signal finally arrives at a quadrature mixer (K) that is coupled to the original microwave signal. The X and Y phases are captured by a high-frequency oscilloscope (L), and the final readout is the magnitude of these two components taken together as $\sqrt{X^2 + Y^2}$. Appendix C has the circuit components listed in more detail.

2.2.2 *The Resonator*

We fabricate microstrip resonators (Figure 2.2) for frequencies within the experimental setup range (2-18 GHz) in house by means of double-layer photolithography and deposition of a sticking layer of 10 nm titanium, 120 nm copper, and a capping layer of 10 nm gold on a commercial GaAs wafer (the recipe for which is given in Appendix D). For the measurements in this chapter we used a 15 GHz resonator, which is achieved by a 140 μm thick, 500 μm wide, and 3 mm long gold-plated copper central line separated from the feeding line by a 140 μm coupling gap and the transmission line by a 400 μm gap (see Figure 2.2, top). The coupling gap is designed to critically couple the resonator to the incoming

microwave signal, while a larger transmission gap is used to avoid affecting the quality factor of the resonator unnecessarily while still allowing enough signal to be transferred for measurements to be done in transmission mode [67]. The microstrip resonator is deposited on top of a 550 μm thick undoped GaAs wafer whose back is gold-plated to form the ground plate. The dimensions are calculated to guarantee a 50 Ω matching impedance with the feeding coaxial lines and prevent power losses by reflection.

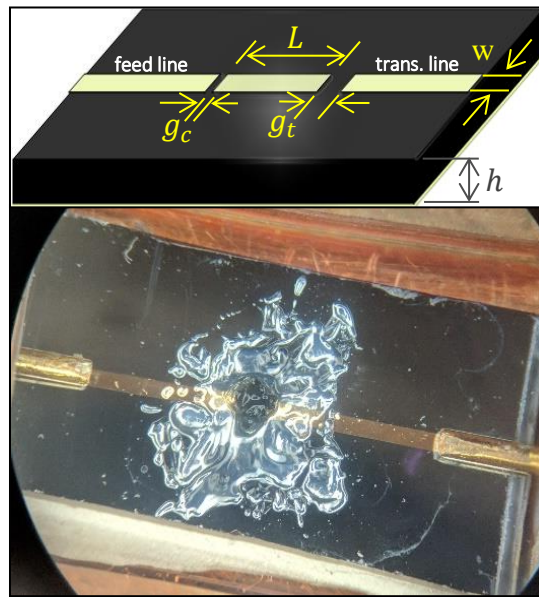


Figure 2.2: The Microstrip Resonator

Top: A 3D representation of the transmission resonator design with the characteristic functional parameters: Line resonator length (L) and width (w), coupling gap (g_c), transmission gap (g_t), and GaAs substrate thickness (h), which separates the resonator line and the back plate. Bottom: The coal sample is shown mounted to the surface of the resonator mounted in solid copper housing box using standard cryogenic vacuum grease.

The microstrip resonator chip is mounted in a solid OFHC copper housing box and held in place with a back layer of conductive silver paint. Nonmagnetic SMA connectors are used for the connections to the housing box, with gold-plated beryllium copper center contacts placed in physical contact with the resonator feedlines. The housing box is kept in good thermal contact with the dilution refrigerator coldfinger by two brass screws and Apiezon thermalizing vacuum grease, and the resonator is oriented

with the smaller coupling gap facing the input line, such that the maximum microwave power reaches the sample for the initial pulses. The total losses at 15 GHz through the housing box and a 15GHz resonator is -7 dB, and the specific resonator used in these experiments had a quality factor of $Q \approx 50$.

2.2.3 The Dilution Refrigerator

To properly isolate the sample from high temperatures, several thermalization stages are present in the dilution refrigerator as shown in Figure 2.3. Starting from the top, the microwave stimuli are conducted through a 0.75 m long semirigid copper coaxial connected to the room temperature circuit. At the 4K plate the coaxial transitions into a 0.5 m long niobium superconducting line which reaches down to the 1K plate. Then, a 0.15m long stainless steel coaxial is used to connect to the mixing chamber, from which a 0.3 m copper microcoaxial along the length of the cold finger is used to transport the signal down to the housing box. The different coaxial line stages are included to allow for the inclusion of attenuators, circulators or cryogenic amplifiers as needed. The same configuration applies to the returning coaxial lines. The total power losses at 15GHz through each side of the lines is -8dB at low temperature. Considering a maximum output power of 30dBm at the room temperature amplifier, we estimate that the microwave pulses at 15GHz reach the housing box with a power of ~ 22 dBm (160 mW).

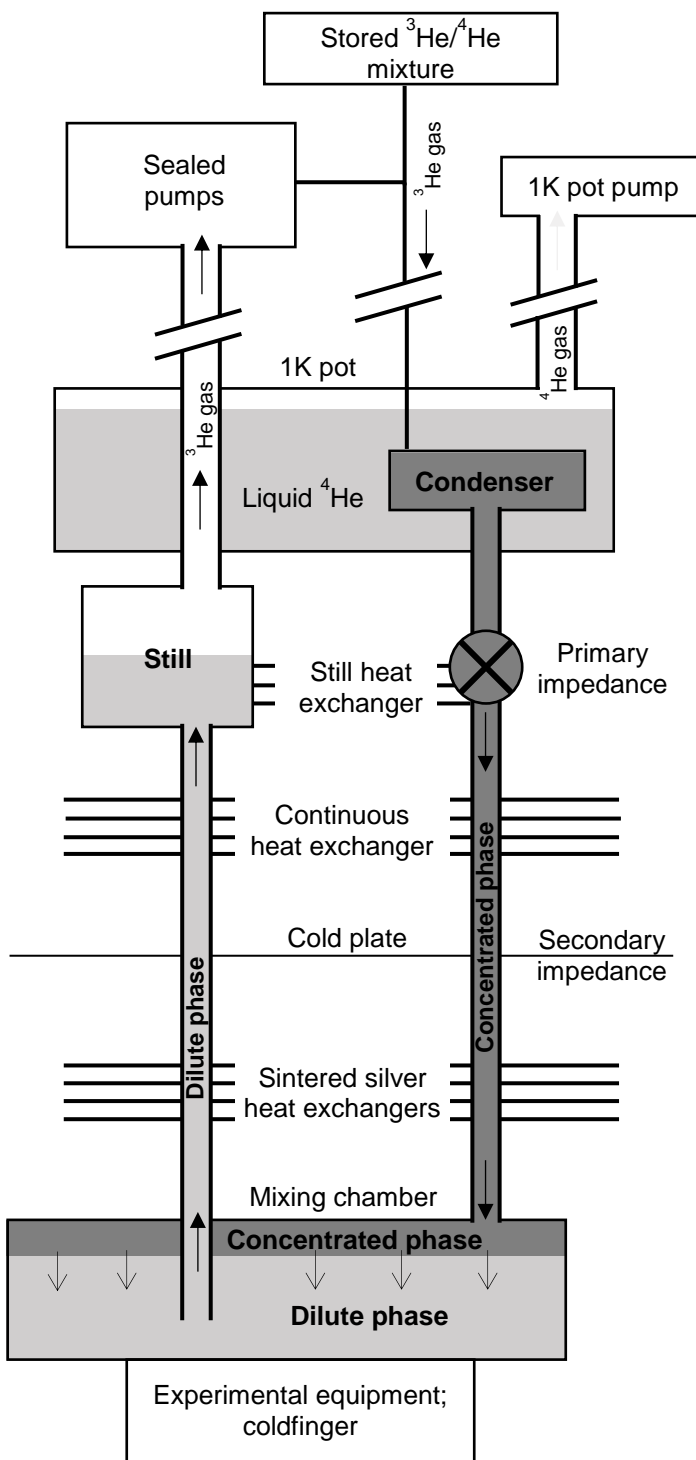
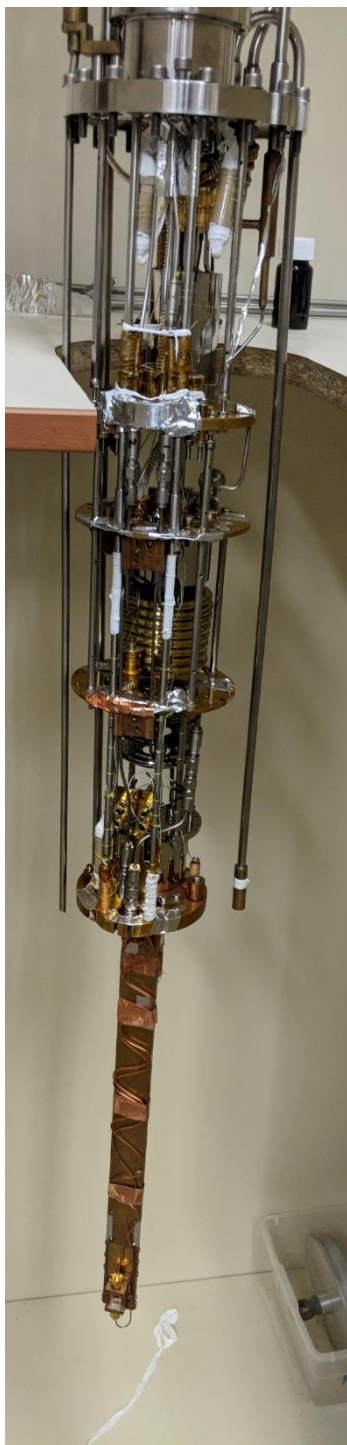


Figure 2.3: The Dilution Refrigerator

Left: Photo of the dilution refrigerator outside of the magnet without vacuum sleeve and radiation shield. Right: Diagram of dilution refrigerator principle of operation.

2.3 Experimental Results

The spin echo signal intensity was used as a direct indicator of spin polarization as a function of temperature as per (2.1). A Bruker coal calibration sample [68] with a very strong echo response was placed in the center of the microstrip resonator (see Figure 2.2). The Hahn echo sequence discussed in the introduction was applied to the sample at temperatures ranging between 100 to 800 mK. The echo height is proportional to the difference in population between the ground and excited spin states that are involved in the microwave absorption. When only the ground state is populated in steady-state, the sample reaches full spin polarization. Accordingly, as expected from (2.1), the spin echo signal should increase as the sample's temperature decreases and saturate when the full spin polarization is achieved, which for the magnetic field and frequency employed in this experiment occurs around 100 mK. However, undesired heating of the sample through the coaxial lines by the microwave pulses would result in an artificial saturation of the spin echo at temperatures significantly higher than 100 mK. Therefore, the observation of the theoretical expectation of spin polarization becomes an excellent indicator of a preservation of the sample temperature as dictated by the dilution refrigerator.

Initially, continuous wave EPR was performed to establish the resonant magnetic field of the sample at 15 GHz, which is found at $H = 0.505$ T, as expected for a spin $\frac{1}{2}$ system at this frequency. Then, the field was held constant at 0.505 T and microwave radiation was supplied at 15.62 GHz to the spin echo circuit (slightly away from the resonance maximum to improve sensitivity). A series of different pulse lengths for a dephasing time of $t_{delay} = 100$ ns was systematically applied to the sample at $T = 2$ K (where microwave heating would be negligible) to locate the largest observable magnitude of the echo signal. The optimal pulse sequence was found to be $200\text{ ns} \rightarrow t_{delay} \rightarrow 400\text{ ns} \rightarrow t_{delay} \rightarrow echo$. Spacing the pulse sequences by at least 5 seconds was necessary to see a steady increase in echo height down to

100mK. To ensure that no heating occurred due to the repetition rate of the pulses even at the lowest sample temperature (100 mK), a period of 10 s was used to space each pulse sequence sent to the sample for all subsequent studies.

2.3.1 Polarization of the Spins; Heating the Sample

To determine the heating effect of the pulses, the sample was cooled overnight to below 100 mK and the height of the echo was studied as a function of the temperature. The echo heights obtained for a pulse sequence of $200\text{ ns} \rightarrow t_{\text{delay}} = 400\text{ ns} \rightarrow 400\text{ ns}$ for different experimental temperatures in the range of 100 to 800 mK is shown in Figure 2.4. The echo heights have been normalized assuming a full spin polarization at 100 mK, as expected from theory. The theoretical expectation of the spin polarization is also shown in Figure 2.4 (continuous line) and is in excellent agreement with the experimental data. The perfect match between experiment and theory demonstrates a proper thermalization of the spins while spin echo measurements are undertaken, proving that the microwave pulses used in this particular spin echo sequence do not perturb the temperature of the sample even down to the lowest temperatures of the study. In other words, our microstrip-based spin echo spectroscopic setup enables studies of spin dynamics in magnetic systems at temperatures sufficiently low to ensure a full spin polarization of the system, allowing studies of quantum dynamics of spin and decoherent mechanisms intrinsic to the system while avoiding dephasing from fluctuations of the dipolar interactions which are relevant in condensed solid-state spin samples.

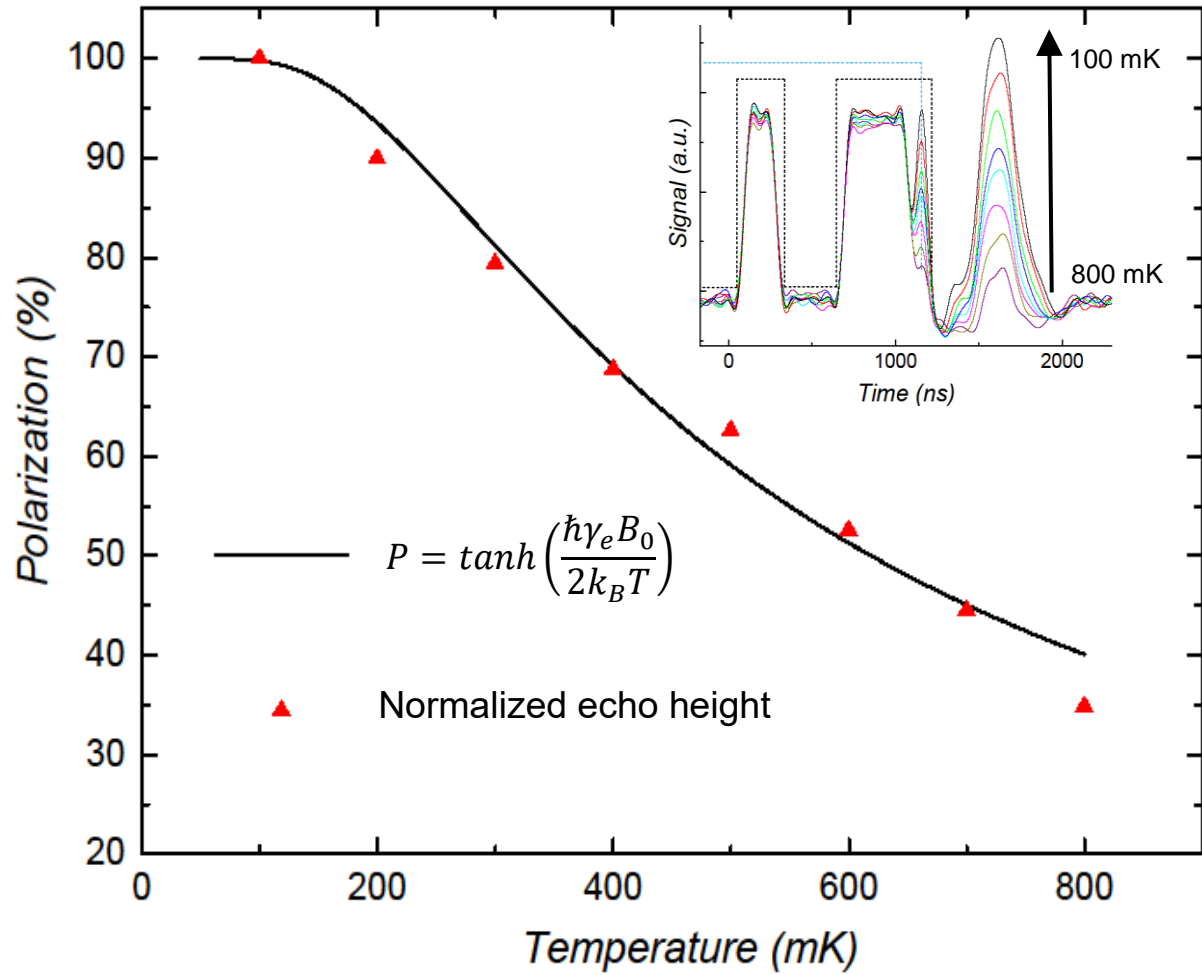


Figure 2.4: Spin Bath Polarization at Low Temperatures

Main panel: Thermal polarization of the spin bath as a function of temperature. The theoretical curve (black line) has been plotted according to Eq. (1). The experimental data points (red triangles) are normalized so that 100mK is assumed 100% polarization. Data was taken with a $200\text{ ns} \rightarrow t_{\text{delay}} = 400\text{ ns} \rightarrow 400\text{ ns}$ pulse sequence and a 10 s repetition period. Inset: Pulse sequence and echo signal for various temperatures. The solid blue line at the top represents the pulse sequence sent to the sample, while the solid black line above it represents the opening of the screening switch to allow the echo signal through. These are shown to explain the observed “peak” just before the echo, which is the remainder of the second pulse bleeding through the screening switch.

2.3.2 Spin-Spin Relaxation Time

As a final test, we allowed the sample to again cool to below 100 mK and performed spin echo with the $200\text{ ns} \rightarrow t_{\text{delay}} \rightarrow 400\text{ ns}$ pulse sequence to extract an estimate of T_2 for the coal spin marker by varying the delay time between pulses and recording the height of the spin echo. The results are shown in Figure 2.5, where the dependence of the height of the spin echo as a function of delay time is fitted to an exponential decay (continuous lines) for two temperatures ($T = 100$ and 600 mK). Our estimate for T_2 was calculated to be $2.7 \pm 0.4\text{ }\mu\text{s}$; It is important to note that this coal sample has a very strong instantaneous diffusion component that will affect the spin-spin relaxation time, and accurate measurements of T_2 at very low temperatures is almost impossible [69]. However, the observed transverse relaxation time lies within the expected values for this sample ($T_2 = 500\text{ ns}$ has been reported at room temperature [16]). We did not observe any significant change in T_2 within our range of temperatures. We associate this to a saturation at higher temperatures when decoherence becomes dominated by nuclear dephasing, rather than interactions with vibrational oscillations of the lattice (phonons).

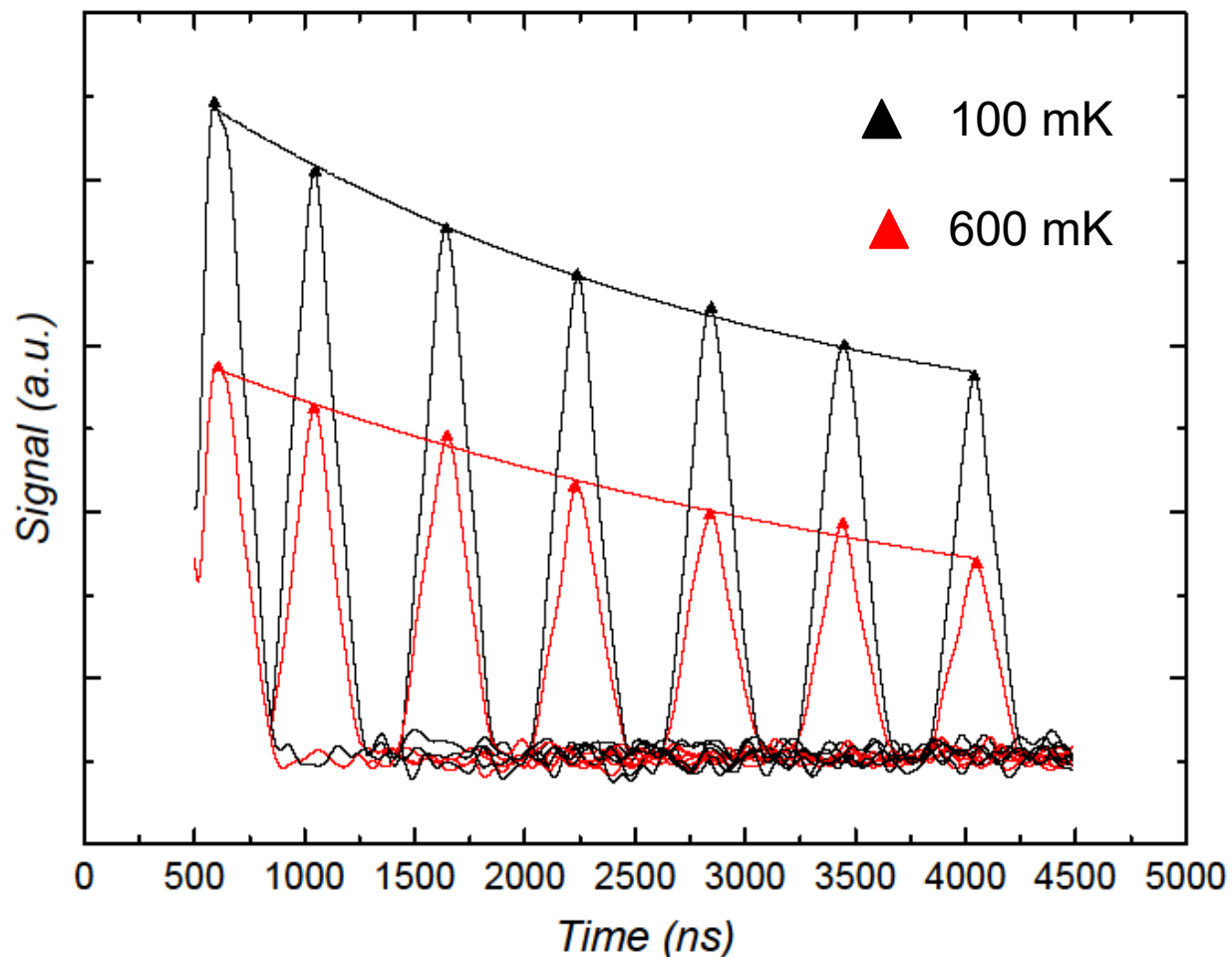


Figure 2.5: Extracting the Spin-Spin Relaxation Time T_2

Exponential decay fit to the echo heights for a series of a $200 \text{ ns} \rightarrow t_{\text{delay}} \rightarrow 400 \text{ ns}$ pulse sequences. The delay times used were 100, 300, 600, 900, 1200, 1500, and 1800 ns. Data was taken at 100 mK, with a 10 s period (black), and 600 mK, with a 0.5 s period (red). T_2 was extracted from both sets of data with the following equation of fit: $y = A_1 \times \exp\left(\frac{-x}{T_2}\right) + y_0$.

2.4 Discussion and Summary

While pulsed EPR experiments have already been achieved below 1 K, to our knowledge no implementation of a sub-Kelvin pulsed EPR apparatus has been made specifically to address the decoherence inherent to low dimensional spin systems, such as condensed crystalline samples of single-molecule magnets, with the ability to study thin films and molecules deposited on the surface of the

microstrip resonators employed in our setup. Here we have demonstrated our ability to perform pulsed EPR experiments successfully and without heating of the sample at temperatures down to 100 mK on a planar microstrip resonator, using the echo height at different temperatures as a direct measure of the thermal spin polarization (2.1) to prove we can achieve $\approx 100\%$ polarization of the spin bath at magnetic fields below 1 T.

As mentioned in the introduction, superconducting planar microstrip and coplanar waveguide resonators with nano-constrictions may be employed to drive spin-photon interactions into the strong coupling regime (the topic of the next chapter), which is extremely important for studies of quantum dynamics of the spin of SMMs in view of potential applications in quantum computation. In addition, the ability to study the quantum dynamics of SMMs at ultra-low temperatures and low magnetic fields ensures observing spin dynamics associated with the molecules' intrinsic magnetic anisotropy. This opens an avenue to operations involving highly mixed superposition spin states, as well as to exploring the interaction between such sophisticated quantum states and their intrinsic sources of decoherence (such as nuclear spins and phonon couplings), even in magnetically condensed samples as a result of a full polarization of the spin bath. This technique will in turn facilitate investigations of interesting quantum behaviors of SMMs which are driven by their intrinsic magneto-anisotropy, including Rabi oscillations that are not Zeeman-dominated and thus not necessarily well-defined (as when the quantization axis results from a competition between the uniaxial anisotropy axis and the externally applied field). Additionally, our setup offers the capability to amplify signals at cryogenic temperatures, opening the door to experiments involving low numbers of photons in the strong coupling regime. We do not see any major technical limitation to extend this capability to temperatures down to 20mK, which is the base temperature achievable in our cryostat.

Ultimately, in this chapter we have achieved our goal of enabling pulsed EPR experiments on well-ordered single crystal SMMs at relatively low magnetic fields, opening the door to examining the three main sources of decoherence (dipolar, nuclear, and phonon dephasing) in the same experiment (something impossible to do with very high magnetic fields and frequencies), to be performed in-house; there are many intriguing pathways that may be explored in the future using this technical method.

References

- 1 Friedman, J. R., Sarachik, M. P., Tejada, J. & Ziolo, R. *Macroscopic Measurement of Resonant Magnetization Tunneling in High-Spin Molecules*. Physical Review Letters **76**, 3830-3833, (1996).
- 2 Thomas, L. et al. *Macroscopic Quantum Tunnelling of Magnetization in a Single Crystal of Nanomagnets*. Nature **383**, 145-147, (1996).
- 3 Hernández, J. M. et al. *Field Tuning of Thermally Activated Magnetic Quantum Tunnelling in Mn12-Ac Molecules*. Europhysics Letters (EPL) **35**, 301-306, (1996).
- 4 Ziemelis, K. *The Difficult Middle Ground*. Nature Physics, S19, (2008).
- 5 Luis, F. et al. *Long-Range Ferromagnetism of Mn12 Acetate Single-Molecule Magnets under a Transverse Magnetic Field*. Physical Review Letters **95**, 227202, (2005).
- 6 del Barco, E., Kent, A. D., Rumberger, E. M., Hendrickson, D. N. & Christou, G. *Symmetry of Magnetic Quantum Tunneling in Single Molecule Magnet Mn12-Acetate*. Physical Review Letters **91**, 047203, (2003).
- 7 Foss-Feig, M. S. & Friedman, J. R. *Geometric-Phase-Effect Tunnel-Splitting Oscillations in Single-Molecule Magnets with Fourth-Order Anisotropy Induced by Orthorhombic Distortion*. EPL (Europhysics Letters) **86**, 27002, (2009).
- 8 Morello, A., Bakharev, O. N., Brom, H. B., Sessoli, R. & de Jongh, L. J. *Nuclear Spin Dynamics in the Quantum Regime of a Single-Molecule Magnet*. Physical Review Letters **93**, 197202, (2004).
- 9 Kent, A. D. et al. *Low-Temperature Magnetic Hysteresis in Mn12 Acetate Single Crystals*. Europhysics Letters (EPL) **49**, 521-527, (2000).
- 10 Martínez-Hidalgo, X., Chudnovsky, E. M. & Aharony, A. *Dipolar Ordering in Fe8?* Europhysics Letters (EPL) **55**, 273-279, (2001).
- 11 Torres, F., Hernández, J. M., Bohigas, X. & Tejada, J. *Giant and Time-Dependent Magnetocaloric Effect in High-Spin Molecular Magnets*. Applied Physics Letters **77**, 3248-3250, (2000).
- 12 Fominaya, F., Villain, J., Gandit, P., Chaussy, J. & Caneschi, A. *Heat Capacity Anomalies Induced by Magnetization Quantum Tunneling in a Mn12-Acetate Single Crystal*. Physical Review Letters **79**, 1126-1129, (1997).
- 13 López-Ruiz, R., Luis, F., González, V., Millán, A. & García-Palacios, J. L. *Nonlinear Response of Single-Molecule Nanomagnets: Equilibrium and Dynamical*. Physical Review B **72**, 224433, (2005).
- 14 del Barco, E., Kent, A. D., Yang, E. C. & Hendrickson, D. N. *Quantum Superposition of High Spin States in the Single Molecule Magnet Ni4*. Physical Review Letters **93**, 157202, (2004).

- 15 Tokman, I. D., Pozdnjakova, V. I., Vugalter, G. A. & Shvetsov, A. V. *Electromagnetic Superradiance from Single-Molecule Magnets in the Presence of a Classical Driving Magnetic Field*. Physical Review B **77**, 094414, (2008).
- 16 Takahashi, S. *et al.* *Pulsed Electron Paramagnetic Resonance Spectroscopy Powered by a Free-Electron Laser*. Nature **489**, 409, (2012).
- 17 Stamp, P. C. E. & Gaita-Ariño, A. *Spin-based Quantum Computers Made by Chemistry: Hows and Whys*. Journal of Materials Chemistry **19**, 1718-1730, (2009).
- 18 Affronte, M. *Molecular Nanomagnets for Information Technologies*. Journal of Materials Chemistry **19**, 1731-1737, (2009).
- 19 Ghirri, A., Candini, A. & Affronte, M. *Molecular Spins in the Context of Quantum Technologies*. Magnetochemistry **3**, (2017).
- 20 Ghirri, A., Troiani, F. & Affronte, M. Vol. 164 383-430 (2014).
- 21 Mannini, M. *et al.* *Magnetic Memory of a Single-Molecule Quantum Magnet Wired to a Gold Surface*. Nature Materials **8**, 194, (2009).
- 22 Camarero, J. & Coronado, E. *Molecular vs. Inorganic Spintronics: The Role of Molecular Materials and Single Molecules*. Journal of Materials Chemistry **19**, 1678-1684, (2009).
- 23 Kim, G.-H. & Kim, T.-S. *Electronic Transport in Single-Molecule Magnets on Metallic Surfaces*. Physical Review Letters **92**, 137203, (2004).
- 24 Leuenberger, M. N. & Mucciolo, E. R. *Berry-Phase Oscillations of the Kondo Effect in Single-Molecule Magnets*. Physical Review Letters **97**, 126601, (2006).
- 25 González, G. & Leuenberger, M. N. *Berry-Phase Blockade in Single-Molecule Magnets*. Physical Review Letters **98**, 256804, (2007).
- 26 Timm, C. & Elste, F. *Spin Amplification, Reading, and Writing in Transport through Anisotropic Magnetic Molecules*. Physical Review B **73**, 235304, (2006).
- 27 Jo, M.-H. *et al.* *Signatures of Molecular Magnetism in Single-Molecule Transport Spectroscopy*. Nano Letters **6**, 2014-2020, (2006).
- 28 Henderson, J. J., Ramsey, C. M., del Barco, E., Mishra, A. & Christou, G. *Fabrication of Nanogapped Single-Electron Transistors for Transport Studies of Individual Single-Molecule Magnets*. Journal of Applied Physics **101**, 09E102, (2007).
- 29 Zobbi, L. *et al.* *Isolated Single-Molecule Magnets on Native Gold*. Chemical Communications, 1640-1642, (2005).

- 30 *Molecular Spintronics and Quantum Computing*. Journal of Materials Chemistry **19**, 1670-1671, (2009).
- 31 Cornia, A. & Seneor, P. *The Molecular Way*. Nature Materials **16**, 505, (2017).
- 32 Jiang, S., Goß, K., Cervetti, C. & Bogani, L. *An Introduction to Molecular Spintronics*. Vol. 55, (2012).
- 33 Jenkins, M. *et al.* *Coupling Single-Molecule Magnets to Quantum Circuits*. New Journal of Physics **15**, 095007, (2013).
- 34 Schlegel, C., van Slageren, J., Manoli, M., Brechin, E. K. & Dressel, M. *Direct Observation of Quantum Coherence in Single-Molecule Magnets*. Physical Review Letters **101**, 147203, (2008).
- 35 Takahashi, S. *et al.* *Coherent Manipulation and Decoherence of S=10 Single-Molecule Magnets*. Physical Review Letters **102**, 087603, (2009).
- 36 Morley, G. W., Brunel, L.-C. & van Tol, J. *A Multifrequency High-Field Pulsed Electron Paramagnetic Resonance/Electron-Nuclear Double Resonance Spectrometer*. Review of Scientific Instruments **79**, 064703, (2008).
- 37 Stich, T. A. *et al.* *Multifrequency Pulsed EPR Studies of Biologically Relevant Manganese(II) Complexes*. Applied Magnetic Resonance **31**, 321, (2007).
- 38 Yang, Z. *et al.* *Pulsed ESR Dipolar Spectroscopy for Distance Measurements in Immobilized Spin Labeled Proteins in Liquid Solution*. Journal of the American Chemical Society **134**, 9950-9952, (2012).
- 39 Bertaina, S. *et al.* *Quantum Oscillations in a Molecular Magnet*. Nature **466**, 1006, (2010).
- 40 Luis, F., L. Mettes, F., Tejada, J., Gatteschi, D. & Jongh, L. J. *Observation of Quantum Coherence in Mesoscopic Molecular Magnets*. Vol. 85, (2000).
- 41 Bonizzoni, C., Ghirri, A. & Affronte, M. *Coherent Coupling of Molecular Spins with Microwave Photons in Planar Superconducting Resonators*. Vol. 3, (2018).
- 42 Collett, C. *et al.* *A Clock Transition in the Cr7Mn Molecular Nanomagnet*. Vol. 5, (2019).
- 43 Liu, J. *et al.* *Electric Field Control of Spins in Molecular Magnets*. Physical Review Letters **122**, 037202, (2019).
- 44 Shiddiq, M. *et al.* *Enhancing Coherence in Molecular Spin Qubits via Atomic Clock Transitions*. Nature **531**, 348, (2016).
- 45 Takahashi, S. *et al.* *Decoherence in Crystals of Quantum Molecular Magnets*. Nature **476**, 76, (2011).

- 46 Bal, M. *et al.* *Non-Equilibrium Magnetization Dynamics in the Fe₈ Single-Molecule Magnet Induced by High-Intensity Microwave Radiation*. *Europhysics Letters (EPL)* **71**, 110-116, (2005).
- 47 Jenkins, T. *et al.* *Controlled Dimerization of Mn₁₂ Single-Molecule Magnets*. **56**, 14755-14758, (2017).
- 48 Godfrin, C. *et al.* *Operating Quantum States in Single Magnetic Molecules: Implementation of Grover's Quantum Algorithm*. *Physical Review Letters* **119**, 187702, (2017).
- 49 Godfrin, C. *et al.* *Electrical Read-Out of a Single Spin Using an Exchange-Coupled Quantum Dot*. *ACS nano* **11**, 3984-3989, (2017).
- 50 Affronte, M. *et al.* *Single Molecule Magnets for Quantum Computation*. *Journal of Physics D: Applied Physics* **40**, 2999-3004, (2007).
- 51 Moreno-Pineda, E., Godfrin, C., Balestro, F., Wernsdorfer, W. & Ruben, M. *Molecular Spin Qudits for Quantum Algorithms*. *Chemical Society reviews* **47**, 501-513, (2018).
- 52 Moreno-Pineda, E. *et al.* *Observation of Cooperative Electronic Quantum Tunneling: Increasing Accessible Nuclear States in a Molecular Qudit*. *Inorganic Chemistry* **57**, 9873-9879, (2018).
- 53 Morita, T. *et al.* *Comparison of the Magnetic Anisotropy and Spin Relaxation Phenomenon of Dinuclear Terbium(III) Phthalocyaninato Single-Molecule Magnets Using the Geometric Spin Arrangement*. *Journal of the American Chemical Society* **140**, 2995-3007, (2018).
- 54 Ferrando-Soria, J. *et al.* *A Modular Design of Molecular Qubits to Implement Universal Quantum Gates*. *Nature Communications* **7**, 11377, (2016).
- 55 Stamp, P. C. E. & Tupitsyn, I. S. *Coherence Window in the Dynamics of Quantum Nanomagnets*. *Physical Review B* **69**, 014401, (2004).
- 56 Chudnovsky, E. M. *Universal Decoherence in Solids*. *Physical Review Letters* **92**, 120405, (2004).
- 57 Meier, F. & Loss, D. *Electron and Nuclear Spin Dynamics in Antiferromagnetic Molecular Rings*. *Physical Review Letters* **86**, 5373-5376, (2001).
- 58 Morello, A., Stamp, P. C. E. & Tupitsyn, I. S. *Pairwise Decoherence in Coupled Spin Qubit Networks*. *Physical Review Letters* **97**, 207206, (2006).
- 59 de Loubens, G. *et al.* *High Frequency EPR on Dilute Solutions of the Single Molecule Magnet Ni₄*. *Journal of Applied Physics* **103**, 07B910, (2008).
- 60 Habib, F. *et al.* *The Use of Magnetic Dilution To Elucidate the Slow Magnetic Relaxation Effects of a Dy₂ Single-Molecule Magnet*. *Journal of the American Chemical Society* **133**, 8830-8833, (2011).

- 61 Long, J. R. *et al.* *Study of the Influence of Magnetic Dilution over Relaxation P in a Zn/Dy Single-Ion Magnet by Correlation between Luminescence and Magnetism.* RSC Advances **6**, 108810-108818, (2016).
- 62 Titos-Padilla, S. *et al.* *Dilution-Triggered SMM Behavior under Zero Field in a Luminescent Zn₂Dy₂ Tetranuclear Complex Incorporating Carbonato-Bridging Ligands Derived from Atmospheric CO₂ Fixation.* Inorganic Chemistry **52**, 9620-9626, (2013).
- 63 Gregson, M. *et al.* *A Monometallic Lanthanide bis(methanediide) Single Molecule Magnet with a Large Energy Barrier and Complex Spin Relaxation Behaviour.* Chemical Science **7**, 155-165, (2016).
- 64 Takahashi, S., Hanson, R., van Tol, J., Sherwin, M. S. & Awschalom, D. D. *Quenching Spin Decoherence in Diamond through Spin Bath Polarization.* Physical Review Letters **101**, 047601, (2008).
- 65 Yap, Y. S., Tabuchi, Y., Negoro, M., Kagawa, A. & Kitagawa, M. *A Ku Band Pulsed Electron Paramagnetic Resonance Spectrometer using an Arbitrary Waveform Generator for Quantum Control Experiments at milliKelvin Temperatures.* Review of Scientific Instruments **86**, 063110, (2015).
- 66 Jenkins, M. *et al.* *Nanoscale Constrictions in Superconducting Coplanar Waveguide Resonators.* Vol. 105, (2014).
- 67 Quddusi, H. M. *et al.* *On-Chip Integration of High-Frequency Electron Paramagnetic Resonance Spectroscopy and Hall-Effect Magnetometry.* Review of Scientific Instruments **79**, 074703, (2008).
- 68 Weber, R. T. *ELEXSYS E 580 Pulse EPR Spectrometer User's Manual.* Bruker Biospin Corporation, (2001).
- 69 Ranguelova, K. on behalf of Bruker BioSpin Corp. to R. Cebulka. *T₂ Relaxation Time for Bruker Coal Sample*, 2018.

CHAPTER 3: COLLECTIVE COUPLING OF MOLECULAR SPINS TO LOW NUMBERS OF PHOTONS IN THE STRONG COUPLING REGIME

The physics resulting from the rules which govern the interaction of a single photon with a single spin are of extreme interest in the fields of quantum computing and information [1-13]. The field of research that probes this spin-photon coupling in a wide variety of energy ranges is still highly active, incorporating experiments both in the weak coupling regime and the strong coupling regime. In the first chapter I gave a brief introduction of the two regimes, and in the second chapter we looked at an experiment tailored to a weakly coupled system; in the current chapter we will delve deeper into the strong coupling regime, particularly as it relates to low numbers of photons and spins.

The structural monodispersity, the ease of magnetic dilution, and the large tunnel splittings provided by mononuclear SMMs in a solid crystalline form make these types of systems ideal candidates for an experimental investigation into the coupling between the spin of a SMM (in the simplest case, approximated as a two-level atom) and the harmonic excitations of a resonance cavity with a high quality factor (e.g. photons in a superconducting resonator). In particular, some crystalline mononuclear SMMs have been shown to provide a substantially increased spin-photon coupling factor when compared to other spin systems [14] (such as NV centers in diamond) due the involvement of large spins and highly mixed states as well as the high degree of monodispersity, where all spins are identical and feel a radiation field of wavelength larger than the size of the crystal.

By combining this enhanced spin-photon coupling parameter with the intensified applied microwave magnetic field that is expected in an extremely high-quality factor nano-constricted superconducting resonator, one may realize an experimental setup which could feasibly allow measurements of the coherent collective coupling of a set of molecular spins and a very low number of

photons (including, possibly, even a single photon). In fact, the techniques discussed in the following sections may eventually allow reaching the strong coupling regime with a single molecular spin, a something which has not yet been achieved (to our knowledge). Furthering experimental development in this area will likely be transformative to our understanding of the quantum dynamics of various spin systems. The eventual result of our approach here should be to enable further increases in the coupling parameter g by virtue of narrowing the central line of a CPW resonator down to nanometer scales. A similar procedure has been proposed to couple superconducting resonators to the spins of donor defects in both sapphire and diamond [15,16] as well as to flux qubits in the context of advancements in quantum computing [17-25].

3.1 Vacuum Rabi Oscillations

A secondary goal of this dissertation (aside from studying the sources of decoherence in the weak coupling regime) is to explore the possibility to observe the vacuum Rabi splitting which develops in the strong coupling regime, separating the symmetric and antisymmetric spin-photon superposition states as shown previously in Figure 1.12. The spin in a *mononuclear* SMM comes from the single, only, magnetic constituent; in the simplest case this can be approximated by a two-level system with the spin being either in the ground state (for example, spin down) or in the first excited state (for example, spin up). For most SMMs at very low temperatures, this is an excellent approximation as any additional excited states will most likely be well-separated from the two lowest energy states. We thus aim to understand the interaction of this two-level spin system with the various photon modes (or allowed photon wave numbers k_x , k_y , k_z) in a cavity with a high-quality-factor.

3.1.1 The Jaynes-Cummings Hamiltonian, Revisited

In general terms, the coupling between a photon in a resonant cavity and a two-level spin system placed inside can be described by the Jaynes-Cummings Hamiltonian, which as you may recall from the introductory chapter is given by

$$H_{JC} = \frac{\hbar}{2}\omega_0\sigma_z + \hbar\omega a^\dagger a + \hbar g(a^\dagger\sigma^- + a\sigma^+) \quad (3.1)$$

where the first term represents the energy between the split spin levels of the molecule (described as a two-level system), the second term represents the cavity with $N = a^\dagger a$ photons, and the third term accounts for the coupling between the spin and the photon, with g being the rate of creation or annihilation ($\sigma^+ a, \sigma^- a^\dagger$) of a photon. This rate is none other than the so-called vacuum Rabi frequency; that is, it represents the oscillation frequency between a photon existing in some resonant mode of the surrounding cavity, and the spin existing in the energized state. Now, in the absence of spontaneous decay or an external damping force, the coupled spin-photon system will coherently oscillate (that is, remaining in one or the other of two “pure” states, $|1, 0\rangle$ or $|0, 1\rangle$) between an atomic excitation (molecular spin) and a filled photonic mode in the cavity. This oscillation between states is what is known as vacuum Rabi oscillation. It may be interpreted as some vacuum electromagnetic fluctuations which will stimulate photon emission and absorption by the atom to/from the resonant cavity.

The vacuum Rabi frequency, g , may be given by the strength of the Zeeman coupling between the spin, S , and the magnetic field of the cavity vacuum fluctuations, B_{RF} , as below

$$g \equiv f_{Rabi} = \frac{2g_L\mu_B S B_{RF}}{\hbar} \quad (3.2)$$

where g_L is the Landé g-factor. Recall that this g-factor belongs to an electron with both spin and orbital angular momentum and is used to describe the energy levels of an atom in a weak magnetic field as

$$g_L \approx 1 + \frac{j(j+1) + s(s+1) - l(l+1)}{2j(j+1)} \approx 2 \quad (3.3)$$

(with $J = \sqrt{j(j+1)}$, $S = \sqrt{s(s+1)}$, $L = \sqrt{l(l+1)}$ being the total, spin, and orbital angular momenta, respectively). In order for coherent oscillations to be made possible, that is, for more than one exchange of energy to occur observably, the Rabi frequency must overcome the inherent decay rates of both the photon and the spin lifetimes. For a cavity of loaded quality factor Q_L , the decay rate k_{photon} of an excitation (i.e., a populated photon mode) at resonance ($E = \hbar\omega_r$) is given by

$$k_{\text{photon}} = \frac{\omega_r}{Q_L} \quad (3.4)$$

[26]. In the case of a two-level SMM spin system, the lifetime decay of the excited spin state may be expressed by the decoherence rate

$$\gamma_\varphi = \frac{\hbar}{T_2 \Delta_0} \quad (3.5)$$

(where T_2 is the spin-spin relaxation time and Δ_0 is the tunnel splitting between the two spin states), which is governed by the dephasing sources that have been discussed in previous chapters (magnon, phonon, and nuclear). Thus, for a cavity with a resonant frequency of 10 GHz and Q-factor 10,000, k_{photon} is on the order of 1 MHz; for the Fe_8 SMM discussed in Figure 1.11, at 100 mK and magnetic fields of less than 1 T, γ_φ may be on the order of 10 MHz. When a large number of coherent oscillations are completed before the photon exits the cavity or the atom decays, the system is considered to have reached the Quantum Electrodynamics (QED) strong coupling limit:

$$n_{Rabi} = \frac{2g}{k_{photon} + \gamma_{\varphi}} \quad (3.6)$$

(n_{Rabi} being the number of Rabi oscillations).

It is possible to enhance the coupling parameter g by utilizing two separate approaches. One may attempt coupling of a single photon cavity mode coherently to a large number of spins all at once (corresponding to the situation studied by Tavis and Cummings in [27], where the Rabi splitting was enhanced by a factor of \sqrt{N}). This method has already been successfully demonstrated in a wide assortment of low-spin systems, including NV centers in diamond [28], standard EPR materials [29,30], N-doped buckyballs [31], and Cr impurities in ruby [16] among other systems with larger numbers of spins [32,33]. However, one may instead (or in addition) attempt to approach the issue by involving smaller numbers of large individual spins, using materials with strongly mixed spin states (as may be found in some mononuclear SMMs [14]), or by technically improving the resonator (for example, increasing the quality-factor or the concentration of the microwave magnetic field at the sample position). This second class of methods may even eventually provide a way of strongly coupling a single spin to a single photon; they are the focus of our approach to the strong coupling regime.

3.2 The Strong Coupling Limit: The Story so Far

A significant amount of energy has been devoted in recent years to improving the coupling between potential qubits and QED circuits. Molecular spins in particular have elicited interest in this regard. Efforts to reach the strong coupling regime with spin ensembles have begun to bear fruit, although as yet there seems to be no concrete evidence of doing so with a single qubit-photon system. Bonizzoni, et. al. have recently published their work on coherent coupling of molecular spins to planar superconducting resonators [34,35], illustrating the difference between weak and strong coupling in

various systems (see Figure 3.1). Coherent Rabi oscillations have been observed in several systems, including in a gadolinium-doped CaWO_4 single crystal (an example is shown in Figure 3.2).

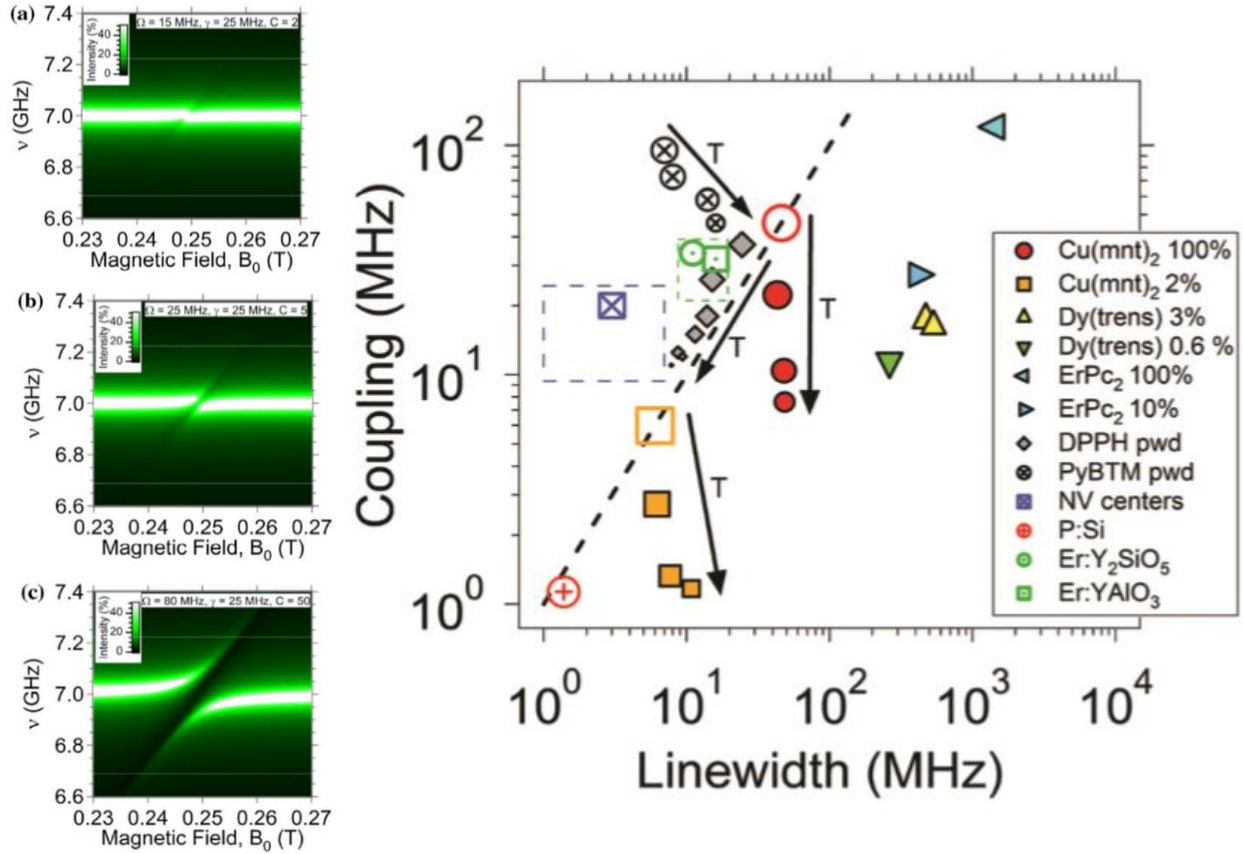


Figure 3.1: Coupling Regimes in Microstrip Resonators

Left: Simulated transmission spectra for a YBCO coplanar resonator in the weak coupling (a), high cooperativity (b), and strong coupling (c) regimes [34]. The peak splitting indicative of strong coupling clearly emerges at resonance. Right: Coupling parameter g plotted vs spin linewidth (lifetime) γ_ϕ for various spin systems. The dashed line represents the boundary between weak and strong coupling, where $g = \gamma_\phi$. Data for the same compound taken at different temperatures T are marked by the solid black arrows as well as the size of the symbol, with a larger symbol meaning a higher temperature [35].

Increasingly high blocking temperatures have been reported in lanthanide SMM complexes [36-38], up to and including liquid nitrogen temperatures [39]. Various resonators specifically designed for high quality factors are being designed, including microstrip [40] and loop-gap resonators [41,42], and perhaps most

exciting has been the recent successful implementation of a quantum algorithm using a SMM by Godfrin, et. al. [43].

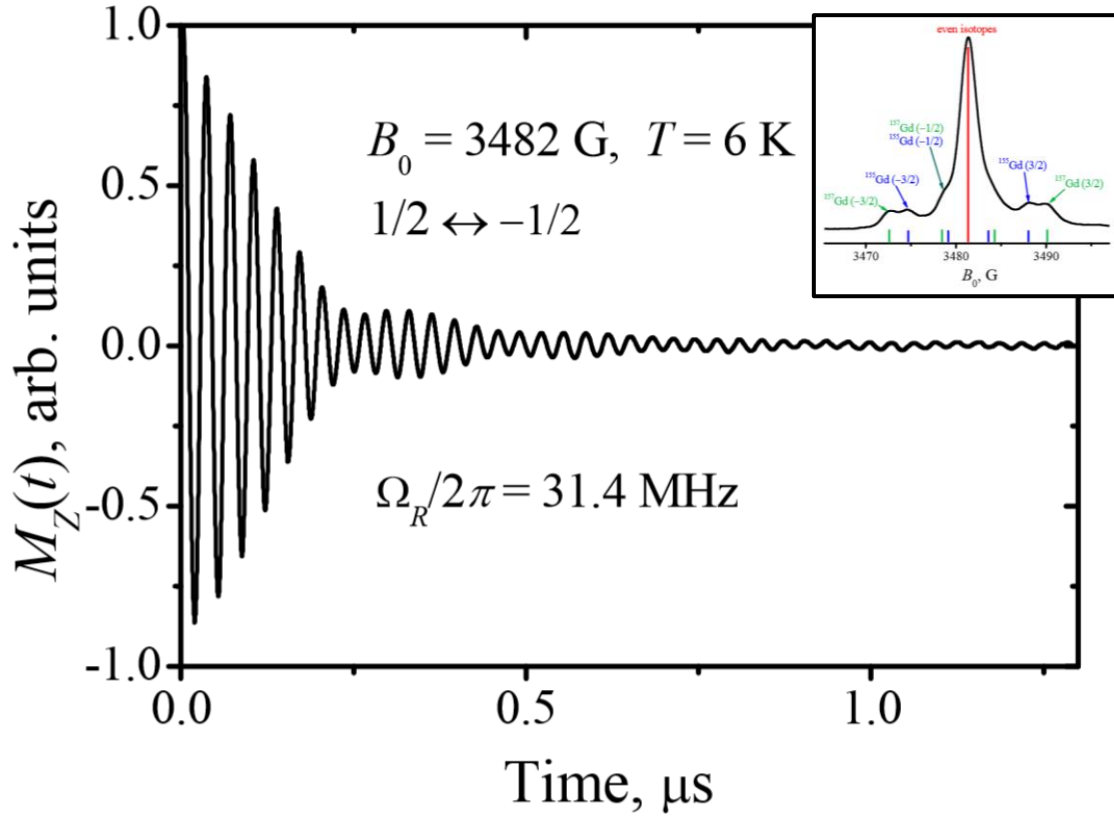


Figure 3.2: Coherent Rabi Oscillations in Gd-doped CaWO_4

Rabi oscillations between the $S = +1/2$ and $S = -1/2$ states for Gd-doped CaWO_4 obtained in a cylindrical cavity resonator at 6K and 9.75 GHz. Inset: EPR spectrum of the $m = +1/2$ to $-1/2$ EPR transition, showing fine structure contributions due to additional Gd isotopes present in the crystal. [44]

3.2.1 An Example: Fe_8

In addition to the studies of low-spin systems described above, spectroscopic observation of the vacuum Rabi splitting in SMMs has been reported by Jonathan Friedman and his research group [45]. Their experiment was performed at 4 K, with a standard EPR cylindrical cavity with a resonant frequency of approximately 150 GHz, a quality factor of about 1000, and a large number of photons ($N \approx 10^8$) which

were coupled to a single solid crystal of undiluted Fe_8 . However, the authors did note that when accounting for the degree of dispersion that is typically present in a crystal of Fe_8 (that is, the degree to which the individual single molecules of Fe_8 do not behave uniformly), they were unclear as to how each molecule could be simultaneously meeting the requirements to achieve coherent coupling.

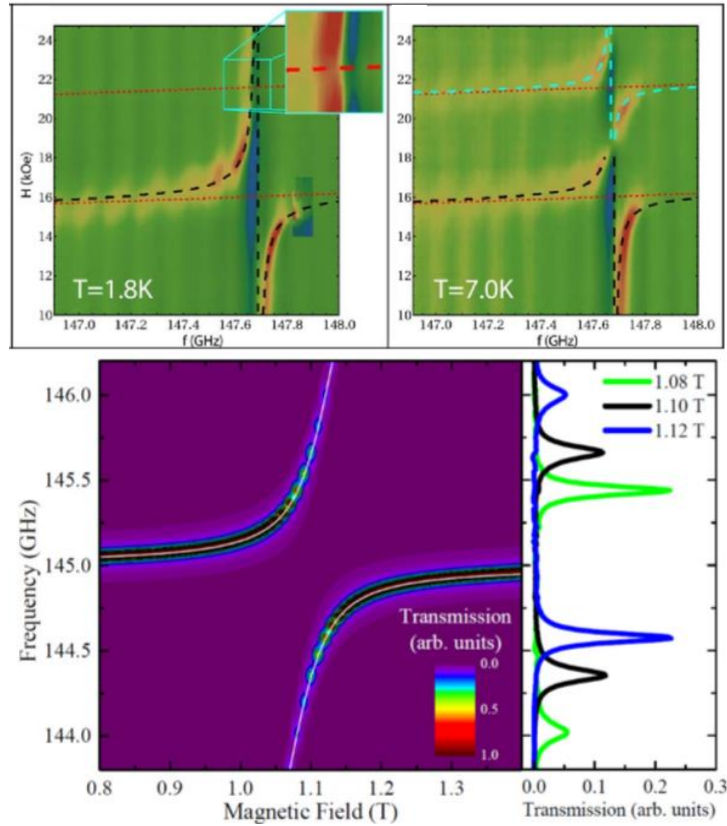


Figure 3.3: Strong Coupling in Fe_8

Top: Power absorption (red and yellow indicate significant absorption) as a function of magnetic field H and frequency f at $T = 1.8$ K (left) and $T = 7$ K (right) for Fe_8 in a cylindrical cavity. The lower dashed red line represents the ground state $m = -10$ to -9 transition, while the upper dashed red line represents the first excited state (populated only for higher temperatures) $m = -9$ to -8 transition [45]. Bottom: Transmission as a function of magnetic field and frequency at $T = 3$ K for the Fe_8 $m = -10$ to -9 transition in a cylindrical cavity. The right panel displays a cross section of the transmission at three distinct magnetic fields, clearly showing the peak splitting inherent to the strong coupling regime [46].

Indeed, the dephasing rate γ_φ for Fe_8 at temperatures near 4K is influenced heavily by dipolar fluctuations and as a consequence is quite fast, with $\gamma_\varphi \sim 10^9$ Hz; due to the \sqrt{N} dependence, this necessitates coupling to greater than 10^{16} individual SMM spins within the crystal to even barely reach the strong coupling regime and requires a very fast Rabi frequency on the order of γ_φ , or 1 GHz. Figure 3.3 shows their results, along with results from Muhandis Shiddiq concerning the same compound.

3.2.2 Magnetic Dilution

As discussed in the first chapter, coherence in a magnetically diluted SMM crystal (as well as in spin-polarized systems which have not been diluted) is constrained primarily by phonon and nuclear dephasing, with some recent results [47] demonstrating lifetimes of up to 40 μs . This would suggest that dephasing rates $\gamma_\varphi = 0.1$ MHz or lower can be expected in magnetically dilute systems. Our nano-constricted superconducting resonators that will be discussed in the next section have a high quality factor ($Q \approx 10^5 - 10^6$), which should guarantee photon lifetimes of 100 μs or larger (corresponding to $k_{\text{photon}} \approx 0.01$ MHz). Thus, the dephasing in the spin system should become the limiting factor on the number of coherent vacuum Rabi oscillations. In other words (or equations),

$$k_{\text{photon}} \ll \gamma_\varphi; \quad k_{\text{photon}} + \gamma_\varphi \approx \gamma_\varphi. \quad (3.7)$$

While these lifetimes may still be two orders of magnitude smaller than those found in NV centers in diamond [28], we may be able to enhance the coupling parameter g by almost two orders of magnitude by virtue of the high spin and large tunnel splittings which may be supplied in some SMMs. As shown in [14,37,38], lanthanide-based mononuclear SMMs (e.g., TbW_{30} or GdW_{30}) are the most reliable options for this approach of coupling enhancement, due to their easily obtainable large tunnel splittings and comparably high resistance to decoherence. In case of point, the increase in the coupling parameter that

may be provided by the large spins and tunneling states in some lanthanide-based mononuclear SMMs, when combined with high quality factor superconducting resonators which utilize nano-constrictions, may even allow the feasibility of strongly coupling a single photon cavity mode with a single molecular spin, something which to our knowledge has not yet been achieved.

3.3 Superconducting, Nano-constricted, CPW Resonators

Portions of this section have been written using references [26,48-50].

Over the course of many years, a large number of different resonant/traveling wave microwave apparatuses have been utilized in EPR studies. Three commonly used variants are microwave cavities, in which microwaves are confined within a hollow (or dielectric-filled) physical cavity to form standing waves at resonance between the walls; loop-gap resonators, in which microwaves are either inductively (through a wire loop above a circular hole) or capacitively (through a straight wire above a straight-edged gap) coupled to the cavity-like resonator; and planar resonators, including microstrip (a single transmission line of a specific length) and coplanar waveguide (a center transmission line of specific length with “infinite” grounding planes on both sides) configurations. Figure 3.4 illustrates the difference between these resonant geometries.

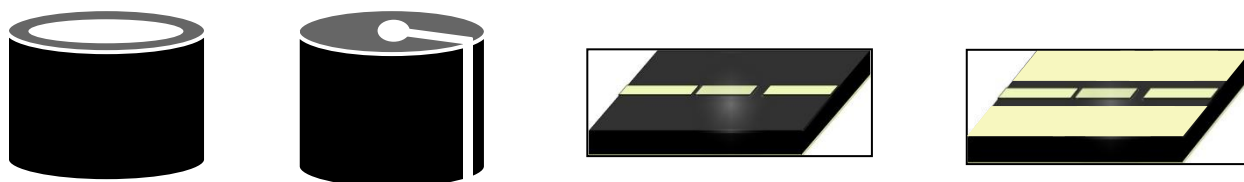


Figure 3.4: Resonant Geometries

Left: Schematic of a cylindrical resonant cavity. Middle left: Schematic of a loop-gap resonator. Middle right: Schematic of a microstrip planar resonator. Right: Schematic of a CPW planar resonator.

Microwave cavities work well at high frequencies and can have impressive quality factors combined with simple manufacturing requirements, but at low frequencies the dimensions required

become prohibitively large. Loop-gap resonators are slightly more challenging to machine but are comparatively easy to tune to match the sample resonance while allowing for a higher filling factor with small samples, and are commonly used for EPR measurements below X-band frequencies. Above about 7 GHz, however, the dimensions required are so small that they become impractical to machine. As a side project, we actually attempted to machine an 8.5 GHz loop-gap resonator made of OFHC copper by use of electrical discharge machining (EDM), the only viable machining method due to the size of the smallest dimension being 67 ten-thousandths of an inch (see Figure 3.5). Unfortunately, we were unable to achieve a quality factor greater than that of the microstrip resonators used in the second chapter, and didn't end up using it in any experiments due to technical concerns. Microstrip resonators were used in the previous chapter; they typically have a lower quality factor and higher losses when compared to their CPW counterparts (making them ideal for weak coupling experiments). However, for strong coupling, CPW resonators are significantly better since radiative losses are minimized due to the grounding planes. Making the conductor a superconductor will reduce heating and radiative power loss even further. Finally, narrowing the central resonator line to a nano-constriction will enhance the microwave magnetic field strength at the sample location, and thus the coupling to the sample, by huge amounts. This is the idea behind the design of our nano-constricted superconducting resonators.

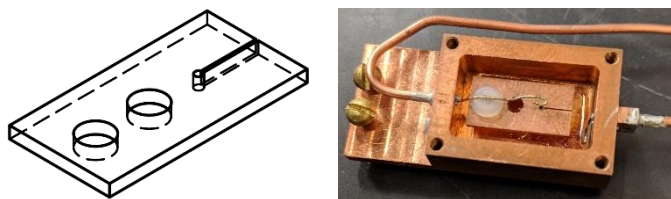


Figure 3.5: Our Loop-Gap Resonator

Our attempted 8.5 GHz loop-gap resonator. Left: Schematic. Right: Image of the loop-gap resonator in its housing box.

The ultimate goal of our investigations into the strong coupling regime will be to continue increasing the coupling parameter g by narrowing the center line of the coplanar waveguide (CPW) resonator down to nanometer scales. These nano-constrictions greatly increase the AC current in the constricted portion of the resonator, corresponding to a significant increase of the microwave magnetic field at the sample position and thus an enhancement of the coupling parameter. It has been estimated that the enhancement due to these nano-constrictions can reach approximately two orders of magnitude, effectively increasing the coupling parameter to $g \approx 0.2$ MHz so as to overcome the intrinsic dephasing times in SMMs and work towards allowing strong coupling between a single cavity mode and a single molecular spin [14].

3.3.1 Design

CPW resonators are at heart simple devices consisting of a regular CPW device constrained to the length of one half of the resonant wavelength and capacitively coupled to the feed lines by two gaps. The fundamental mode frequency is calculated from

$$f_0 = \frac{c}{2l\sqrt{\epsilon_{eff}}} \quad (3.8)$$

where l is the resonator length and ϵ_{eff} is the effective dielectric constant, which depends on the dimensions of the resonator and dielectric properties of the surroundings (c is the speed of light) [14]. We have designed a series of different coupling gap dimensions, chosen blindly to both over-couple and under-couple the resonator to the feedlines, as well as two distinct gap styles: direct and interlocked, as shown in Figure 3.6; the optimal geometry will be identified by characterization of the resonators. Resonator lengths corresponding to frequencies between 7 GHz and 14 GHz have been used.

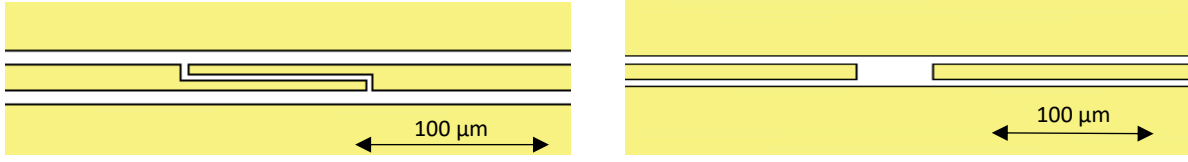


Figure 3.6: Interlocked and Direct Coupling Gaps

Close up of the different types of coupling gaps present in the nano-constricted portion of the resonators, including interlocked (left) and direct (right).

The behavior of this type of resonator can be approximated as a series of parallel LRC circuits coupled to an input and transmission line (see Figure 3.7) [26]. They can be modelled as a combination of many small lumped elements with identical impedances, with each section having a resistance, inductance, conductance, and capacitance (per unit length) of R_l, L_l, G_l , and C_l , respectively. Therefore, each section will have an impedance of

$$Z_0 = \sqrt{\frac{R_l + j\omega L_l}{G_l + j\omega C_l}}. \quad (3.9)$$

For the fundamental mode (corresponding to f_0), the properties for the full length of the transmission line (length = l) can be found to be $R = R_l * l$ (resistance); $C = \frac{C_l * l}{2}$ (capacitance); $L = \frac{2L_l * l}{\pi^2}$ (inductance); and $Z_c = \frac{2Z_0}{\pi}$ (impedance). If we now capacitively couple the resonator/transmission line to both an input and transmission line, we introduce an effective capacitance C_{eff} which shifts the resonant frequency, and resistance (in parallel) R_{eff} which changes the quality factor. The loaded quality factor for this coupled transmission line is then

$$Q_L = \frac{1}{\frac{1}{Q_{ext}} + \frac{1}{Q_{int}}} \quad (3.10)$$

with $\frac{1}{Q_{ext}} = \omega^2 C_{eff}^2 Z_0 Z_c$ and $\frac{1}{Q_{int}} = \frac{Z_c}{R}$.

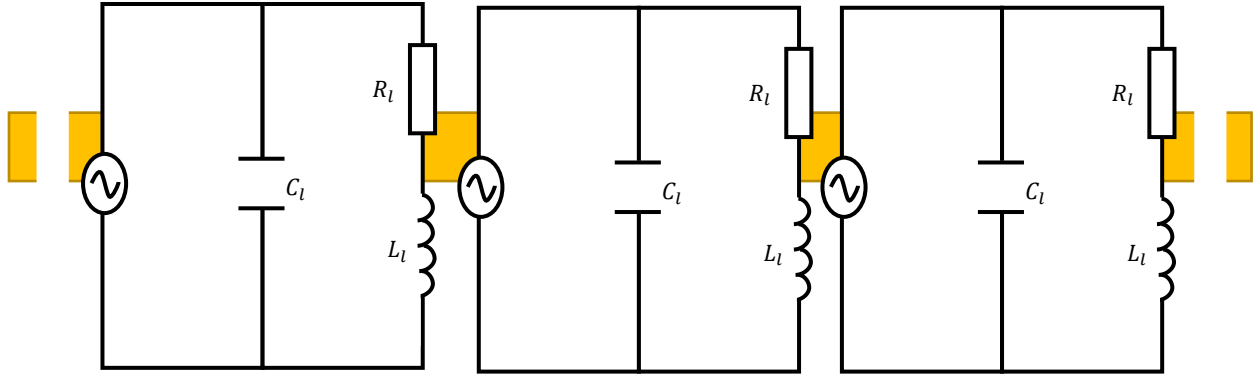


Figure 3.7: The Parallel LRC Circuit

Approximation of the resonator transmission line as a series of parallel LRC circuits.

Just like in a normal transmission line, the electromagnetic radiation mode in a CPW resonator can be described as a current/voltage wave, with the central line current being equal and opposite to the ground plate current (a conducting backing plate may also be employed to both increase thermal connection with the housing box and assist in isolating the resonator line). The zero-point energy of a CPW resonator is stored equally as voltage in the capacitor and current in the inductor of the equivalent lumped element (parallel LRC oscillator). Using estimated values of our devices' parameters L and C for the fundamental resonance of a 7 GHz resonator [51], we find vacuum voltage and current fluctuations to be $V_0 = 1.8 \mu\text{V}$ and $I_0 = 58 \text{ nA}$, respectively. While this works well enough for coupling a cavity photon with a *charge*-based atom (for example, a Cooper-box [26]), where the coupling depends on the electric field between the center line and the ground plane which is typically rather large (E_0 on the order of 0.2 V/m) and you may see vacuum Rabi frequencies in the range of 200 MHz [52], it does not work nearly as well when trying to couple the photon to a *spin*-based atom. This is quite simply due to the fact that the vacuum microwave magnetic field is weaker than the electric field by a factor of c , the speed of light. Using a spin of $S = 1/2$ in (3.2) for the same parameters gives a vacuum Rabi frequency of only $g \approx 100$ Hz. However, this coupling can be enhanced by several orders of magnitude by virtue of combining the

specific nano-engineering of the resonators described here with the high spin and large tunnel-splitting in SMMs, bringing the coupling up to $g \approx 0.2$ MHz [14], making it larger than the spin dephasing rate γ_ϕ .

3.3.2 Fabrication

A series of different micro-coplanar waveguide resonators with $Q > 10^4$ for experiments requiring an enhanced coupling parameter by way of a large microwave magnetic field have been successfully fabricated for frequencies of 7 GHz (central line length of 8 mm) and 14 GHz (central line length of 4 mm). The principle method of operation is designed to work by means of a high temperature/high field superconducting film (YBCO) grown atop a sapphire substrate.

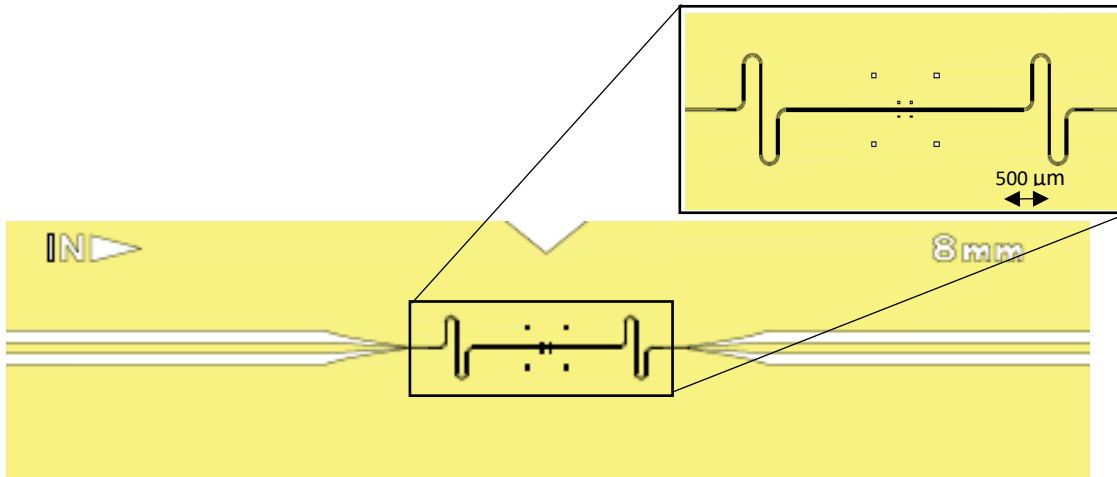


Figure 3.8: CPW Resonator Design

AutoCAD design for one of the interlock-gap 7 GHz CPW resonators. 14 GHz geometries were also fabricated. Outset: Close up of the constricted portion of the resonator.

One such resonator design is shown in Figure 3.8. In each case, the resonator dimensions have been calculated to maximize the unloaded quality factor while maintaining a 50Ω impedance [26,51-53]. Symmetric direct or interdigitated coupling gaps separate the resonator from the input and transmission lines, with gap and central line dimensions set at discrete intervals to allow the opportunity to study both over-and under-coupled resonators at multiple frequencies [51]. They have been designed for a 330 nm

YBCO film deposited on both sides (one as a backing plate, one for patterning) of a 430 μm thick sapphire substrate. 7 GHz and 14 GHz resonators designed for $Q > 10^4$ have already been fabricated by STAR Cryo-electronics, and were recently received by our lab.

The outset in Figure 3.8 shows a micro-constriction embedded into the central line of the resonator, where the microwave magnetic field becomes largest at the fundamental resonance mode. Further narrowing of this constriction, down to nano-scales, will allow for a large enhancement of the microwave magnetic field at the micro-constriction location. Together with the enhancement in the spin-photon coupling offered by some mononuclear lanthanide SMMs, this is imperative for reaching the strong coupling regime between the cavity mode and a reduced number of spins. This should enable a real potential of achieving strong coupling to a single spin for the first time.

3.4 Conclusions

CPW resonators to our specifications have been purchased from and fabricated by STAR Cryo-electronics, with various dimensions and geometries of coupling gaps as well as two different lengths of the central line corresponding to a 7 GHz and 14 GHz resonance. We plan to characterize the different resonator gap lengths and designs to observe performance at magnetic fields up to at least 1 Tesla and temperatures below 100mK. The microwave current density achieved in the constricted area of the resonator for powers above 0 dBm overcomes the critical current density of YBCO at the constriction (center of the line), where the maximum current density is reached for the fundamental resonant mode [14]. This is indicative that the ac current is greatly enhanced in the vicinity of the constricted section of the resonator, which in turn translates into a substantial increase of the ac magnetic field at the sample position, ultimately enhancing the coupling parameter g . The estimated enhancement in the microwave magnetic field in nano-constricted resonators can reach two orders of magnitude, bringing the coupling

parameter up to $g \approx 0.2$ MHz, hopefully overcoming the intrinsic dephasing in SMMs and allowing for strong coupling between a cavity mode and low numbers of spins.

Eventually we plan to study the coupling between a superconducting cavity mode and mononuclear lanthanide-based SMMs in the strong coupling regime. Both single-crystals and isolated molecules deposited on the surface of the resonators will be investigated. Initially the hope is to use these resonators to observe the coherent collective coupling of a large number of spins with a single cavity mode, which will be made possible by the high degree of monodispersity found in single crystals of mononuclear SMMs, where all spins are identical and feel a radiation field of wavelength larger than the size of the crystal. According to the estimates given earlier ($g \approx 0.2$ MHz, $k_{photon} \approx 0.01$ MHz, and $\gamma_\varphi \approx 0.1$ MHz), $N > 100$ molecular spins coherently coupled to a superconducting cavity would be sufficient to generate Rabi oscillations at a rate faster than the system dephasing. Note that a typical magnetically dilute (0.001%) crystal of mononuclear SMMs, with a volume of $10^3 \mu\text{m}^3$, contains roughly 10^{12} molecular spins. In fact, the low number of molecules required to achieve the strong coupling regime will allow the possibility of working with molecules directly deposited on top of the surface of the resonators, rather than a large crystal. In addition, experiments employing ultra-low power microwave stimuli may be performed in order to perform measurements with a low number of photons in the cavity, with the objective of observing the coherent collective coupling of a low number of molecular spins with a single photon. Note that at

$$T = 40 \text{ mK} \left(< T_0 = \frac{\hbar\omega_n}{k_B} = 340 \text{ mK} \right) \quad (3.11)$$

a 10 GHz resonator is in its ground state with a thermal occupancy of $N_{photon} = 0.033$ (number of photons in the cavity). Future efforts are focused on improving the assembly of the microwave lines, and thermalization and cryogenic amplification stages in the dilution cryostat that will enable measurements with an extremely low number of photons.

References

- 1 Wernsdorfer, W., Aliaga-Alcalde, N., Hendrickson, D. N. & Christou, G. *Exchange-Biased Quantum Tunnelling in a Supramolecular Dimer of Single-Molecule Magnets*. Nature **416**, 406, (2002).
- 2 Hill, S., Edwards, R. S., Aliaga-Alcalde, N. & Christou, G. *Quantum Coherence in an Exchange-Coupled Dimer of Single-Molecule Magnets*. Science **302**, 1015, (2003).
- 3 del Barco, E., Kent, A. D., Yang, E. C. & Hendrickson, D. N. *Quantum Superposition of High Spin States in the Single Molecule Magnet Ni₄*. Physical Review Letters **93**, 157202, (2004).
- 4 de Loubens, G., Garanin, D. A., Beedle, C. C., Hendrickson, D. N. & Kent, A. D. *Magnetization Relaxation in the Single-Molecule Magnet Ni₄ Under Continuous Microwave Irradiation*. EPL (Europhysics Letters) **83**, 37006, (2008).
- 5 Quddusi, H. M. *et al.* *Asymmetric Berry-Phase Interference Patterns in a Single-Molecule Magnet*. Physical Review Letters **106**, 227201, (2011).
- 6 Leuenberger, M. N. & Loss, D. *Quantum Computing in Molecular Magnets*. Nature **410**, 789, (2001).
- 7 Tejada, J., Chudnovsky, E. M., Barco, E. del, Hernandez, J. M. & Spiller, T. P. *Magnetic Qubits as Hardware for Quantum Computers*. Nanotechnology **12**, 181-186, (2001).
- 8 Stamp, P. C. E. & Gaita-Ariño, A. *Spin-based Quantum Computers Made by Chemistry: Hows and Whys*. Journal of Materials Chemistry **19**, 1718-1730, (2009).
- 9 Affronte, M. *Molecular Nanomagnets for Information Technologies*. Journal of Materials Chemistry **19**, 1731-1737, (2009).
- 10 Lehmann, J., Gaita-Ariño, A., Coronado, E. & Loss, D. *Quantum Computing with Molecular Spin Systems*. Journal of Materials Chemistry **19**, 1672-1677, (2009).
- 11 Affronte, M. *et al.* *Single Molecule Magnets for Quantum Computation*. Journal of Physics D: Applied Physics **40**, 2999-3004, (2007).
- 12 Chiolero, A. & Loss, D. *Macroscopic Quantum Coherence in Molecular Magnets*. Physical Review Letters **80**, 169-172, (1998).
- 13 Bal, M. *et al.* *Non-Equilibrium Magnetization Dynamics in the Fe₈ Single-Molecule Magnet Induced by High-Intensity Microwave Radiation*. Europhysics Letters (EPL) **71**, 110-116, (2005).
- 14 Jenkins, M. *et al.* *Coupling Single-Molecule Magnets to Quantum Circuits*. New Journal of Physics **15**, 095007, (2013).
- 15 Kubo, Y. *et al.* *Strong Coupling of a Spin Ensemble to a Superconducting Resonator*. Physical Review Letters **105**, 140502, (2010).

- 16 Schuster, D. I. *et al. High-Cooperativity Coupling of Electron-Spin Ensembles to Superconducting Cavities*. Physical Review Letters **105**, 140501, (2010).
- 17 Abdumalikov, A. A., Astafiev, O., Nakamura, Y., Pashkin, Y.A. & Tsai, J. *Vacuum Rabi Splitting due to Strong Coupling of a Flux Qubit and a Coplanar-Waveguide Resonator*. Physical Review B **78**, 180502, (2008).
- 18 Jerger, M. *Experiments on Superconducting Qubits Coupled to Resonators* Doctor of Science thesis, Karlsruhe Institute of Technology, (2013).
- 19 Fedorov, A. *et al. Strong Coupling of a Quantum Oscillator to a Flux Qubit at Its Symmetry Point*. Physical Review Letters **105**, 060503, (2010).
- 20 Forn-Diaz, P. *Superconducting Qubits and Quantum Resonators* Doctor of Philosophy thesis, Barcelona Supercomputing Center, (2010).
- 21 Kakuyanagi, K. *et al. Observation of Collective Coupling between an Engineered Ensemble of Macroscopic Artificial Atoms and a Superconducting Resonator*. Physical Review Letters **117**, 210503, (2016).
- 22 Kemp, A., Saito, S., Munro, W. J., Nemoto, K. & Semba, K. *Superconducting Qubit as a Quantum Transformer Routing Entanglement Between a Microscopic Quantum Memory and a Macroscopic Resonator*. Physical Review B **84**, 104505, (2011).
- 23 Omelyanchouk, A. N., Shevchenko, S. N., Greenberg, Ya S., Astafiev, O. & Il'ichev, E. *Quantum Behavior of a Flux Qubit Coupled to a Resonator*. Low Temperature Physics **36**, 893-901, (2010).
- 24 Yamamoto, T. *et al. Superconducting Flux Qubit Capacitively Coupled to an LC Resonator*. New Journal of Physics **16**, 015017, (2014).
- 25 Yu, D., Kwek, L. C., Amico, L. & Dumke, R. *Superconducting Qubit-Resonator-Atom Hybrid System*. Quantum Science and Technology **2**, 035005, (2017).
- 26 Schuster, D. *Circuit Quantum Electrodynamics* Doctor of Philosophy thesis, Yale University, (2007).
- 27 Tavis, M. & Cummings, F. W. *Exact Solution for an N-Molecule-Radiation-Field Hamiltonian*. Physical Review **170**, 379-384, (1968).
- 28 Balasubramanian, G. *et al. Ultralong Spin Coherence Time in Isotopically Engineered Diamond*. Nature Materials **8**, 383, (2009).
- 29 Abe, E., Wu, H., Ardavan, A. & Morton, J. J. L. *Electron Spin Ensemble Strongly Coupled to a Three-Dimensional Microwave Cavity*. Applied Physics Letters **98**, 251108, (2011).
- 30 Chiorescu, I., Groll, N., Bertaina, S., Mori, T. & Miyashita, S. *Magnetic Strong Coupling in a Spin-Photon System and Transition to Classical Regime*. Physical Review B **82**, 024413, (2010).

- 31 Wu, H. *et al.* *Storage of Multiple Coherent Microwave Excitations in an Electron Spin Ensemble*. Physical Review Letters **105**, 140503, (2010).
- 32 Probst, S. *et al.* *Anisotropic Rare-Earth Spin Ensemble Strongly Coupled to a Superconducting Resonator*. Physical Review Letters **110**, 157001, (2013).
- 33 Ranjan, V. *et al.* *Probing Dynamics of an Electron-Spin Ensemble via a Superconducting Resonator*. Physical Review Letters **110**, 067004, (2013).
- 34 Bonizzoni, C., Ghirri, A. & Affronte, M. *Coherent Coupling of Molecular Spins with Microwave Photons in Planar Superconducting Resonators*. Vol. 3, (2018).
- 35 Bonizzoni, C. *et al.* *Coupling Molecular Spin Centers to Microwave Planar Resonators: Towards Integration of Molecular Qubits in Quantum Circuits*. Dalton Trans **45**, 16596-16603, (2016).
- 36 Le Roy, J. J., Ungur, L., Korobkov, I., Chibotaru, L. F. & Murugesu, M. *Coupling Strategies to Enhance Single-Molecule Magnet Properties of Erbium–Cyclooctatetraenyl Complexes*. Journal of the American Chemical Society **136**, 8003-8010, (2014).
- 37 Prodius, D. *et al.* *Influence of Lanthanides on Spin-Relaxation and Spin-Structure in a Family of Fe7Ln4 Single Molecule Magnets*. Journal of Materials Chemistry C **6**, 2862-2872, (2018).
- 38 Zhang, P., Zhang, L. & Tang, J. *Lanthanide Single Molecule Magnets: Progress and Perspective*. Dalton Transactions **44**, 3923-3929, (2015).
- 39 Guo, F.-S. *et al.* *Magnetic Hysteresis up to 80 Kelvin in a Dysprosium Metallocene Single-Molecule Magnet*. Science **362**, 1400, (2018).
- 40 Torrezan, A. C., Mayer Alegre, T. P. & Medeiros-Ribeiro, G. *Microstrip Resonators for Electron Paramagnetic Resonance Experiments*. Review of Scientific Instruments **80**, 075111, (2009).
- 41 Friedman, J. R. *Loop Gap Resonators for Spin Resonance Spectroscopy*. United States patent (2019).
- 42 Eisenach, E. R. *et al.* *Broadband Loop Gap Resonator for Nitrogen Vacancy Centers in Diamond*. Review of Scientific Instruments **89**, 094705, (2018).
- 43 Godfrin, C. *et al.* *Operating Quantum States in Single Magnetic Molecules: Implementation of Grover's Quantum Algorithm*. Physical Review Letters **119**, 187702, (2017).
- 44 Baibekov, E. *et al.* *Coherent Spin Dynamics in Gadolinium-doped CaWO4 Crystal*. **95**, (2016).
- 45 Eddins, A. W., Beedle, C., Hendrickson, D. & Friedman, J. R. *Collective Coupling of a Macroscopic Number of Single-Molecule Magnets with a Microwave Cavity Mode*. **112**, 120501, (2014).
- 46 Shiddiq, M. *Quantum Entanglement and Coherence in Molecular Magnets* Doctor of Philosophy thesis, Florida State University, (2015).

- 47 Bader, K. *et al.* *Room Temperature Quantum Coherence in a Potential Molecular Qubit*. Nature Communications **5**, 5304, (2014).
- 48 Krawczyk, M. *Microstrip Resonators for Circuit Quantum Electrodynamics* Masters thesis, Technische Universität München, (2011).
- 49 Lewin, W. in *Wave Guides & Resonant Cavities* (MIT OpenCourseWare, <https://ocw.mit.edu/>. License: Creative Commons BY-NC-SA, Massachusetts Institute of Technology, Fall 2012).
- 50 Atkinson, J. H. *Internal Degrees of Freedom and Spin Transitions in Single Molecule Magnets* Doctor of Philosophy thesis, University of Central Florida, (2016).
- 51 Göppl, M. *et al.* *Coplanar Waveguide Resonators for Circuit Quantum Electrodynamics*. Journal of Applied Physics **104**, 113904, (2008).
- 52 Wallraff, A. *et al.* *Strong Coupling of a Single Photon to a Superconducting Qubit using Circuit Quantum Electrodynamics*. Nature **431**, 162, (2004).
- 53 Frunzio, L., Wallraff, A., Schuster, D., Majer, J. & Schoelkopf, R. *Fabrication and Characterization of Superconducting Circuit QED Devices for Quantum Computation*. IEEE Transactions on Applied Superconductivity **15**, 860-863, (2005).

CHAPTER 4: THE IMPACT OF SERVICE-LEARNING COURSEWORK ON UNDERGRADUATE STUDENTS' LERANING PROCESS

The material presented in this chapter is based on the paper "Assessment of the Effect of Service-Learning in Nanoscience on Student's Depth of Learning and Critical Thinking", published in Volume 6 Issue 1 of PRISM: A Journal of Regional Engagement. The authors are myself, Rebecca Cebulka, and my advisor, Enrique Del Barco. The journal's copyright policy is attached in Appendix A, while the IRB approval for the research is attached in Appendix B. The paper was published online in 2017. [1]

In addition to the technical advances detailed in the previous two chapters, there is a wider need to understand nanomagnetism and nanotechnology in general in order to support future experiments and development along this path. Science and technology at the nanoscale are focused on the investigation of structures having one or more dimension being less than several hundred nanometers. These types of structures exhibit phenomena which are unique to their small size and are promising in many applications, with the potential for a significant impact across many fields including physics, biology, chemistry, materials science and engineering. While research into nanoscience unquestionably has and will continue to play a vital role in developing cutting-edge science and engineering technologies, there remains a lack of talented students who have been attracted to fields in nanotechnology. Many universities do not have the capability to introduce or expose their students to the processes involved with nanofabrication and development, regardless of recommendations from both the President's Council of Advisors on Science and Technology and the NSF [2] to improve education and training of the next generation of students so as to graduate with a general understanding of nanoscience and technology. As a direct consequence, among the many teaching and learning activities being developed at the University of Central Florida (UCF) (including large scale-up reversed classes for introductory physics courses, extra-curricular support for physical science students, online and in-person tutoring, and both professional and peer-mentoring programs for Physics majors), a new degree option for a minor in Nanoscale Science and Technology was

initiated and offered for the first time in the Fall 2015 semester. The minor was designed to attract students from a wide variety of disciplines and is structured around three main “nano-courses,” to be taken in any order. These three main courses were tailored to provide exposure to the basics of nanoscale science and technology, both from a physical and computational standpoint as well as examining the societal impact of modern emergent nanotechnologies. More specifically, for these three main courses there exists a three-fold aim:

- i. That undergraduate students at UCF will become familiar with various nanoscience concepts by conducting and presenting individual study into advanced topics linked to the contents of the courses;
- ii. That local middle school students be introduced to some of the most inviting facets of STEM fields of research - those incorporating nanotechnologies or nanoscience which may have a great effect on human society – hopefully with a high likelihood of convincing the younger generation to aspire towards careers in nanoscience; and,
- iii. That local middle school instructors as well as students will benefit from lasting products of their interactive partnership with the undergraduate students in the courses.

The last two goals may seem to point towards a collaboration between the undergraduate students who have enrolled in the courses and a local middle school audience; in point of fact, all three of the main “nano-courses” were designated through UCF to be *service-learning*. For the reader who may be unacquainted, service-learning is described by UCF as “a teaching method that uses community involvement to apply theories or skills being taught in a course” [3]. For a more thorough explanation of service-learning courses and various teaching methods, see [4]. Each of the three main courses has been made to require that enrolled students “teach” at a local middle school for one class period about a part

of the course they thought was exciting, so as to combine more traditional teaching methods with a type of community service. Ideally, this would also contribute to the recruitment of even more young minds towards a career in a STEM-related field. The students who are enrolled should gain an increased feeling of both personal and civic responsibility, through the creation and dissemination of their own interactive lecture in a classroom and by venturing into the local community to impart knowledge and experiences relating to nanotechnology to its younger members, most particularly potential future female STEM workers. The remainder of this chapter concerns itself with a study performed as part of my receipt of a 2015-2016 iSTEM Fellowship, into the effect of service learning on the novel course series on nanoscience described above taught in the UCF physics department.

4.1 Background

"Nanoscience II: Technology and Applications," was the initial course to be offered in the Fall semester of 2015 to a class of 12 students. It was comprised of 60% lecture-related activities and 40% service-learning-related activities. The lecture part of the course consisted of an overview of the basic physics and applications of nanoscience/nanotechnology, and heavily emphasized in-class student interaction with the lecturer and each other. Homework was presented as miniature-research assignments, with either a group of students or individuals investigating a topic related to the lecture material outside of class and then presenting it in-class to their fellow students. In the service-learning aspect, students were divided into groups of 3 and told to choose an area of developing nanoscience applications that interested them. They were to study them on their own, outside of class, to eventually be presented in a local middle school. The middle schools ultimately chosen for these presentations were suggested by the Executive Director of Secondary and Middle Schools in each school district.

The approach behind the course was intentionally chosen so that the majority of student learning would follow from their own research initiative, both individually and through interactions with their fellow students, in addition to experiences with a wider audience at the middle schools through the service-learning portion. As well as being necessary to passing the course the idea was for the service-learning presentations, each of which had at least one female presenting, to have a community service effect. Hopefully they would also encourage middle school students to become more attracted to a career in STEM, in particular young women who still remain underrepresented in a large number of the hard sciences. The presenters, especially the female presenters, who travelled to the local schools would function as role models to the students. Of course, there has been a large volume of research performed concerning the beneficial impact of female role models in recruitment and retention of women in STEM fields [5-8].

The student presenters were placed in contact with the middle school teachers through an intermediary (myself, the course TA) so as to determine which topics would be the best fit for each classroom, as the middle school audience ranged from 6th to 8th grade and were covering different topics in their science lessons. This worked to engender a sense of cooperation between the students enrolled in the course and the surrounding community. As an accompaniment to the scientific subjects being discussed, the presenters also shared with the middle school classes their personal experiences at UCF, involvement in the nanoscience course, and plans for a future career. Academically, the rewards of using service-learning as an instruction method have been known for decades and can be found in numerous studies [9-11]. Documented advantages to the approach include but are not limited to increased critical thinking skills, increased problem-solving skills, increased student engagement in class, and increased engagement in the community.

It was decided to integrate a nanoscience course with service-learning teaching methods because while UCF has a generally impressive record of providing service-learning education options, including an entire department devoted to the application and understanding of experiential learning methods, virtually none of the service-learning courses offered at the time this study began were involved with a scientific topic. As an example, in the Spring semester of 2016 which immediately followed the course discussed in this chapter, two nursing and eleven creative writing, teaching, or other humanities courses made up the majority of the fourteen service-learning designated courses that were offered at UCF. The only service-learning course that semester related to STEM directly was the continuation of the course discussed here. Given the degree of involvement UCF has shown in service-learning activities, it felt obligatory to include a more scientific option by providing nanotechnology courses with a service-learning component to students at an undergraduate level. This series of nanoscience courses is only the second physics service-learning option offered by the department; the other was designed to train future physics instructors. As a consequence, research as to its effectiveness was warranted to help decide if this teaching method for this subject should continue to be implemented in the future.

While a large volume of research has been carried out as to the effect of service-learning on courses which do not focus on science and technology [12-18], at the time this study was performed very little had been aimed towards service-learning in STEM courses in general, and virtually none for nanoscience courses specifically. In the research presented in this chapter, learning assessment results have been used to examine students' depth of learning and critical thinking over the course of the UCF service-learning nanotechnology course. To this end, nanoscience pre- and post-tests [Appendix F] were administered to the enrolled students at the beginning and end of the semester, in order to help quantify general depth of learning. Students were also required to write a critical reflection paper at the end of

the semester, which was intentionally designed to focus on their service-learning experiences. For this paper, each student wrote an initial draft, was given constructive criticism by the instructors, and submitted a final reflection. Both the initial drafts and the completed reflections were made anonymous and provided to the Program Director of Service-Learning at UCF with no student contact. The papers were evaluated in accordance with the Describe, Examine, and Articulate Learning (DEAL) model [15], which has been shown in previous research to be an effective method to assist students in developing their critical thinking skills [19,20] as well as a valid way to evaluate improvement in said skills [15].

4.2 Methodology

4.2.1 Research Participants

Participating in the research study were myself and my advisor (Enrique Del Barco, who taught the majority of the course while I acted as the TA) as the principal investigators (PIs), and the 12 students who were enrolled as the research subjects. The course name was PHZ 3464 Nanoscience II: Technology and Applications and was offered at UCF in the Fall semester of 2015. This study took place during that same semester (Fall 2015). The research subjects were comprised of one sophomore, one junior, and ten seniors, with majors including physics, engineering, biology, and chemistry. Out of the twelve students, nearly half were female. The research purpose was explained to all of the subjects in accordance with IRB protocol and all of the students enrolled in the course did choose to participate.

4.2.2 Course Design

When designing the course, we specifically intended for PHZ 3464 to focus more on learning outside the classroom than on lecture content. The overarching goal was to increase students' experience in research discussions and presentations about scientific topics of their own choice. The total grade was made up of 40% contribution from the service-learning aspect and 60% contribution from more formal

coursework. Table 4.1 shows the grading rubric for the final grades. To facilitate experience in presentations and discussion, homework assignments were to select a topic somehow related to what was currently being discussed in class, research it at home either in groups or individually, and then give a short presentation on that topic in-class. Students were made aware of the presentation grading rubric at the start of the semester. Lectures by the professor were complemented by student discussions about recent articles from academic journals, in addition to time dedicated to research and planning for the end of semester service-learning projects, which are explained in the next paragraph. There were also several student visits to on-campus microfabrication facilities, with hands-on components included.

Table 4.1: Nanoscience Course Rubric

Overall grading rubric for the Nanoscience II: Technology and Applications course.

Service Learning (40%)	In-class presentations (15%)
	Final reflection paper (15%)
	Middle school presentations (10%)
Formal Coursework (60%)	Exams (40%)
	Homework (20%)

For the end of semester service-learning projects students were divided into four groups of three students each and put in contact with local middle school teachers. They chose a modern nanoscience application/technology that interested them, researched it outside of class and prepared an interactive presentation to be “taught” in a middle school class during their normal science period (about 40 minutes). Topics were selected from the journal *Nature*; several articles relating to emergent nanotechnologies were submitted to the TA (myself) who worked with the middle school teachers to select the best options for each class. A total of eight different classes, roughly 20 middle school students per class, and three separate schools were part of the projects. The presenters were asked to emphasize

relatability and classroom interaction and minimize the use of PowerPoint slides and lecturing; some examples of the classroom presentations are shown in Figure 4.1. Ultimately the service-learning projects were graded on a progress report performed during normal class time, before the visits to the local schools; the middle school presentations themselves; and the final reflection paper. Each group also presented a poster about the experience in the middle schools at the end of the semester, which were then submitted to the annual UCF service-learning showcase in the Spring semester of 2016.

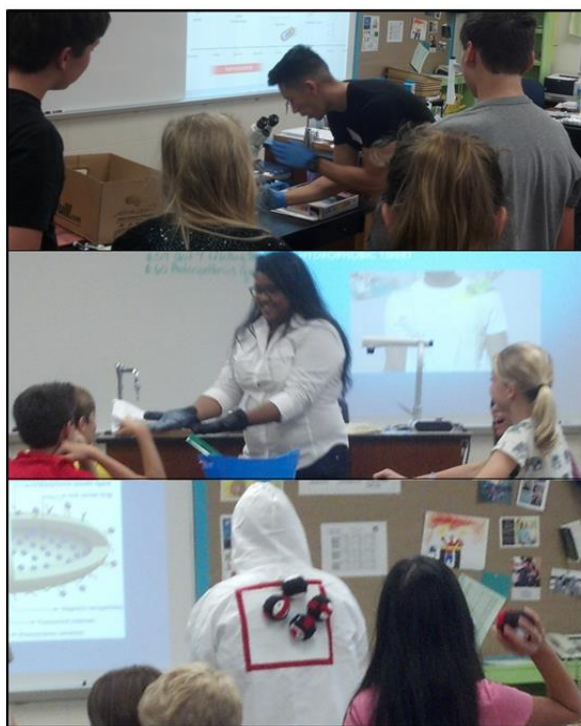


Figure 4.1: Participants Presenting in Middle Schools

Top: One of the study participants presenting on “Using Nanotechnology to filter/purify water” shows a culture of bacteria under a microscope. Middle: The group presenting on “Wearable Nanotechnology” illustrates the difference between a normal glove and a nanoparticle-coated water-repellent glove by inviting the audience to touch them. Bottom: A participant presenting on “Using Nanotechnology to treat/cure diseases” demonstrates the ability of nanoparticles to ‘stick’ to certain cells by involving the audience in an interactive game. [1]

As an aside, the experience with the middle schools was very positive. The teachers were extremely excited about the project and response from the middle school students overall was

encouraging. Remarks from the teachers included “Thanks so much for coming to my class today! I can tell they really enjoyed it! As, did I! It was really great!” [21] and “They really loved it!” [22]. There were requests for additional presentations as well as interest about collaborating again in the future for similar projects.

4.2.3 Assessments

Research subjects were asked to take a pre-test on the first day of class and a post-test on the last day of class made up of 27 multiple-choice questions selected to assess general knowledge of nanoscience topics [Appendix F]. A few previously designed nanoscience concept inventories were found [23,24], but were intended for upper-level courses as opposed to an introductory course, and they put a heavy emphasis on the engineering processes. A more wide-ranging, introductory nanoscience concept inventory was developed by the professor and TA (myself) *before the course curriculum was written*, so as to avoid tailoring it specifically to the course material. As we will see in the next section, significant improvement was seen from the beginning of the course to the end of the semester.

Near the end of the course, subjects were required to write a two-page critical reflection paper about the process of their service-learning project, how they were affected, and how they felt the project affected their local community. A copy of the DEAL model rubric that was used to score the reflections [Appendix G, [25]] was made available to them before they started their first drafts. Once completed, those drafts were read by the course instructors (including myself) and returned to the subjects with feedback and criticism. The subjects then handed in their final reflection papers on the last day of class, to be anonymously scored together with their initial drafts by the Program Director of Service-Learning at UCF. They were judged by the same DEAL model rubric that had been provided to the subjects. All versions of the critical reflections, from all students, had the formatting standardized as well as titles and

the student's names removed. Additionally, each paper was assigned a different random number as an identifier, with drafts mixed in with final versions. All were scored by one person who had no previous contact with the students. The reason behind scoring the critical reflections in this manner was to evaluate the development of critical thinking skills while increasing overall objectivity during the scoring. As will be discussed in section 4.3, the results did show improvement.

After the conclusion of the semester, we requested that research participants complete a post-survey [Appendix H] asking them to rate statements about the impact of their service-learning experience on themselves and the community, as well as the contribution service-learning had towards the overall learning in the classroom, from Strongly Agree to Strongly Disagree. This survey was based on a survey utilized by the UCF Arboretum [26] to assess the impact that service-learning courses involving work in the Arboretum had on students' educational experiences. Participants were informed that their professor would be unable to see the individual respondents, to encourage honest responses. Anything related to the submission or scoring of the post-survey was taken care of by the TA, with the professor only being shown the statistics presented in this chapter. Nine of the twelve students chose to participate in the survey.

4.3 Results

The results of this study showed a distinct increase both in nanoscience subject knowledge and general critical thinking skills. Results were quantified through the use of paired, two-tailed T-tests and the calculation of the percent gain as in (4.1). A paired T-test is used as a method of statistical analysis when comparing two data samples which are linked, particularly in cases of before-and-after studies. It can help determine if the "between" methods had a significant impact on the sample means. *Two-tailed* refers to the hypothesis used to test whether the difference between before and after samples is

meaningful, or due to random fluctuations; a paired two-tailed p-test starts from the hypothesis that the difference *is* meaningful to start, and that the direction of that difference does not matter. Therefore, performing this manner of analysis will inform us as to whether our service-learning method had a meaningful effect on students' learning. A walkthrough of a simple paired T-test is presented in [27]; the values presented in this section were calculated using Excel's built-in paired T-test formula. The meaning of the t- and p-values is to determine how likely it is that there was no significant difference between the before-and-after sample means. The larger the magnitude of the t-value, or the farther it is from zero, the more likely the difference is significant. The smaller the magnitude of the p-value, conversely, the more likely it is that the difference between the two means is statistically significant. Commonly accepted nomenclature is to refer to p-values <0.05 as "statistically significant," and <0.001 as "statistically highly significant," with the former having less than a 1 in 20 chance of being wrong and the latter having less than 1 in 1000 chance. The percent gain is somewhat easier to understand. It simply calculates how much improvement was shown out of how much was possible, scaled to the initial score. The formula used here is

$$\% \text{ gain} = 100 * \frac{(\text{finalscore} - \text{initialscore})}{\text{initial score}} . \quad (4.1)$$

In summary, the post-test showed an average percent gain of 28.86% from the pre-test, with a p-value of 0.000321 and t-value of -5.1435. The initial mean score (out of 100) was 59.88 with standard deviation of 16.246 and standard error of 4.69, and the final mean score was 77.16 with standard deviation of 7.03 and standard error of 2.03 (see Figure 4.2). The critical reflection papers showed an average percent gain of 11.54%, with a p-value of 0.00326 and t-value of -3.7407. By accepted nomenclature, that makes the improvement seen in the concept inventories statistically highly significant and improvement in the reflection papers statistically significant.

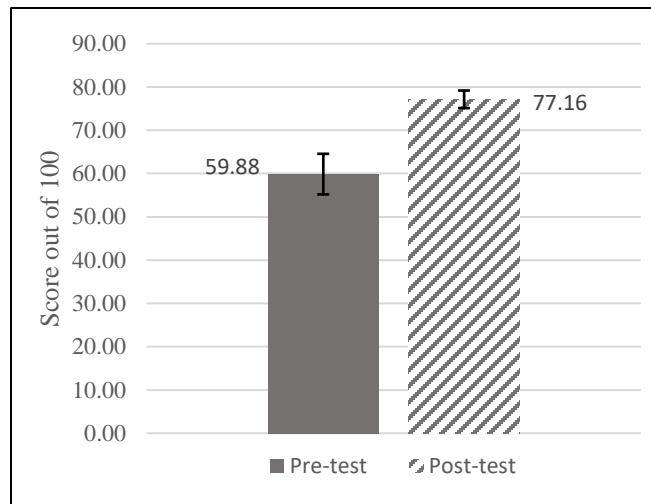


Figure 4.2: Overall Concept Inventory Scores

Average nanoscience concept inventory total scores (out of 100) for the pre- and post-test. Error bars shown represent the standard error calculated for each concept inventory. [1]

4.3.1 Pre/Post-Tests

The pre/post-test questions were grouped into the following five categories: Undergraduate Quantum Mechanics, Semiconductor Physics, Micro-device Fabrication, Nanoscience, and Nanotechnology/ Applications. The percent gains for each topic, averaged over the twelve study participants, are shown in Figure 4.3 above the average total scores for each topic. As can be seen in the figure, Nanoscience and Nanotechnology/Applications exhibit the greatest average percent gain over the semester, in addition to having some of the lowest pre-test scores. As would be expected for a nanoscience course that sets its focus on technological applications, those two topics showed the most overall improvement.

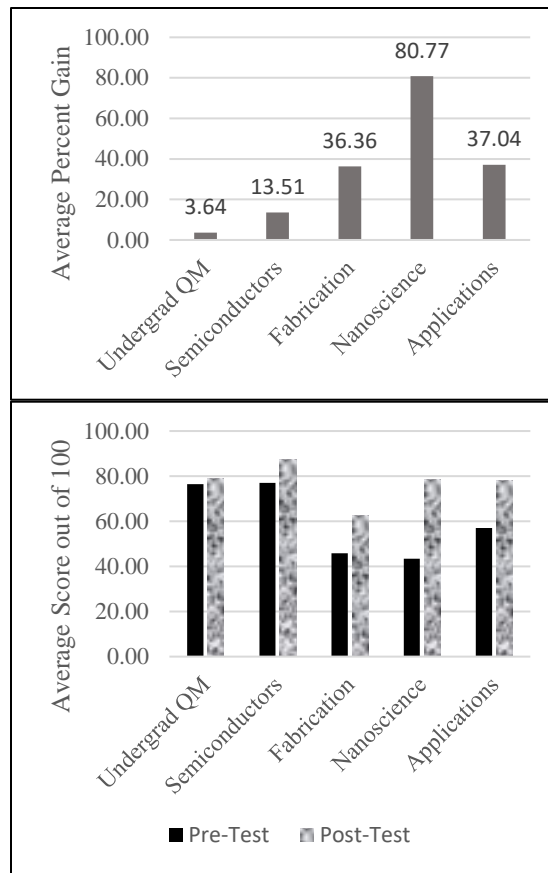


Figure 4.3: Concept Inventory Scores by Topic

Improvement on the nanoscience concept inventory in each topic. Top: Average percent gains per topic. Bottom: Average total scores (out of 100) per topic, for both pre- and post-tests. [1]

4.3.2 Critical Reflections

Participants achieved good scores on both the drafts and final submissions of the critical reflection papers, with an average score for the drafts (out of 100) being 88.7 and that of the final submissions being 98.9. Critical reflections scoring was grouped into the following eleven categories (with an explanation of each):

- i. *Integration*: ability to draw connections between the experience and the learning
- ii. *Relevance*: discussion remained focused on the learning
- iii. *Accuracy*: statements were accurate and well-supported

- iv. *Clarity*: provided examples, illustrated points, and defined terms
- v. *Precision*: gave specific descriptions or data
- vi. *Writing*: no typographical, spelling, or grammatical errors
- vii. *Depth*: avoided oversimplifying; addressed questions arising from statements made
- viii. *Breadth*: considered alternate points of view or alternate interpretations
- ix. *Logic*: conclusions consistently followed the line of reasoning
- x. *Significance*: substantially addressed the most significant issue(s) raised by the experience
- xi. *Fairness*: represented others' perspectives without bias.

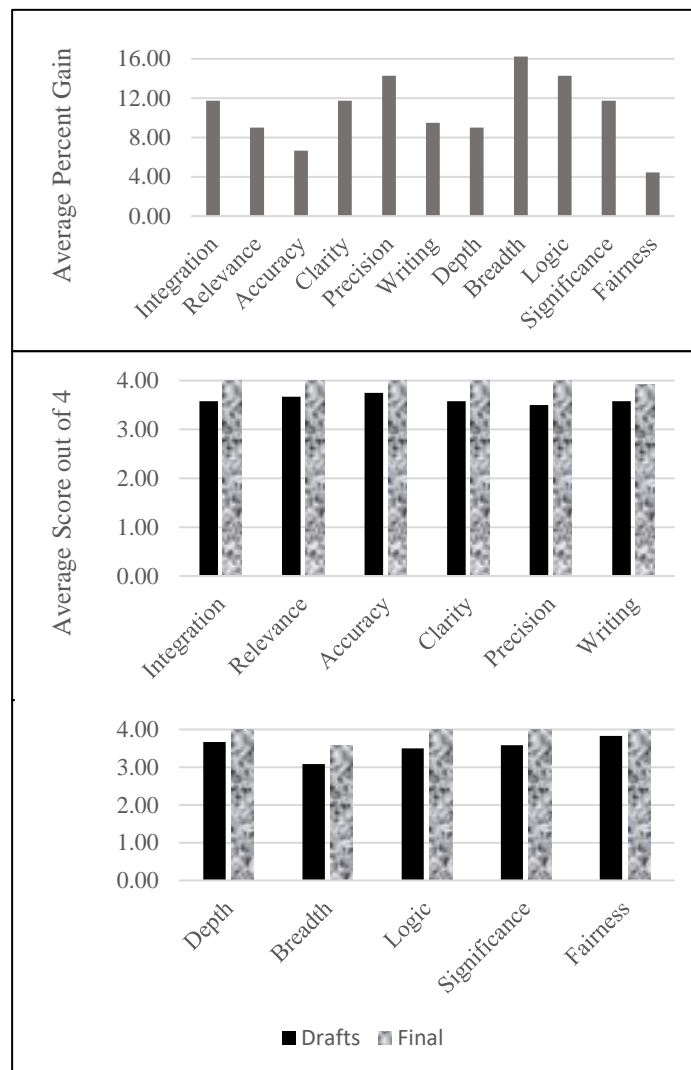


Figure 4.4: Critical Reflection Scores

Top: Average percent gain for each category. Bottom: Average total scores (out of 4) in each category for both drafts and final submissions. [1]

The average percent gains as well as the average scores for both drafts and final submissions are shown in Figure 4.4, broken down by category. With the exception of the Writing and Breadth categories, each area received a perfect score on the final critical reflection submission. The main category participants struggled with was the breadth of their reflections; that is [Appendix G], “Giving meaningful consideration to alternative points of view and making good use of them in shaping the learning.”

4.3.3 *Post-Survey*

To finish, the service-learning post-survey [Appendix H] showed very optimistic responses to the service-learning experience in general and encouraging reactions to the impact on their more conventional classroom learning. Participants confirmed their desires to continue involvement with the community after the course and conveyed that they discovered a clearer image of their career goals while becoming more marketable in their ideal profession as a direct consequence of the service-learning experience. Regarding academic engagement, participants did report an increased interest in the course material relating to their service-learning projects, encouraging them to voluntarily study those topics on their own in more detail than they would have in a standard, non-service-learning course.

The below statements have been selected as being the most relevant to identifying the service-learning experience’s impact on *academic* learning in the classroom:

“Q2: The community work I did increased my ability to understand and apply the academic course material.

Q4: The reflection activity added to my learning experience by helping me to consider course concepts more deeply.

Q14: Outside of class time and service hours, I frequently thought about the issues raised in class.

Q19: I have a better understanding of nanoscience and technology because of my service experience.” [Appendix H]

The participant responses to these statements (ranked from Strongly Agree to Strongly Disagree) are shown in Figure 4.5. All but one participant agreed that the service-learning experience increased their understanding of the course material as well as nanoscience and technology in general. Most of the participants agreed that the critical reflection influenced them to consider concepts more deeply, and almost half said they frequently thought about issues raised in class outside of the requirements of the course.

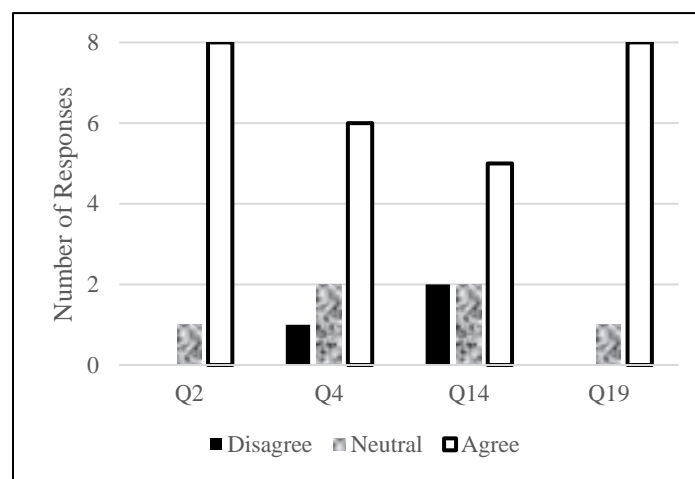


Figure 4.5: Post-Survey Responses

Student responses to the post-survey questions discussed in text. Responses have been grouped in three categories: Agree (includes both Agree and Strongly Agree), Neutral (Neither Agree nor Disagree), and Disagree (includes both Disagree and Strongly Disagree). The total number of responses for each question is 9. [1]

4.4 Discussion and Summary

The assessments of student depth of learning and critical thinking skills demonstrate a positive development over the course of the semester. Although it is possible that this improvement could be attributed to the lecture and formal coursework aspects of the class, the response from study participants show indication that improvement is at least somewhat due to the service-learning project and related

classroom preparation. Specific comments from the participants as well as the post-survey responses point to the substantial impact of service-learning on both participants' traditional learning and their future careers. We associate the observed learning gains with increased student engagement in the course, resulting from the service-learning projects. This conclusion is supported by the participant replies to survey questions as well as their comments to the course instructors about the effect service-learning had on their interest in the course.

As an interesting aside, the statements isolated from the post-survey in the last paragraph of section 4.3.3 are bear some resemblance to several questions asked of students in the service-learning focus groups in [28], including "Did participating in service learning help you to learn or understand the course material better?" and "Did service learning help you to learn specific skills or knowledge that you might not learn in college classes that did not offer service learning?" As a direct consequence of the positive student responses to both focus group interviews and more standard assessments explained further in their report, Prentice & Robinson concluded that service-learning appeared to be a decisively positive contributing factor to students' academic learning. For their assessments (although not their focus group interviews) they were also able to gather data from similar courses both with and without service-learning as a comparison, which was unfortunately not possible in the study discussed in this chapter.

Obviously, there were some limitations to this study, including the small number of students who participated in the course and lack of a non-service-learning comparison group. There also was only one person who scored all of the critical reflection papers; while this removes any question of interrater reliability, it necessitates accepting one single appraisal of participants' critical thinking skills. The conclusions drawn thus rely somewhat on student response and opinion, and although critical reflection

improvement was quantitatively observed it would be an improvement moving forward to have multiple scorers to help ensure grading is as fair, impartial, and accurate as possible. Nevertheless, we see this to be an encouraging starting point for evaluating the effect that service-learning has on students' overall learning, knowledge and critical thinking skills in nanoscience-based courses. Although it was initially implemented in just the last few years, the new UCF "Nanoscience and Nanotechnology" degree did continue beyond the first installment studied in this paper, with the other two core courses having been offered in consecutive semesters. If student response continues to be positive, incorporating service-learning may prove to constitute a way of drawing more undergraduates towards STEM fields and nanoscience, addressing the need for qualified graduates in the workforce. Additional outreach initiatives have been implemented by the PIs following this study, such as the development of the *Physics Youth Scholastic and Instructing Camp for Orlando Scientists* (PhYSICOS) in conjunction with the already established Chemistry and Biology summer camps at UCF. PhYSICOS had its inaugural session in the Summer of 2017 and was offered at no cost to high-performing local high school students. The curriculum was written, sessions were taught, and the camp as a whole was organized entirely by graduate students (particularly the first year, in which my research group oversaw it). Students who participate in the PhYSICOS summer camp experience instructional sessions and enrichments activities that focus on magnetism and giving attendees an overview of some undergraduate introductory physics material. In particular, hands-on experiences with lab experiments and basic device fabrication are provided. PhYSICOS has since transitioned into primarily being organized by the Graduate Society of Physics Students (GSPS) and the Physics Women Society (PWS) in our department.

References

- 1 Cebulka, R. & del Barco, E. *Assessment of the Effect of Service-Learning in Nanoscience on Student's Depth of Learning and Critical Thinking*. PRISM: A Journal of Regional Engagement **6**, (2017).
- 2 Roco, M. C. & Bainbridge, W. S. (Arlington, Virginia, 2001).
- 3 University of Central Florida. *Service Learning*, in <https://www.ucf.edu/services/s/service-learning/> (2018).
- 4 Heffernan, K. *Service-Learning in Higher Education*. Journal of Contemporary Water Research and Education **119**, (2001).
- 5 Craig, A. in *Proceedings of the 3rd Australasian Conference on Computer Science Sducation* 41-47 (ACM, The University of Queensland, Australia, 1998).
- 6 Butler, D. M. & Christensen, R. *Mixing and Matching: The Effect on Student Performance of Teaching Assistants of the Same Gender*. Political Science & Politics **36**, 781-786, (2003).
- 7 Robst, J., Keil, J. & Russo, D. *The Effect of Gender Composition of Faculty on Student Retention*. Economics of Education Review **17**, 429-439, (1998).
- 8 Etzkowitz, H., Kemelgor, C., Nueschütz, M. & Uzzi, B. in *Who Will Do Science? Educating the Next Generation* (eds W. Jr. Pearson & A. Fetcher) Ch. 3, (Johns Hopkins University Press, 1994).
- 9 Giles, D. Jr. & Eyler, J. *The Impact of a College Community Service Laboratory on Students' Personal, Social, and Cognitive Outcomes*. Journal of Adolescence **17**, 327-339, (1994).
- 10 Markus, G. B., Howard, J. P. & King, D. C. *Integrating Community Service and Classroom Instruction Enhances Learning: Results from an Experiment*. Educational Evaluation and Policy Analysis **15**, 410-419, (1993).
- 11 Bringle, R. G. & Hatcher, J. A. *Institutionalization of Service Learning in Higher Education*. The Journal of Higher Education **71**, 273-290, (2000).
- 12 Whitley, M. A. *A Draft Conceptual Framework of Relevant Theories to Inform Future Rigorous Research on Student Service-Learning Outcomes*. Michigan Journal of Community Service Learning **20**, 19-40, (2014).
- 13 Molee, L. M., Henry, M. E., Sessa, V. I. & McKinney-Prupis, E. R. *Assessing Learning in Service-Learning Courses through Critical Reflection*. Journal of Experiential Education **33**, 239-257, (2010).
- 14 Warren, J. L. *Does Service-Learning Increase Student Learning?: A Meta-Analysis*. Michigan Journal of Community Service Learning **18**, 56-61, (2012).

- 15 Ash, S. L. & Clayton, P. H. *Generating, Deepening, and Documenting Learning: The Power of Critical Reflection in Applied Learning*. Journal of Applied Learning in Higher Education **1**, 25-48, (2009).
- 16 Giles, D. Jr. & Eyler, J. *Review Essay: The Endless Quest for Scholarly Respectability in Service-Learning Research*. Michigan Journal of Community Service Learning **2A and 2B**, 53-64, (2013).
- 17 Moely, B. E. & Illustre, V. *The Impact of Service-Learning Course Characteristics on University Students' Learning Outcomes*. Michigan Journal of Community Service Learning **21**, 5-16, (2014).
- 18 Lockeman, K. S. & Pelco, L. E. *The Relationship between Service-Learning and Degree Completion*. Michigan Journal of Community Service Learning **20**, 18-30, (2013).
- 19 Fisher, J. & Mittelman, M. *Applied Learning in Online Education: A Comparative Study Employing DEAL Critical Reflection*. Journal of Applied Learning in Higher Education **5**, 3-14, (2013).
- 20 Bai, J., Larimer, S. & Riner, M. *Cross-Cultural Pedagogy: Practical Strategies for a Successful Interprofessional Study Abroad Course*. Journal of the Scholarship of Teaching and Learning **16**, 72-81, (2016).
- 21 Francher, M. to R. Cebulka. *Personal Communication*, 2015.
- 22 Bennett, K. to R. Cebulka. *Personal Communication* 2015.
- 23 Kumar, D. *et al.* in *2012 ASEE Annual Conference & Exposition* (ASEE Conferences, San Antonio, Texas, 2012).
- 24 Mitin, V., Liu, X., Bell, M. & Fulmer, G. *Developing a Test for Assessing Undergraduate Engineering Students' Knowledge and Understanding of Nanoelectronics Concepts*. Journal of Materials Education **31**, 175-200, (2009).
- 25 Ash, S.L. & Clayton, P.H. *Learning Through Critical Reflection: A Tutorial for Service-learning Students*. Ash, Clayton & Moses, (2009).
- 26 University of Central Florida Arboretum. *Service Learning*, in <https://arboretum.ucf.edu/get-involved/students/service-learning/> (2015).
- 27 Mathematics Learning Support Centre. *1.1 - Paired t-Tests*, in Statistics: General Leaflets. https://www.lboro.ac.uk/media/wwwlboroacuk/content/mlsc/downloads/1.1_Pairedttest.pdf (2019).
- 28 Prentice, M. & Robinson, G. *Improving Student Learning Outcomes with Service Learning*. American Association of Community Colleges, (2010).

CHAPTER 5: CONCLUSION

Accompanying the current global interest aimed towards emerging quantum technologies, the field of molecular magnetism has focused on understanding the quantum dynamical properties of the spin in single-molecule and single-ion magnets. They have turned their eyes to exploring the real possibilities of utilizing the unique characteristics inherent in these systems in existing quantum technologies. In this dissertation I have sought to bring together an integration of experimental and educational frameworks geared towards the study, understanding, and dissemination of knowledge of the quantum dynamics of spin in molecular nanomagnets. I have been primarily concerned with the nature of light-matter interaction in SMMs, and with enabling coherent quantum control over the molecular spin. I have described the experimental setups I have accomplished in order to investigate this interaction in both the weak and strong coupling regimes.

The larger SMM community has only recently begun to develop our understanding of the effects of light-matter interaction in molecular nanomagnets as well as the intrinsic sources of decoherence in their crystalline form, with the limiting factor in most experiments being dipolar dephasing. To overcome this limitation, common practices include diluting the samples in solution and polarizing the spin bath via a large applied magnetic field. Drawbacks of these methods include the loss of a crystalline, monodisperse structure as well as the simultaneous requirement for high magnetic fields and therefore high microwave frequencies, meaning the molecules' intrinsic magnetic properties are subsumed by the large Zeeman interaction. A different approach has therefore been needed if studies into the intrinsic sources of decoherence in a well-ordered crystalline magnetic structure are to be performed; this was the subject of chapter 2 of this dissertation.

To this end, I have developed and tested a unique electron spin-echo experimental setup which can operate at frequencies near 10 GHz and temperatures below 100 mK, while allowing for the possibility of studying 2D films and potentially even single molecules. This has placed our research group in an unprecedented position to undertake time-resolved studies of spin quantum dynamics in non-diluted crystals of SMMs, allowing the probing of ground states involving quantum spin superpositions dictated by the anisotropy of the system. These types of studies should permit measurements of decoherence rates several orders of magnitude lower than what has been achieved at higher fields/temperatures previously. The continuance of this project will focus on time-resolved determination of the spin-lattice and the spin-spin relaxation times of mononuclear SMMs, particularly those based on lanthanide complexes. Ideally, investigation will be done on both T_1 and T_2 as a function of magnetic dilution and molecular composition (which lanthanide is used); this should assist in gaining deep insights into the factors governing decoherence of spins in SMMs. In addition, there are plans in place currently to control the quantum state of the systems' spins by means of Rabi nutation experiments that will be achieved by extending the current spin-echo setup capabilities to higher powers. This may be done by the acquisition of a high-power microwave amplifier, providing a minimum output power of 20 W in the 4.5- 18 GHz frequency range, with a maximum of 65 W at ≈ 10 GHz (such an amplifier has already been identified). This would represent almost two orders of magnitude improvement in the available microwave power with respect to the current capability of 1 W.

In the strong coupling regime, the topic of chapter 3, high quality factor superconducting resonators with micro-constrictions have been designed and fabricated for use in investigating the vacuum Rabi splitting between a photon and the spins of SMMs. The purpose behind the design of these resonators was to continue increasing the coupling parameter by narrowing the center line of the coplanar

waveguide (CPW) resonator down to nanometer scales. CPW resonators fabricated by STAR Cryo-electronics with various geometries of coupling gaps and lengths of the central line have been purchased and received in our lab. They will be characterized at magnetic fields up to 1 T, and at temperatures below 100 mK. These resonators, coupled with some modifications to our dilution refrigerator, will permit measurements of coherent collective coupling between molecular spins and a low number of photons, ideally down to a single photon. In particular, the use of mononuclear SMMs, which bring enhanced spin-photon coupling, may even allow reaching the strong coupling regime with only a single spin. The ultimate plan is to eventually investigate the coupling between a superconducting cavity mode and both single-crystal and isolated molecules of mononuclear SMMs. The initial focus will be on observation of coherent coupling of a large number of spins to a single cavity mode. Ultra-low power microwave experiments are also being developed, so as to take measurements with a low number of photons inside the cavity. Our dilution fridge will need to be configured with the appropriate cryogenic attenuation and amplification stages to accomplish this.

Finally, to marry the scientific aspect of this dissertation to a broader context, I performed some research concerning the best methods of educating new minds in the field of nanotechnology/nanomagnetism. While research and development of new nanoscale materials and applications is still certainly a hot topic, there remains a lack of qualified, interested students who continue into relevant careers. To this end, we designed and implemented a service-learning nanoscience course through the university (UCF), and conducted a study into its effectiveness on student learning. Learning assessment results showed a significant improvement in students' depth of learning and critical thinking throughout the course. Students expressed their approval of the service-learning aspect and its impact on their learning and interest in the course material, as well as future careers.

To summarize, molecular nanomagnets have great potential for use in ultra-high-density integration and quantum information processing; therefore, the experiments that have been enabled during my tenure as a graduate student here at UCF may lead to new and revolutionary quantum technologies. Diminishing and controlling sources of decoherence in SMM/SIMs will enable the large number of gate operations demanded by quantum algorithms and quantum error correction protocols. New interest in the field of nanotechnology and nanomagnetism has been and continues to be fostered through the availability of inclusive STEM courses for college students and even my development of a physics summer camp for local high school students. Over the course of this dissertation I have successfully demonstrated a combination of my scientific and technical training with educational and science education research exposure, with wide-ranging benefits not only to the scientific community but also the world at large.

**APPENDIX A: AUTHOR COPYRIGHT POLICY FOR PRISM: A
JOURNAL OF REGIONAL ENGAGEMENT**

Below is a pdf copy of the author rights for papers published in PRISM: A Journal of National Engagement. It states that the author is free to use the work in any way she/he wishes so long as acknowledgement to PRISM is made. The full policy may be found at

<https://encompass.eku.edu/prism/policies.html>

Rights for Authors

Authors retain copyright but grant exclusive first publication rights and a non-exclusive license to have the work reproduced in other ways, including in electronic databases and on-line. Once an author's work has been published in *PRISM*, the author is free to use it in any way she/he wishes, so long as that use is consistent with the license given *PRISM* to continue to use the work for the duration of its copyright in all languages, throughout the world, in all media. The journal asks only that authors acknowledge in subsequent works the publication of earlier versions in *PRISM*.

The author may include the officially published version of the article (version of record) in an institutional or disciplinary repository, provided the posting includes a prominent statement of the full bibliographical details, and a link to the online edition of the journal.

APPENDIX B: IRB APPROVAL LETTER



University of Central Florida Institutional Review Board
Office of Research & Commercialization
12201 Research Parkway, Suite 501
Orlando, Florida 32826-3246
Telephone: 407-823-2901 or 407-882-2276
www.research.ucf.edu/compliance/irb.html

Approval of Exempt Human Research

From: **UCF Institutional Review Board #1**
FWA00000351, IRB00001138

To: **Rebecca S. Cebulka**

Date: **September 09, 2015**

Dear Researcher:

On 09/09/2015, the IRB approved the following activity as human participant research that is exempt from regulation:

Type of Review: Exempt Determination
Project Title: Assessment of the Effect of Service Learning on Student's Depth
of Learning and Critical Thinking
Investigator: Rebecca S. Cebulka
IRB Number: SBE-15-11499
Funding Agency:
Grant Title:
Research ID: N/A

This determination applies only to the activities described in the IRB submission and does not apply should any changes be made. If changes are made and there are questions about whether these changes affect the exempt status of the human research, please contact the IRB. When you have completed your research, please submit a Study Closure request in iRIS so that IRB records will be accurate.

In the conduct of this research, you are responsible to follow the requirements of the [Investigator Manual](#).

On behalf of Sophia Dziegielewski, Ph.D., L.C.S.W., UCF IRB Chair, this letter is signed by:

A handwritten signature in black ink that reads "Kanille Chay" with a long horizontal flourish extending to the right.

IRB Coordinator

APPENDIX C: DETAILED LIST OF SPIN ECHO CIRCUIT COMPONENTS

- A) Agilent E8364B PNA Series Network Analyzer
- B) Agilent 87301D Directional Coupler Opt 240
- C) Pasternack Circulator Model no. PE8404 w/50 ohm terminator on port 2
- D) HP SPST 33144A Microwave Switch with HP 33190B driver ($T_{\text{rise}} = 5\text{ns}$, $T_{\text{fall}} = 7\text{ns}$ maximum)
- E) Agilent 81110A Pulse Generator
- F) SH Series 11SH10-2000/U18000-O/O 2-18GHz BP filter
- G) Agilent 83020A Microwave System Power Amplifier (30dB gain, 30dBm maximum output)
- H) MiniCircuits CD Block BLK-18+ up to 18GHz
- I) dilution refrigerator (KelvinoxMX100) inside vector magnet (3-axis American Magnetics Inc)
- J) In-House Fabricated Microstrip Resonator (see Appendix D for recipe)
- K) Quinstar Technology, Inc. QCY-150600P000 Cryogenic Circulator
- L) CalTech CIT618 Cryogenic HEMT Cryogenic Signal Amplifier (see Appendix E for more details)
- M) MiniCircuits CD Block BLK-18+ up to 18GHz
- N) Pasternack Circulator Model no. PE8404 w/50 ohm terminator on port 2
- O) AMC Solid State Switch Model no. SWM-DJV-1DT-2ATT Opt. no. 20F ($T_{\text{rise}} = 2\text{ns} = T_{\text{fall}}$ maximum)
- P) SH Series 11SH10-2000/U18000-O/O 2-18GHz BP filter
- Q) Mini-Circuits Amplifier ZVE-3W-183+ (35dB gain, 35dBm maximum output)

R) CTT Amplifier APM/180-2741-22 (66087) (41dB gain, 27dBm maximum output)

S) Stellex Quadrature Mixer M38UC

T) Aeroflex Weinschel Model 981 Coaxial Phase Shifter

U) Agilent Infiniium DS08194A Oscilloscope

APPENDIX D: MICROSTRIP RESONATOR FABRICATION RECIPE

Chemicals and Equipment Needed:

- Isopropyl, Methanol, Acetone, DI water
- GaAs wafer
- LOR and Shipley photoresists, CD-26 developer
- Pipettes, beakers, tweezers
- Nitrogen gas supply
- Gold, Copper, and Titanium pellets
- UV exposure mask, mask aligner, hot plate, spin coater, e-beam evaporation chamber

Spin Coating Procedure:

- Clean GaAs wafer with Acetone, Methanol, Isopropyl (in that order) then blow dry with Nitrogen gas.
- Spin LOR resist with following recipe: 2s at 500rpm, 30s at 3000rpm, 2s at 0rpm. Bake on hotplate for 5 minutes at 175°C.
- Spin Shipley resist with following recipe: 2s at 500rpm, 30s at 5000rpm, 2s at 0rpm. Bake on hotplate for 2 minutes at 120°C.

Mask Aligning Procedure:

- Select mask and clean with Acetone, Methanol, IPA, and DI water then blow dry with Nitrogen gas.
- Place wafer on mask aligner using cut away Parafilm to ensure sample vacuum. Follow SOP for the mask aligner you are using.
- Once the wafer is aligned with the resonator pattern on the mask, check the intensity of the UV-light so as to choose the time of exposure correctly. The relation should be

$$\frac{\text{intensity}}{126 \frac{\text{mJ}}{\text{cm}^2}} = \text{time (s)} \quad (\text{D.1})$$

Evaporation and Liftoff Procedure:

- Clean the patterned wafer by dry plasma etching in an O₂ plasma at 53mTorr for 15 seconds.
- Carefully place sample on sample holder and mount in chamber.
- Evaporations should occur at less than 5e-6 Torr.
- Evaporate 10nm of Titanium, followed by 125nm of Copper, followed by 10nm of Gold.
- Remove wafer from evaporation chamber and place in acetone on a hot plate at 30°C until the metal lifts off. Use a pipette to squirt acetone across the surface gently if needed.

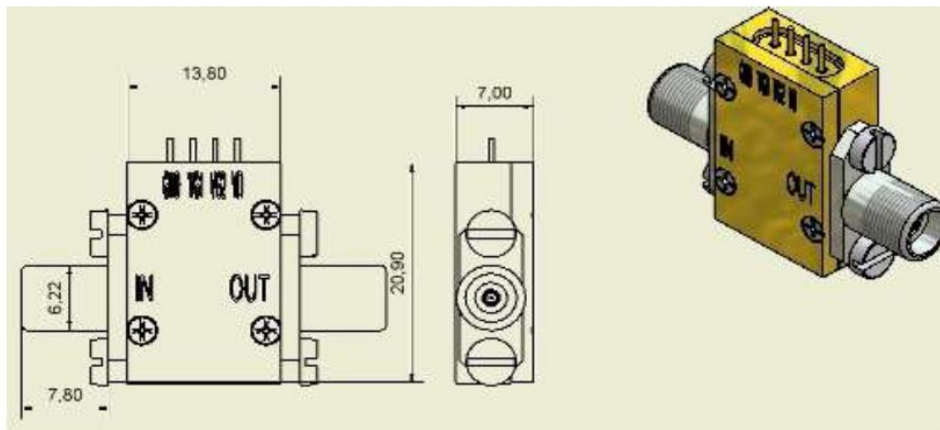
APPENDIX E: CRYOGENIC AMPLIFIER

CIT618 Cryogenic HEMT Low Noise Amplifier, purchased from Caltech.

The CIT618 is a GaAs HEMT cryogenic, low noise, broadband amplifier. In its standard configuration it comes with female K connectors (mate with SMA) on the RF-input and output and a 4-pin 2 mm pitch header for the DC. The amplifier requires one drain voltage in the 0.5V to 1.5V range and one gate voltage in the -3 V to +1 V range (terminals Vg1 = Vg2) into 11K DC resistance. If desired the gate supply can be eliminated (open pins on Vg1 and Vg2) at slightly less than optimum performance.

The amplifier may be operated at room temperature to give a noise figure < 1.9dB and gain ~35dB. Note that a more negative gate supply voltage, typically -1.5V is required at room temperature but the amplifier is not damaged (but has no gain) if the gate voltage for cryogenic operation, typically 0V, is applied at room temperature. Input and output return loss change very little from 300K to 4K.

Outline Drawing



Typical Performance at 19K and 6 to 18 GHz

Gain	38dB \pm 2 dB
Noise temperature	<9K
Noise figure	< 0.13 dB
Input Return Loss	>5 dB (stable, all frequencies) >10 dB 6 to 12 GHz
Output Return Loss	>10dB, 2 to 18 GHz
Operating temperature:	4.2 K- 320 K
RF output power	<.005W, < +7dBm
Maximum input power	.01W, +10dBm
DC power @ 18 K:	Vd = 1.2V at 24 mA (29mW)

Figure E.1: Cryogenic Amplifier

Top: Schematic of the cryogenic amplifier purchased from Caltech to enable ultra-low-power studies to be performed in our dilution refrigerator. Bottom: Performance data for the amplifier.

APPENDIX F: NANOSCIENCE AND TECHNOLOGY CONCEPT INVENTORY

BIRTH MONTH/DAY: (MM/DD) (/)

GENDER: F M

Nanoscale science and technology concept inventory

(Choose only one answer per question)

1. The Wave-Particle duality refers to the phenomenon in which atomic particles while in motion
 - a. appear to float around
 - b. create waves in collisions
 - c. behave sometimes as waves and sometimes as particles
 - d. cause ripple effects
2. Quantization of energy refers to the observation that
 - a. energy is radiated or absorbed in discrete "quanta" or "energy packets"
 - b. small quantum amounts of energy must be used for best results
 - c. restricted use of energy leads to quantization of energy
 - d. a fair distribution of energy requires its division into equal parts or "quanta"
3. The Uncertainty Principle states that
 - a. nothing in nature is certain
 - b. the outcome of any experiment at the nanoscale cannot be predicted
 - c. the simultaneous measurement of position and momentum is inherently inaccurate
 - d. ambiguity leads to uncertainty
4. The Schrodinger equation
 - a. specifies when the quantum state of a physical system does not change with time
 - b. is used to measure dimensions below 100 nanometers
 - c. enables studying the inner side of atomic particles
 - d. is to quantum mechanics what Newton's second law of motion is to classical mechanics
5. According to the Pauli Exclusion Principle
 - a. particles with the highest energy are excluded from any stable system
 - b. no two identical particles may occupy the same quantum state simultaneously
 - c. particles with low energy and those with high energy interact in an exclusive manner
 - d. antisymmetry in wave functions of particles is the result of chemical bonds
6. The term quantum tunneling refers to the phenomenon when a particle
 - a. reaches the other side of a potential energy barrier that it classically could not be surmount
 - b. displays the wave-particle duality of matter
 - c. both a and b
 - d. neither a nor b

7. *Energy bands*
- are ranges of allowed energies for electrons moving in periodic potentials, such as in a crystal lattice*
 - are the energies of a beam of particles when moving together*
 - are associated with sound (i.e., mechanical vibrations) in crystals*
 - are related to light moving inside nanoscopic materials*
8. *Fermi energy*
- is the energy of the highest occupied quantum state in a system of electrons at absolute zero*
 - relates to the energy of systems that conduct electricity in a non-Ohmic way*
 - characterizes the quantum energy of atomic vibrations in solids*
 - is the energy of a free electron at rest in vacuum*
9. *What is a single-electron transistor?*
- a transistor made of semiconductor material*
 - a device which works with thermal electrons*
 - a device operating with tunneling of electrons one at a time*
 - a transistor that cannot be replicated*
10. *Why is graphene, a two-dimensional atomically flat sheet of carbon atoms, so relevant in nanoelectronics?*
- Because of its excellent mechanical properties*
 - Because of its transparency to visible light*
 - Because of its high electrical mobility and absence of a band-gap*
 - Because electrons move quantum-mechanically*
11. *The photolithography process is analogous to which of the following processes?*
- writing on stone*
 - photographic process*
 - scanning process*
 - curing process*
12. *The Moore's law is due to*
- Price of silicon reduction over time*
 - Larger silicon wafers*
 - Transistor size scaling*
 - Modern circuit architectures*
13. *The process responsible for creating N-type and P-type regions in a semiconductor is known as*
- mixing*
 - annealing*
 - deposition*
 - implantation*
14. *Which process can be used to transfer material onto a wafer?*
- Physical and chemical deposition*
 - Electrochemical etching*
 - Nanowire transferring*
 - None of the above*

15. What characteristic optical response can you obtain in a nanosized metallic particle?
- transparency
 - plasmonic resonance
 - mirror reflection
 - spherical refraction
16. Colloidal suspensions of nanosized particles display different colors due to
- their intrinsic color
 - the laser effect in nanotechnology
 - the Heisenberg Uncertainty Principle
 - the size of the particles in suspension
17. A photonic crystal is
- A crystal able to reflect all photons at all frequencies
 - A periodic structure that interacts resonantly with a particular wavelength
 - A crystal that behaves as a metal for photons
 - A crystal made of nanoscale crystallites oriented all in the same direction
18. Spintronics is
- Electronics employing the spin degree of freedom of electrons
 - Electronics employing the charge degree of freedom of electrons
 - Electronics with magnetic devices
 - Electronics of circular devices (e.g., nanocoils) in which electrons spin
19. What is the typical size of a magnetic domain inside a ferromagnetic material?
- 1 Å
 - 1 nm
 - 100 nm
 - 1 μm
20. A carbon nanotube displays amazing mechanical properties, such as
- It is 1/6 the weight of steel and 100 times its tensile strength
 - It is 6 times the weight of steel
 - It is 100 times harder than steel
 - It conducts electricity an order of magnitude better than copper
21. What is a NEMS?
- a nano-electromagnetic system
 - a nano-electromechanical system
 - a non-electromagnetic system
 - a native electromechanical system
22. Nanostructures are relevant in catalysis because
- their small size allows fabricating devices with small size
 - they maximize the active surface area to promote chemical reactions
 - nanoparticles move faster than macroscopic materials
 - they would produce innocuous byproducts

23. In what way can nanoparticles can be used as biosensors?
- Increasing contact between proteins*
 - Facilitating transport of medicines through cell membranes*
 - Copying DNA strands of a virus or a bacteria*
 - Tagging antibodies to determine what infection may be present*
24. Optical tweezers
- use light to break large molecules in small parts*
 - use light to manipulate nanoscale biological systems*
 - are small tweezers (nano-scale) which can only be seen under an optical microscope*
 - tweezers used to trap optical photons*
25. Nanofluidics deals with
- the flow of liquids through nanoscale channels*
 - liquids made of nano-bio-systems (such as proteins)*
 - slippery surfaces in nanoscale biological tissues*
 - the flow of blood and other bio-systems in veins and arteries*
26. Nanoencapsulation of drugs by nano-shells allows
- drugs to be delivered faster into the blood stream*
 - curing illnesses related to open viruses*
 - drugs to be delivered to the brain*
 - producing small-sized pills*
27. Nanoparticles could be used
- to fight cancer by directly slowing tumor growth*
 - as contrast agents in MRI*
 - to prevent sunburn by bonding to skin cells*
 - to promote stronger muscles*

APPENDIX G: DEAL MODEL RUBRIC USED TO SCORE CRITICAL REFLECTIONS

DEAL Model Critical Thinking Rubric

[Modified source: Paul, R & Elder, L. 2001. The Miniature Guide to Critical Thinking. The Foundation for Critical Thinking. Santa Rosa, CA. www.criticalthinking.org]

	(1)	(2)	(3)	(4)
CT Set A				
<i>Integration</i>	Provides no clear connection between the experience and the learning	Provides minimal and/or unclear connection between the experience and the learning	Provides adequate and reasonably clear connection between the experience and the learning	Provides thorough and very clear connection(s) between the experience and the learning
<i>Relevance</i>	Misclassifies the learning and/or inappropriately shifts from one category of learning goal to another; fails to keep the discussion specific to the learning	Discusses learning that is relevant to the category of learning goal, but much of the discussion is not related to the learning	Discusses learning that is relevant to the category of learning goal and keeps the discussion reasonably well focused on the learning	Discusses learning that is relevant to the category of learning goal and keeps the discussion well-focused on the learning
<i>Accuracy</i>	Consistently makes inaccurate statements and/or fails to provide supporting evidence for claims	Makes several inaccurate statements and/or supports few statements with evidence	Usually but not always makes statements that are accurate and well-supported with evidence	Consistently makes statements that are accurate and well-supported with evidence
<i>Clarity</i>	Consistently fails to provide examples, to illustrate points, to define terms, and/or to express ideas in other ways	Only occasionally provides examples, illustrates points, defines terms, and/or expresses ideas in other ways	Usually but not always provides examples, illustrates points, defines terms, and/or expresses ideas in other ways	Consistently provides examples, illustrates points, defines terms, and/or expresses ideas in other ways
<i>Precision</i>	Consistently fails to provide specific information, descriptions, or data	Only occasionally provides specific information, descriptions, or data	Usually but not always provides specific information, descriptions, or data	Consistently provides specific information, descriptions, or data
<i>Writing</i>	Consistently makes typographical, spelling, and/or grammatical errors	Makes several typographical, spelling, and/or grammatical errors	Makes few typographical, spelling, and/or grammatical errors	Makes very few or no typographical, spelling, and/or grammatical errors
CT Set B				
<i>Depth</i>	Fails to address salient questions that arise from statements being made; consistently over-simplifies when making connections; fails to consider any of the complexities of the issue	Addresses few of the salient questions that arise from statements being made; often over-simplifies when making connections; considers little of the complexity of the issue	Addresses some but not all of the salient questions that arise from statements being made; rarely over-simplifies when making connections; considers some but not all of the full complexity of the issue	Thoroughly addresses salient questions that arise from statements being made; avoids over-simplifying when making connections; considers the full complexity of the issue
<i>Breadth</i>	Ignores or superficially considers alternative points of view and/or interpretations	Gives minimal consideration to alternative points of view and/or interpretations and makes very limited use of them in shaping the learning being articulated	Gives some consideration to alternative points of view and/or interpretations and makes some use of them in shaping the learning being articulated	Gives meaningful consideration to alternative points of view and/or interpretations and makes very good use of them in shaping the learning being articulated
<i>Logic</i>	Draws conclusions and/or sets goals that don't follow at all from the line of reasoning presented	Draws conclusions and/or sets goals that only occasionally follow reasonably well from the line of reasoning presented	Draws conclusions and/or sets goals that usually follow well from the line of reasoning presented	Draws conclusions and/or sets goals that consistently follow very well from the line of reasoning presented
<i>Significance</i>	Draws conclusions and/or sets goals that don't address the most significant issue(s) raised by the experience	Draws conclusions and/or sets goals that only minimally address the significant issue(s) raised by the experience	Draws conclusions and/or sets goals that usually address fairly significant issue(s) raised by the experience	Draws important conclusions and/or sets meaningful goals that substantially address the most significant issue(s) raised by the experience
<i>Fairness</i>	Consistently represents others' perspectives in a biased or distorted way	Occasionally represents others' perspectives in a biased or distorted way	Often but not always represents others' perspectives with integrity	Consistently represents others' perspectives with integrity (without bias or distortion)

PHC Ventures, 2011

APPENDIX H SERVICE-LEARNING POST-SURVEY

Nanoscience II: Technology and Applications Service Learning Post Survey

A) For the following questions please rate your response from 1 - 5; 1-Strongly Agree, 2-Agree, 3-Neither Agree nor Disagree, 4-Disagree, 5-Strongly Disagree.

- 1) The community service aspect of this course helped me to see how the subject matter can be used in everyday life.

1	2	3	4	5
---	---	---	---	---
- 2) The community work I did increased my ability to understand and apply the academic course material.

1	2	3	4	5
---	---	---	---	---
- 3) The academic course material (e.g. readings and lectures) enhanced the service that I performed.

1	2	3	4	5
---	---	---	---	---
- 4) The reflection activity added to my learning experience by helping me to consider course concepts more deeply.

1	2	3	4	5
---	---	---	---	---
- 5) The reflection activity helped me to see the connections between my service experience and the course material.

1	2	3	4	5
---	---	---	---	---
- 6) I feel I would have learned more from this course if more time was spent in the classroom instead of doing work with the community.

1	2	3	4	5
---	---	---	---	---
- 7) The service aspect of the course showed me how I can become more involved with my community.

1	2	3	4	5
---	---	---	---	---
- 8) I feel that my service-learning work in this course benefitted the community.

1	2	3	4	5
---	---	---	---	---
- 9) I will probably continue to volunteer or participate with the community after this course.

1	2	3	4	5
---	---	---	---	---
- 10) The community service involved in this course helped me to become more aware of the needs of my community.

1	2	3	4	5
---	---	---	---	---
- 11) This learning engagement helped me to gain a clearer idea of my educational goals (for example, my major or minor).

1	2	3	4	5
---	---	---	---	---
- 12) This learning engagement helped me to gain a clearer idea of my professional goals (for example, my career).

1	2	3	4	5
---	---	---	---	---

- 13) The service I performed and the skills I developed will make me more marketable in my chosen profession when I graduate.

1 2 3 4 5

- 14) Outside of class time and service hours, I frequently thought about the issues raised in class.

1 2 3 4 5

- 15) The service component caused me to think about my attitudes, values and perspectives.

1 2 3 4 5

- 16) During my service learning, I engaged in positive interactions with people from different social, economic, and ethnic backgrounds than mine.

1 2 3 4 5

- 17) This class caused me to feel more concern about social problems in the community.

1 2 3 4 5

- 18) I have a better understanding of complex scientific issues because of my service experience.

1 2 3 4 5

- 19) I have a better understanding of nanoscience and technology because of my service experience.

1 2 3 4 5

- 20) I have a better understanding of STEM education issues because of my service experience.

1 2 3 4 5

B) For the following statements please rate your response from 1 - 4; 1-Significantly, 2-Moderately, 3-Slightly, 4-Not at all.

- 1) My service-learning experience in the UCF Nanoscience II course impacted my ability to engage in/commit to service in the community

1 2 3 4

- 2) My service-learning experience in the UCF Nanoscience II course impacted my ability to be socially responsible

1 2 3 4

- 3) My service-learning experience in the UCF Nanoscience II course impacted my ability to use knowledge/skills in a work situation

1 2 3 4

- 4) My service-learning experience in the UCF Nanoscience II course impacted my ability to apply course content to the real world

1 2 3 4

- 5) My service-learning experience in the UCF Nanoscience II course impacted my ability to pursue my career goals

1 2 3 4

- 6) My service-learning experience in the UCF Nanoscience II course impacted my ability to take initiative

1 2 3 4

- 7) My service-learning experience in the UCF Nanoscience II course impacted my ability to volunteer for new roles

1 2 3 4

C) Please list any additional comments regarding your service-learning experience in the UCF Nanoscience II course: